

Strategies to Access Triplet Excited State in Core-Twisted Perylenediimides

A thesis submitted for the degree of

Doctor of Philosophy

in

Chemistry

by

Kalaivanan N.



Indian Institute of Science Education and Research
Thiruvananthapuram
Thiruvananthapuram – 695016
Kerala, India

October 2016

Declaration

I hereby declare that the Ph. D. thesis entitled "***Strategies to Access Triplet Excited State in Core-Twisted Perylenediimides***" is an independent work carried out by me at School of Chemistry, Indian Institute of Science Education and Research Thiruvananthapuram (IISER-TVM), under the supervision of Dr. Mahesh Hariharan and it has not been submitted anywhere else for any other degree, diploma or title.

In keeping with the general practice of reporting the scientific observations, due acknowledgements have been made wherever the work described is based on the findings of other investigators.

Place: IISER Thiruvananthapuram

Kalaivanan N.

Date: 31-10-2016

Certificate

This is to certify that the work embodied in the thesis entitled "***Strategies to Access Triplet Excited State in Core-Twisted Perylenediimides***" has been carried out by Kalaivanan N. (PHD11108) under my supervision and guidance at the School of Chemistry, Indian Institute of Science Education and Research Thiruvananthapuram (IISER-TVM) and the same has not been submitted elsewhere for a degree.

Place: IISER Thiruvananthapuram

Date: 31-10-2016

Dr. Mahesh Hariharan

(Thesis supervisor)

Dedicated To

My Amma...

எப்பொருள் யார்யார்வாய்க் கேட்பினும் அப்பொருள்
மெய்ப்பொருள் காண்ப தறிவு.

- குறள் 423

To discern the truth in everything, by whomsoever
spoken, is wisdom.

- Kural 423

ACKNOWLEDGEMENTS

The thesis dissertation marks the end of a long and eventful journey for which there are many people that I would like to acknowledge for their support along the way.

First and foremost, I would like to express my special appreciation and thanks to my advisor Dr. Mahesh Hariharan, for his constant guidance and support, and for providing excellent research environment during my doctoral study. His advice on both research as well as on my career have been invaluable. He gave me the freedom to pursue my interests, simultaneously keeping me on the research track. I am extremely thankful to him for his enormous help, discussions without any limit, constant guidance and support throughout my Ph. D. work. He has constantly encouraged me to push my limits farther and farther. It is indeed a rare privilege to work under his guidance.

My sincere thanks to Prof. V. Ramakrishnan and Prof. E. D. Jemmis, present and former Directors of IISER-TVM, for allowing me to use the facilities of IISER-TVM to carry out my research work. I am grateful to my doctoral committee members, Prof. K. George Thomas and Dr. Reji Varghese for their support, guidance and helpful suggestions. I extend my gratitude to all my Ph. D. course instructors. I thank all the faculty members of School of Chemistry, IISER- TVM for all the support and motivation.

I am indebted to Council of Scientific and Industrial Research-University of Grant Commission (CSIR-UGC) and Department of Science and Technology (DST), Government of India, and IISER-TVM for the financial assistance. I thank them for ensuring a continuous funding during my doctoral study.

I will take this opportunity to thank Dr. Gopidas, NIIST-TVM, Dr. Babu Varghese, IIT-Madras, Prof. Fred Lewis, Northwestern University, Dr. Siva Ranjana Reddy, Dr. Vinesh Vijayan, Dr. Padmanaban, Dr. Anil Shaji and Dr. Shaijumon IISER-TVM for fruitful discussions and helpful suggestions.

It is my pleasure to express my sincere thanks to Dr. Suresh Das, former director, NIIST Trivandrum for allowing me to use the experimental facilities in his institute. I express my sincere gratitude to Dr. Joshy, Dr. Karunakaran, Dr. M. L. P. Reddy, Mr. Bejoy, Mrs. Silja, Mr. Vedanarayanan, Mr. Shanmugasundaram NIIST Trivandrum for their timely help during the last five years.

I am deeply indebted to all my present and past group members: Dr. Rijo T. C., Mr. Shinaj K. Rajagopal, Dr. Ajith R. Mallia, Mr. Abbey M. Philip, Ms. Somadrita, Dr. Salini, Dr. Nandita G. Nair, Mr. Nagaraj, Ms. Gopika Gopan, Ms. Remya Ramakrishnan, Ms. Shubhasmin Rana, Ms. Amalu Mohan, Mr. Ebin Sebastian for their help and fruitful discussions during my Ph. D. work. During the course of my Ph. D. work, I had the pleasure of working with several project, students Ms. Priyanka M. M., Ms. Reshma V. Nair, Ms. Aparna, Ms. Souparnika, Ms. Riya, Mr. Pavan Sharma, Mr. Syed M. Bilal, Mr. Harish Banda, Mr. Murugan, Mr. Vignesh, Mr. Nybeen, Ms. Keerthi Muraleedharan, Mr. Febin Kuriakose, Ms. Ramarani Sethi, Mr. Vinayak Bhat, Ms. Asha, Mr. Ashik Hemanth, Ms. Devika, Mr. Ashwin, Ms. Ishamol, Ms. Anagha S., Ms. Athira., Ms. Hridya P., Ms. Ambili. Their assistance during the presented work is gratefully acknowledged. I thank Mr. Likhin, Mr. Dijo for collaborative work. Special mention to Mr. Abbey M. Philip and Ms. Gopika Gopan for spending their time to correct my thesis.

My wholehearted thanks goes to Mr. Alex P. Andrews for single crystal X-ray diffraction measurements; Mr. Adarsh for NMR experiments, Mr. Aneesh for SEM analysis; Mr. Nibith, Mr. Shiju, Mr. Manoj for GC-mass, elemental and IR analysis and Mr. Shebin George for the graphical artworks. I thank Dr. Morison, Dr. Rajesh, Mr. Navaneethan, Mr. Harikrishna, Mr. Yoganandam, and Mr. Prashant from Laser Spectra Services, Bangalore for their technical support.

I would like to thank several people who made this work possible, and who have made my stay at IISER-TVM enjoyable. I remember the 2011 Ph. D. batch students of IISER-TVM: Mrs. Jiji A. C., Ms. Shine K. Albert, Mr. Sandeep, Mrs. Sabnam, Mrs. Rohini K., Dr. Ajith R. Mallia, Dr. Nijamudheen, Mr. Ramachandra Prasad Pola for their unconditional love and care; Mr. Mohan Rao, Mr. Soumik Mondal, Dr. Atchuth Rao, Dr. Vidyasgar, Dr. Anoop Thomas, Ms. Hema, Mrs. Reshmi Thomas, Mrs. Shyama, Ms. Priyakumari, Dr. Vidya, Dr. Vinayak, Mr. Shine A., Dr. Subila, Mr. Amol and Dr. Pratap Zalake for their timely help. Special mention to Mr. Chandrashekar and Mr. Jyothish Joy for helping me with the computational studies; I thank Mr. Murali, Mr. Hari Veera Prasad, Mr. Libin, Mr. Perumal, Mr. Vignesh, Mr. Manoj, Ms. Jobha, Mr. Baiju, Dr. Pradeep D., Mr. Harshad, Ms. Parvathy, Ms. Dhanya, Mrs. Anu, Ms. Asha, Mr. Purnachandra Rao, Mrs. Soumiya, Ms. Elizabeth Ms. Swathi and Ms. Hemna for their support and affection.

I take this opportunity to express my immense gratitude towards all my teachers, Mr. Marimuthu, Mr. Nataraj, Mrs. Seetha, Mr. Shanmugam, Mrs. Mariyammal, Mrs.

Kalaiselvi, Mrs. Jegadeeshwaran, Mrs. Sengottayan, Mr. Vajravel, Mrs. Kanjana, Mr. N. M. Subramaniyan (NMS), Mrs. Kannamma, Mr. Radhakrishnan, Mrs. Kamalaveni, Mr. K. M. Subramaniyam, Mrs. Saraswathi, in Panchayat Union Middle School, Salangapalayam; Mr. Senniyappan, Mr. Arangasamy, Mr. Aranganathan, Mr. Subramaniyam, Mr. Shanmugam, Mr. Sundaramoorthi, Mrs. Sarojadevi, Mrs. Sampooranam, Mr. Gopalakrishnan, in Govt. Boys Higher Sec. School, Kavindapadi; Dr. Raju, Dr. Ilamparithi, Dr. Gopalswamy, Mr. Maniyan, Mr. Mani, Mr. Viswanathan, Mrs. Manimegalai, Mr. Kannapiran, Mr. Kalaimani, Mr. Appasamy in Gobi Arts and Science College, Gobichettipalayam; Dr. Nanjundan, Dr. Sivasankaran, Dr. Sadasivam, Dr. Shanthi, Dr. Kannan, Dr. Murugesan, Dr. Umaphathi, Dr. Subramaniyan, Dr. Maheshwari, Dr. Sangeetha, Dr. Sarojadevi, Dr. B. Varatharajan (IIT Madras), Dr. D. Ramana (Malldi Drugs Ltd.) in Anna University Chennai for the motivation to keep high standard in my life starting from schooling till my graduation studies. I am thankful to each and every one of them for helping me to pursue my passion and the continuous support and care that they have provided.

It is important to mention Ms. Anjana, Dr. Shyamala T., Mrs. Varsha, Mr. Nithiyanandan, Mr. Prathap, Mr. Selvakumar, Mr. Prabu, Mr. Ramkumar, Ms. Arthi, Mr. Balaganesh, Ms. Joshya Shyamala and Mr. Kalaiselvan for their continuous support and care. I would like to thank all my friends at Gobi Arts and Science College, Erode, Anna University, Chennai, Biocon Pharmaceuticals, Bangalore and Hindustan Unilever Research Center, Bangalore for their support and affection. My special mention to Dr. Mahesh Hariharan's family, Dr. Vinesh Vijayan's family, Dr. Siva Ranjana Reddy's family, Mr. Shine A's family, Mr. Sandeep's family and Ms. Shine K. Albert's family for their love and care during my stay here. I would like to thank all the teaching and non-teaching (library, IT, purchase, finance and mess) staff of IISER-TVM.

I am extremely thankful to Mr. Parthipan, my brother for solely taking the responsibility of my family and supporting me to pursue my research. Special thanks to Mr. Jaganathan, my periyappa for his constant motivation in all my activities.

Above all, I would like to acknowledge the tremendous sacrifices that my parents (Mrs. Pathmavathi, Mr. Nagarajan and Mrs. Kausalya) made to ensure that I had an excellent education. For this and much more, I am forever in their debt. Along the line, I would like to thank the almighty for all the blessings poured on me.

Kalaivanan N.

Preface

Majority of the organic molecules are electronically neutral and possessing closed shell configurations have net spin zero, live in the ground state as singlet. Upon excitation, the excited organic molecules could have paired and unpaired electronic configuration leading to excited singlet and triplet states respectively. Generation of singlet excited state is spin allowed process whereas intersystem crossing which generates triplet excited state is spin forbidden. Excited singlet and triplet states can be well differentiated based on their photophysical properties. Longer lifetime (μs - ms) and paramagnetic nature of triplet excited states when compared to diamagnetic short-lived (ns - μs) singlet excited states make them to be used in various applications such as photocatalysis, bio-imaging, high performance solar cells and photovoltaics. But among the ocean of organic molecules, only handful of families such as organometallics, aromatic ketones, aromatic thiones, hetero-aromatics, and low molecular weight polyaromatic hydrocarbons possess inherent ability to access triplet excited state. It is very necessary to develop metal free organic phosphorescent/triplet active materials in different fields of applications. Perylenediimides (PDIs) are one among the versatile chromophoric systems that have been widely used in applications due to their remarkable photo, chemical and thermal stability. Reported methods to access triplet state of PDI in solution make use of bimolecular triplet sensitization, substitution with heteroatoms, charge transfer (CT) complex and heavy metals induced intersystem crossing (ISC). Slip-stacked arrangement in the polycrystalline thin film of 2,5,8,11-tetraphenyl PDI offers singlet exciton fission (SF) mediated triplet population. Designing of heavy atom free, PDI systems for efficient ISC is still burgeoning area of research. In this thesis, we have attempted different strategies to access the triplet excited state in PDIs through chemical and structural modifications.

The best approach to develop metal free phosphorescent material could be covalently attaching the heavier halogen atoms such as bromine and iodine. Heavy atoms promote intersystem crossing to access triplet excited state due to their spin orbit coupling. Studies have demonstrated that bromination could enhance the rate of intersystem crossing in organic molecules significantly. Unfortunately in the case of perylene family dyes, mono-bromination is not sufficient to enhance the intersystem crossing. We have attempted to sequentially substitute bromine atoms at the bay region of PDI to yield PDI-Br₀₋₄ in chapter 2. Crystal structures of PDI-Br₃₋₄ show the core-twisted nature of the derivatives, which perturbs the excitonic interaction in the crystalline state. Electrochemical analysis shows that the electron affinity of the PDIs is increased consecutively upon sequential bromination.

Basic photophysical measurements in toluene show characteristic PDI absorption and partially quenched fluorescence upon successive bromination. Nano and femtosecond transient absorption measurements show ultrafast intersystem crossing in core-twisted derivatives in toluene solution. The quantum yield of triplet generation in core-twisted perylenediimide calculated to be 5 and 18% in PDI-Br₃ and PDI-Br₄ respectively. Enhanced intersystem crossing in the core-twisted PDIs upon successive bromination is attributed to the energy gap reduction between the excited singlet and nearby triplet excited state. Slip-stacked arrangement of the PDI-Br₄ in the crystalline state could promote possibility of singlet fission (SF) mediated triplet generation. Nanosecond transient absorption measurements show enhanced triplet quantum yield of 105±5% in polycrystalline thin film of PDI-Br₄ upon excitation with 355 nm.

Structural deformation from coplanar to non-planar geometry in the molecules is considered to enhance nonradiative decay pathway such as intersystem crossing from singlet excited state. Twisting the perylenediimide molecule could lead to improved triplet generation arising from the non-planar geometry. It is uncertain to conclude that intersystem crossing observed in PDI-Br_{3,4}, discussed in chapter 2, is due to the presence of heavy atom effect or core-twisted nature of the derivatives. In order to deconvolute the heavy atom effect from core-twist, heavy atom free "twist-only" bearing PDI structures were designed.

In chapter 3 we discuss the synthesis, crystal structure and "twist-only" promoted intersystem crossing in the systematically twisted perylenediimide based chromophores. Designed contorted chromophores 1c and 2d were synthesised by Suzuki coupling of one and two phenanthrene units respectively with 1-bromo and 1,7-dibromo perylenediimide (PDI) followed by the metal catalysed Scholl dehydrocyclisation reaction. Planar model derivative 3c was synthesised by Suzuki coupling of two benzene with 1,7-dibromo PDI followed by Scholl reaction. Red fluorescent crystals of the derivatives 1c and 2d were obtained from the chloroform and toluene solution respectively. Repulsion between the hydrogens at the cove regions of the derivatives 1c and 2d twist the chromophores from planarity. The dihedral angle between the non-planar units in 1c and 2d is found to be 40-44°. Cyclic voltammogram analysis exhibits higher negative reduction potential when compared to the model derivative 3c, indicating the weaker electron acceptor strength of the derivatives 1c and 2d. UV-vis absorption and partially quenched fluorescence show the possibility of intersystem crossing in contorted chromophores. Nano and femtosecond transient absorption measurements show significant 10±1 and 30±2% of triplet generation in the contorted derivatives 1c and 2d respectively when compared to the negligible triplet

generation in the planar derivative 3c. Quantum chemical calculations indicate that out of plane C=C and C-H vibrations can allow efficient ISC driven by vibronic coupling.

Photoinduced electron transfer processes in electron donor (D) - acceptor (A) systems are widely studied to understand the charge transfer rates and efficiencies. Earlier investigations on multichromophoric systems had shown that the important recombination pathway of charge transfer ($D^{+\bullet}-A^{\bullet}$)* state consists of intersystem crossing to yield triplet excited state of the units. In chapter 4, we attempted to synthesise perylenediimide based donor-acceptor systems which can undergo efficient charge transfer followed by the generation of triplet excited state in PDI upon excitation. The photophysics of molecular dyads and triads consisting of perylenediimide (PDI) covalently connected to the donor anthracene (AN) or pyrene (PY) at the bay positions is presented in chapter 4. Desired dyads and triads were synthesised by performing Suzuki reaction of 1-bromo/1,7-dibromo PDI with 9-anthracenyl and 1-pyrenyl boronic acid. Density Functional Theory (DFT) calculations of the dyads (AN-PDI, PY-PDI) and triads (AN-PDI-AN, PY-PDI-PY) reveal a near-orthogonal geometry between the donor and acceptor units. UV-vis absorption spectra of the derivatives show summed absorption of donor and acceptor along with the ground state charge transfer band at the long wavelength region. Upon excitation of toluene solution at 375 nm, dyads and triads exhibit higher stokes' shifted (100-150 nm) emission spectra which is attributed to charge transfer emission. Charge transfer characteristics of the triads were further confirmed by Lippert-Mataga analysis and the solvent dependent excited state properties. Femtosecond and nanosecond transient absorption spectroscopic techniques were performed to understand the excited state properties of the triads (AN-PDI-AN and PY-PDI-PY).

Upon excitation with 355 nm, 10 ns laser pulse in non-polar solvent such as toluene, AN-PDI-AN yielded the triplet excited state localised on PDI ($\Phi_T = 40\%$) moiety ($AN-PDI^3-AN$)* having a lifetime of 500 ns. In a moderately polar solvent such as chloroform, an equilibrium between localised triplet state ($AN-PDI^3-AN$)* and long lived ($\tau_T = 5 \mu s$) charge transfer $^3(AN^{+\bullet}-PDI^{\bullet}-AN)^*$ is observed. But in more polar solvent such as N,N-dimethylformamide, long lived charge transfer $^3(AN^{+\bullet}-PDI^{\bullet}-AN)^*$ is the only species observed in the transient absorption measurement. The other triad PY-PDI-PY also exhibits same behaviour upon excitation with 355 nm. To further understand the kinetics of triplet formation, femtosecond transient absorption measurement was performed. Upon excitation with 400 nm, 110 fs laser, both the triads exhibit ultrafast ISC to generate triplet species in chloroform solution.

Contents

List of Figures	
List of Tables	
List of Schemes	
List of Abbreviations	
1. Triplet Excited State in Organic Chromophores	
1.1. Introduction.....	1
1.2. Singlet and triplet excited state.....	1
1.3. Jablonski diagram.....	4
1.4. Applications of triplet excited state.....	6
1.4.1. Higher performance solar cells.....	6
1.4.2. Phosphorescent bio-probes.....	8
1.4.3. Photodynamic therapy.....	9
1.4.4. Phosphorescent displays.....	9
1.5. Characterisation of triplet excited state.....	10
1.5.1. Electron paramagnetic resonance (EPR).....	10
1.5.2. Phosphorescence spectroscopy.....	12
1.5.3. Generation of singlet oxygen.....	13
1.5.4. Transient absorption spectroscopy.....	14
1.6. Triplet excited state in organic molecules.....	16
1.7. Perylenediimide dyes.....	21
1.7.1. Electrochemical properties.....	22
1.7.2. Optical properties.....	22
1.7.3. Applications of PDI.....	23
1.7.3.1. Non-fullerene acceptor in solar cells.....	23
1.7.3.2. Artificial photosynthesis.....	24
1.7.4. Disadvantages of PDI.....	25
1.7.5. Strategies reported in the literature.....	26
1.8. Objective of the thesis.....	26
2. Access to Triplet Excited State in Core-Twisted Perylenediimides	
2.1. Introduction.....	30
2.2. Synthesis, characterization and crystal structure of PDI-Br ₍₀₋₄₎	32
2.3. Results and discussions.....	36
2.3.1. Electrochemical studies.....	36
2.3.2. Photophysical studies in solution state.....	37
2.3.3. Transient absorption measurement in solution state.....	39
2.3.3.1. Femtosecond transient absorption spectroscopy.....	39
2.3.3.2. Nanosecond transient absorption spectroscopy.....	41

2.3.4. Optical properties of PDI-Br ₍₀₋₄₎ in polycrystalline thin film.....	43
2.3.5. Transient absorption measurement in polycrystalline thin film.....	46
2.3.6. Singlet exciton fission in polycrystalline thin film.....	47
2.4. Conclusions.....	50
2.5. Experimental section.....	51
2.5.1. Synthesis and characterisation.....	51
2.6. Appendix.....	53
3. Enhanced Intersystem Crossing in Core-Twisted Aromatics	
3.1. Introduction.....	62
3.2. Synthesis, characterisation and crystal structure of twisted aromatics.....	64
3.3. Results and discussions.....	69
3.3.1. Electrochemical studies.....	69
3.3.2. Photophysical characterisation in solution state.....	69
3.3.3. Transient absorption measurements.....	72
3.3.3.1. Nanosecond transient absorption measurements.....	72
3.3.3.2. Femtosecond transient absorption measurements.....	73
3.4. Conclusions.....	75
3.5. Experimental section.....	77
3.5.1. Synthesis and characterisation.....	77
3.6. Appendix.....	82
4. Charge-Transfer Facilitated Triplet Generation in Perylenediimide based Orthogonal Dyads and Triads	
4.1. Introduction.....	86
4.2. Synthesis and characterisation.....	89
4.3. Results and discussions.....	91
4.3.1. Structure optimisation.....	91
4.3.2. Electrochemical analysis.....	92
4.3.2.1. Rehm-Weller analysis.....	94
4.3.3. Photophysical properties of the dyads and triads.....	94
4.3.4. Characterisation of singlet excited charge transfer states.....	97
4.3.5. Charge recombination.....	100
4.3.6. Transient absorption spectroscopy.....	102
4.3.6.1. Nanosecond transient absorption spectroscopy.....	102
4.3.6.2. Femtosecond transient absorption spectroscopy.....	105
4.4. Conclusions.....	107
4.5. Experimental section.....	108
5. Bibliography	113
6. List of publications	127
7. Presentations at conferences	129
8. Copyrights and permission	131

List of Figures

Figure	Title	Page
1.1.	A) Ground state and B) excited state singlet and triplet in an orbital configuration scheme. The arrows indicate the electron spin.	2
1.2.	Vector diagram illustrating the relative orientations of the two electron spins for the singlet and the triplet excited states.	3
1.3.	Jablonski diagram showing possible transition in the molecule upon excitation.	4
1.4.	Functional mechanism of a bilayer organic solar cell upon excitation of the donor.	7
1.5.	A) Confocal luminescence images of fixed KB cells stained with phosphorescent and fluorescent under same excitation conditions (405 nm) with different laser scan times; B) decay profiles of fluorescent (channel 1) and phosphorescent (channel 2) images.	8
1.6.	A) Working principle of PDT; B) photophysical processes involved in the formation of reactive oxygen species.	9
1.7.	Induction of the spin state energies of triplet excited state as a function of the magnetic field B_0 ; arrows indicate the possible transition in the presence of external magnetic field.	11
1.8.	A) Jablonski diagram showing the difference between fluorescence and phosphorescence; B) comparison of absorption, fluorescence and phosphorescence spectra of chrysene.	12
1.9.	Jablonski diagram showing the triplet – triplet energy transfer process leading to the singlet oxygen (1O_2) population upon excitation.	14
1.10.	Jablonski diagram showing possible transient absorption of a molecule from the excited state.	16
1.11.	Examples of known organic phosphors; A) polyaromatic hydrocarbon along with fullerene C_{60} ; B) organometallic complexes Ir and Pt complexes; C) aromatic ketone, thione and heterocyclic aromatics.	18
1.12.	Rate of ISC of naphthalene upon substitution with halogen atoms.	19
1.13.	Energy level ordering of localised and charge transfer singlet and triplet excited states of donor-acceptor systems.	19
1.14.	Mechanism of singlet exciton fission.	20
1.15.	Chemical structure of perylene and its derivative explored during different time period.	22
1.16.	A) Absorption and emission spectra of un-substituted PDI in toluene; B) frontier molecular orbitals HOMO and LUMO calculated from B3LYP/6-31++G**.	23
1.17.	Molecular structure of PDI based polymer and corresponding I-V plot obtained for the polymer bulk heterojunction solar cell.	24
1.18.	A) Model for the columnar PDI aggregates; B) self-assembled artificial photosynthetic system based PDI chromophore	25
2.1.	Crystal packing of the derivatives PDI-Br ₂₋₄ . A), B) and C) side view of the	36

	dimers in PDI-Br ₂ , PDI-Br ₃ and PDI-Br ₄ respectively; D), E) and F) corresponding top view.	
2.2.	A) Cyclic voltammogram and B) tabulation of the first and second reduction potential of the derivatives PDI-Br ₀₋₄ in dichloromethane.	37
2.3.	A) Absorption; B) emission ($\lambda_{ex} = 480$ nm) and C) time-dependent fluorescence studies ($\lambda_{ex} = 480$ nm and monitored at their emission maxima) of the derivatives PDI-Br ₀₋₄ in toluene.	38
2.4.	A), B), C), D) and E) fTA spectra of the derivatives PDI, PDI-Br, PDI-Br ₂ , PDI-Br ₃ and PDI-Br ₄ respectively; F), G), H), I) and K) corresponding decay associated difference spectra obtained from SVD analysis.	40
2.5.	nTA spectra of PDI-Br ₄ in toluene upon excitation with 532 nm laser; Inset shows the kinetics of bleach recovery and triplet decay monitored at respective wavelength.	42
2.6.	A) Powder XRD pattern of polycrystalline thin film of PDI-Br ₄ along with the stimulated P-XRD pattern obtained from single crystal; B) profilometric traces of PDI-Br ₄ polycrystalline thin film (thickness is 60±10 nm).	44
2.7.	A) Absorption and B) emission ($\lambda_{ex} = 480$ nm) spectra of the derivative PDI-Br ₀₋₄ in polycrystalline thin film state.	45
2.8.	A) nTA spectra of PDI-Br ₄ in polycrystalline thin film upon excitation at 532 nm; B) corresponding kinetics profile of the triplet decay monitored at 600 nm.	47
2.9.	A) calculated singlet and triplet energy levels (ISC- intersystem crossing; SF- singlet fission); B) triplet state decay kinetics of PDI-Br ₄ in polycrystalline thin film monitored at 600 nm upon excitation with 355 and 532 nm.	48
2.10.	Plausible Jablonski diagram of PDI-Br ₄ in monomer and polycrystalline thin film; energy levels are calculated from TDDFT (B3LYP/6-311G++(d,p) method. (IC - internal conversion; ISC - intersystem crossing; SF - singlet fission; Φ_F - fluorescence quantum yield; Φ_T - triplet quantum yield).	49
3.1.	A) and C) crystal structure of the core-twisted derivatives 1c and 2d; B) and D) corresponding side view.	68
3.2.	Energy optimized twisted and wagging conformation of the derivative 2d along with the corresponding crystal structure.	68
3.3.	A) Cyclic voltammogram analysis of the derivatives 1c, 2d and 3c in dichloromethane; B) FMO analysis obtained from the TD-DFT calculations.	70
3.4.	A) Absorption; B) emission spectra ($\lambda_{ex} = 480$ nm); C) time dependent emission spectra ($\lambda_{ex} = 480$ nm and monitored at their emission maxima) of the derivatives 1c, 2d and 3c in toluene.	71
3.5.	Temperature dependent A) emission ($\lambda_{ex} = 480$ nm) and B) excitation spectra ($\lambda_{em} = 600$ nm) of the derivative 1b in toluene.	71
3.6.	A) and C) nTA spectra of the core-twisted derivatives 1c and 2d respectively; B) and D) kinetics profile of the transient species (triplet decay and bleach recovery) in the derivatives 1c and 2d respectively in toluene upon excitation with 355 nm, 10 ns laser pulse.	72
3.7.	A) and C) fTA spectra of the core-twisted derivatives 1c and 2d respectively; B) and D) kinetics profile of the transient species (triplet and singlet decay) in the	74

	derivatives 1c and 2d respectively in toluene upon excitation with 300 nm, 110 fs laser pulse.	
3.8.	A), B) and C) out-of-plane mode C-H vibration; D), E) and F) out-of-plane mode C=C vibration in the derivatives 1c, 2d and 3c respectively (obtained from DFT calculation, Gaussian 09).	76
4.1.	An energy level diagram for the donor-acceptor (D-A) dyads illustrates the different photoinduced processes that occur in these molecules. The triplet state that is reached through RP-ISC can be localized on either the donor or the acceptor.	87
4.2.	A) Electrochemical analysis of the triads in dichloromethane along with PDI; B) frontier molecular orbital diagram of the triads calculated from DFT calculations.	93
4.3.	Steady-state absorption spectra of A) dyads and B) triads along with PDI in toluene; normalised steady state fluorescence spectra of C) dyads and D) triads along with PDI ($\lambda_{ex} = 350$ nm) in toluene.	95
4.4.	A) Solvent dependent fluorescence spectra of the triad AN-PDI-AN upon excitation with 350 nm; B) corresponding Lippert-Mataga plot.	98
4.5.	Time resolved fluorescence emission profile of the triad AN-PDI-AN in toluene, chloroform and DMF upon excitation with 375 nm.	99
4.6.	Steady state CW-EPR spectra of A) and B) AN-PDI-AN in the absence and presence of light of excitation at 77 K; C) and D) PY-PDI-PY in the absence and presence of light of excitation at 77 K.	102
4.7.	nTA spectra of the derivative PY-PDI-PY in A) toluene; B) chloroform and C) DMF upon excitation with 355 nm, 10 ns pulse. D), E) and F) corresponding SVD analysis.	103
4.8.	Model energy level diagrams for the excited states of dyads and triads in toluene, chloroform and DMF.	104
4.9.	fTA spectra of the triads A) AN-PDI-AN and B) PY-PDI-PY in chloroform upon excitation with 400 nm laser; insets show the spectra obtained from the corresponding SVD analysis.	106

List of Tables

Table	Title	Page
2.1.	Crystallographic data and refinement parameters for the derivatives PDI-Br ₂₋₄ .	33
2.2.	Photophysical properties of derivatives PDI-Br ₀₋₄ in toluene solution.	38
2.3.	Photophysical properties of derivatives PDI-Br ₀₋₄ in polycrystalline thin film.	45
3.1.	Single crystal analysis parameter of the derivatives 1c and 2d.	67
4.1.	Electrochemical properties of the derivatives along with the model derivatives in dichloromethane; HOMO and LUMO energy levels obtained from DFT calculations.	92
4.2.	Photophysical properties of the dyads and triads along with PDI in toluene.	96

List of Schemes

Scheme	Title	Page
2.1.	A) Chemical structure of PDI, thionated PDI and Pt-PDI complex; B) energy level diagram for singlet exciton fission between two interacting chromophores 1 and 2; C) schematic of singlet fission in polycrystalline thin film of slip-stacked PDI	30
2.2.	Synthesis scheme for PDI-Br _{0.4} .	34
2.3.	Molecular structures of the derivatives under study.	35
3.1.	Molecular structure of non-planar chromophores studied for efficient ISC along with the carbon allotropes graphene and fullerene C ₆₀ ; efficiency and the rate of ISC are mentioned in the scheme.	63
3.2.	Molecular structure the core-twisted derivative 1c and 2d along with the model derivative 3c; arrows indicate cove and bay regions in the derivatives.	64
3.3.	Synthesis of the core-twisted derivatives 1c, 2d and the model derivative 3c.	66
4.1.	Molecular structures of the PDI based D-A dyad and D-A-D triad.	89
4.2.	Syntheses scheme for the PDI based dyads and triads.	90
4.3.	Optimised geometries of the dyads and triads obtained using B3LYP/6-311G (d,p) level of theory; θ show the dihedral angle between the donor and acceptor units; imide alkyl chain is omitted for the clarity.	91
4.4.	Basic ISC mechanism from singlet excited CT state.	100

List of Abbreviations

PDI	Perylenediimide
SF	Singlet fission
OLED	Organic light emitting diode
IC	Internal conversion
ISC	Intersystem crossing
EPR	Electron paramagnetic resonance
fTA	Femtosecond transient absorption
nTA	Nanosecond transient absorption
CT	Charge transfer
HOMO	Highest occupied molecular orbital
LUMO	Lowest unoccupied molecular orbital
TD-DFT	Time dependent density functional theory
SOC	Spin orbit coupling
DCM	Dichloromethane
NMR	Nuclear magnetic resonance
IR	Infrared
m. p.	Melting point

Chapter 1

Triplet Excited State in Organic Chromophores

1.1. Introduction

The current achievements of modern material chemistry are implausible without the contribution of organic compounds which are cheap, environmentally safer and flexible for modulation when compared to their inorganic counterparts[1-3]. Enhanced performance of organic fluorescent materials have attracted immense attention in the field of biological imaging, display, lighting systems (such as OLEDs and LCDs) and as for other functional applications[4]. On the otherhand, organic phosphorescent materials have not witnessed same level of achievements as organic fluorescent materials[5]. Understanding the difference between fluorescence and phosphorescence requires the knowledge of electron spin and spin states in the molecules[6].

1.2. Singlet and triplet excited state

Electrons in the atoms revolve around the nucleus with the spin quantum number (s) of $\pm 1/2$. Based on the outer shell electronic configuration, spin states of the atom/molecule are defined by using the formula $2S+1$ where S is total spin quantum number which is equal to $\sum(s_1+s_2+s_3+\dots)$. For example, the spin state of the molecules with a single unpaired electron ($S= 1/2$), doubly paired electrons ($S=0$) and doubly unpaired electrons ($S=1$) are defined as doublet, singlet and triplet

respectively (Figure 1.1A). Based on the Pauli exclusion principle, two electrons in an orbital cannot have the same spin quantum number. So, encountering molecules which live in the triplet spin state is very sparse. However, oxygen lives in the ground state as triplet due to the presence of two unpaired electrons in the degenerate molecular orbitals. Radicals are another class of molecules which can also possess the triplet spin in the ground state.

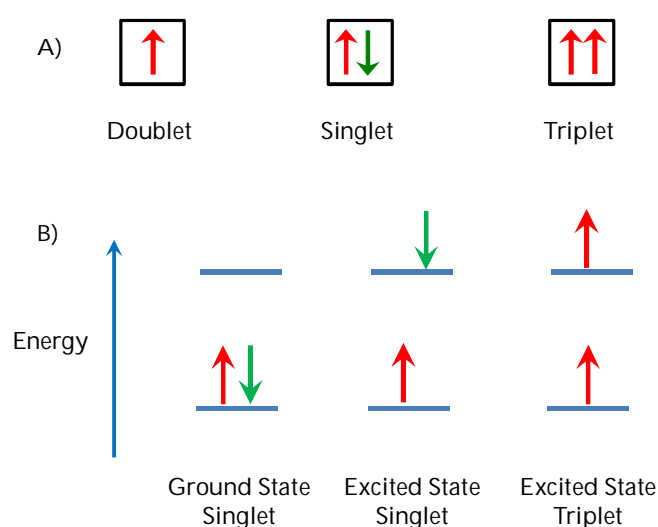


Figure 1.1. A) Ground state and B) excited state singlet and triplet in an orbital configuration scheme. The arrows indicate the electron spin.

Majority of the electronically neutral organic molecules possessing closed shell (paired) configuration have net spin zero, live in the ground state as singlet. Upon excitation, the excited organic molecules could have either paired or unpaired electronic configuration leading to excited singlet and triplet states respectively (Figure 1.1B). Whether an excited molecule is in a spin singlet or triplet state depends only on the relative spin orientation of the excited and ground state electron[7]. Thus, as the spin projection of the electron in the ground state does not

change during the transition, α and β notation for the excited electron spin projection directly corresponds to spin singlet and triplet states of the molecule respectively. The two spins, indicated by arrows, precess around a local magnetic field in z-direction (Figure 1.2)[8]. The anti-parallel and 180° out of phase configuration corresponds to the situation in a singlet state ($S=0$), while the other

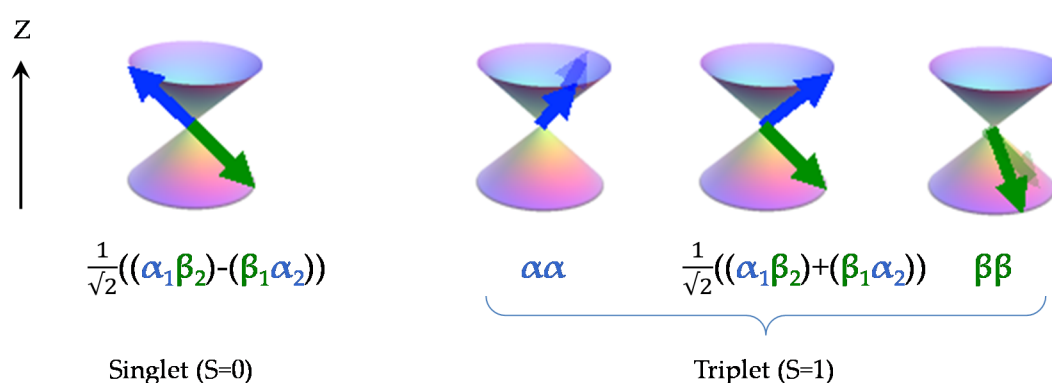


Figure 1.2. Vector diagram illustrating the relative orientations of the two electron spins for the singlet and the triplet excited states.

three in phase configurations yield a triplet state ($S=1$). For the singlet excited state, the total wave function is given as,[9]

$$\Psi_s = \left[\frac{1}{\sqrt{2}} (\varphi_\alpha(1)\varphi_\beta(2) + \varphi_\beta(1)\varphi_\alpha(2)) \right] \left[\frac{1}{\sqrt{2}} (\alpha_1\beta_2 - \beta_1\alpha_2) \right]; M_s=0 \quad \text{----(1.1)}$$

While for the triplet excited state, the possible total wave functions are given as follows,

$$\Psi_T = \left[\frac{1}{\sqrt{2}} (\varphi_\alpha(1)\varphi_\beta(2) - \varphi_\beta(1)\varphi_\alpha(2)) \right] \left[\frac{1}{\sqrt{2}} (\alpha_1\alpha_2) \right]; M_s=1 \quad \text{----(1.2)}$$

$$\Psi_T = \left[\frac{1}{\sqrt{2}} (\varphi_\alpha(1)\varphi_\beta(2) - \varphi_\beta(1)\varphi_\alpha(2)) \right] \left[\frac{1}{\sqrt{2}} (\alpha_1\beta_2 + \beta_1\alpha_2) \right]; M_s=0 \quad \text{----(1.3)}$$

$$\Psi_T = \left[\frac{1}{\sqrt{2}} (\varphi_\alpha(1)\varphi_\beta(2) - \varphi_\beta(1)\varphi_\alpha(2)) \right] \left[\frac{1}{\sqrt{2}} (\beta_1\beta_2) \right]; M_s=-1 \quad \text{----(1.4)}$$

Where φ is spatial function; α and β are spin function; M_s is total spin

The difference between a molecule in the singlet and triplet state is that the molecule is diamagnetic in the singlet state and paramagnetic in the triplet state[10]. This difference in spin state makes the transition from singlet to triplet (or triplet to singlet) more improbable than the singlet to singlet (or triplet to triplet) transitions. Singlet to triplet (or reverse) transition involves a change in spin state, which is forbidden based on the selection rules[11]. The transition between the different spin multiplicities can be explained by a Jablonski diagram (Figure 1.3)[12].

1.3. Jablonski diagram

The Jablonski diagram is a partial energy diagram that represents the energy of molecule in its different energy states (Figure 1.3). The lowest and darkest horizontal line represents the ground-state electronic energy of the molecule which is the singlet state (S_0), majority of the molecules in a solution are in this state at room

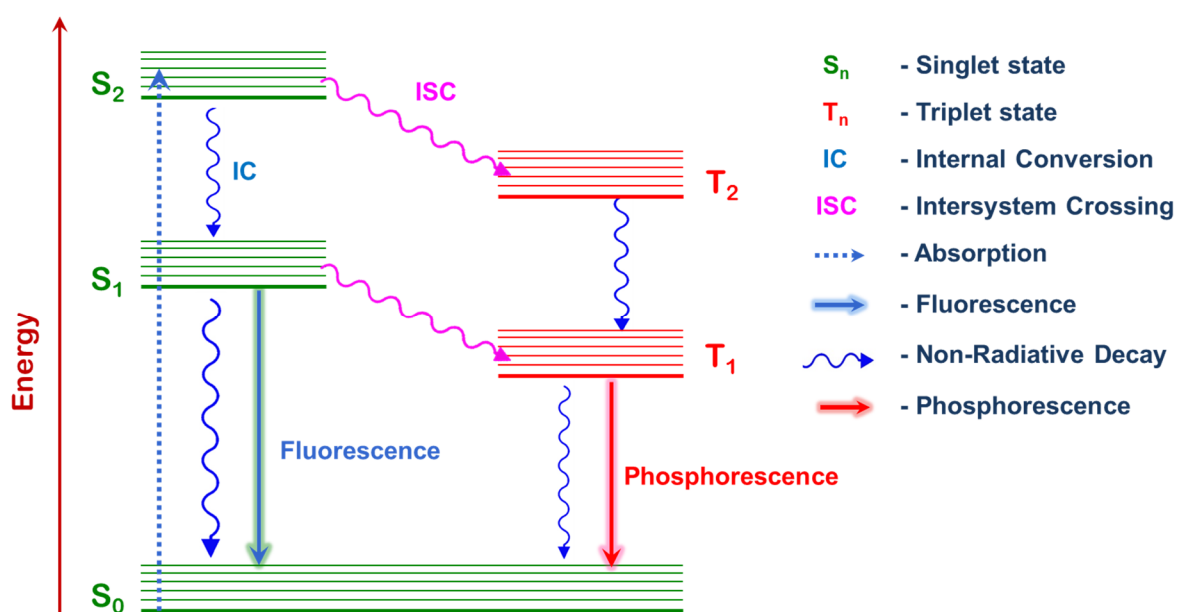


Figure 1. 3. Jablonski diagram showing possible transition in the molecule upon excitation.

temperature. The upper lines represent the excited electronic states: S_1 and S_2 represent the electronic singlet state; T_1 and T_2 represent the electronic triplet state. There are numerous vibrational levels that can be associated with each electronic state as denoted by the thinner lines. Upon excitation, instantaneous transition (absorption) can occur from the ground state (S_0) to various vibrational levels in the singlet excited states (S_n) generating strongly bound electron-hole pair, so called exciton. Transition from S_0 to the triplet electronic state (T_n) is forbidden because of the different spin multiplicity between the two states (spin forbidden). The excited molecule can undergo various deactivation processes to relax back to the ground state.

Internal Conversion (IC): Internal conversion is a spin allowed non-radiative process of molecule that passes to a lower electronic state from higher excited state. It is a crossover of two states with the same multiplicity meaning singlet-to-singlet or triplet-to-triplet states. This process happens in the time scale of 10^{-14} to 10^{-11} s.

Fluorescence: Spin allowed radiative transition from higher singlet excited state to lower singlet excited state or ground state is called fluorescence. Most of the organic molecules fluoresce from the lower singlet excited state (S_1) to ground state (S_0) which phenomenon is governed by the Kasha's rule. Fluorescence occurs in the time scale of 10^{-9} to 10^{-7} s.

Intersystem Crossing (ISC): Intersystem crossing is a process where there is a crossover between electronic states of different multiplicity ($S_n \rightarrow T_n$) as demonstrated

in the Figure 1.3. Due to the spin forbidden nature of ISC, it occurs with time scale of 10^{-11} to 10^{-6} s. Spin-orbit coupling (interaction of spin and orbital motion of the electron) enhances the probability of ISC.

Phosphorescence: After ISC to the triplet excited state, further deactivation can occur through forbidden radiative or non-radiative transition to the ground state. The radiative transition from $T_n \rightarrow S_n$ is called phosphorescence while the non-radiative decay is known as reverse intersystem crossing (RISC). Owing to the forbidden nature of such transition, triplet excited state lives for longer lifetime when compared to the singlet excited states. Hence, phosphorescence happens at a timescale of 10^{-6} to 10^2 s which is longer compared to the spin allowed transitions.

1.4. Applications of triplet excited state

While fluorescent singlet state has been investigated intensively for diverse applications, the recent development of organic triplet active materials is a research goal that continues to attract growing interest over fluorescent molecules for various applications owing to higher lifetime, slow emission and paramagnetic nature[13]. Following are the few examples where the importance of triplet over singlet excited state is well established.

1.4.1. High performance solar cells

Solar cell is a device that converts light energy into electricity by the photovoltaic effect. The efficiency of the device is estimated from the efficiency of

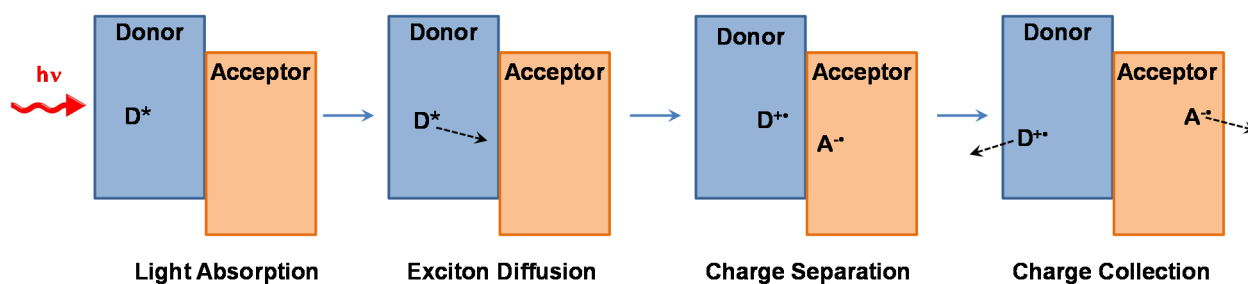


Figure 1. 4. Functional mechanism of a bilayer organic solar cell upon excitation of the donor.

the following sequential processes[14]. 1) light absorption; 2) exciton diffusion; 3) charge separation and 4) charge collection (Figure 1.4). Among the four processes, exciton diffusion and charge collection efficiencies depend on the lifetime of the exciton generated.

$$L_D = \sqrt{D\tau} \quad \text{--- (1.5)}$$

where, L_D is exciton diffusion length (cm); D is exciton diffusion co-efficient (cm^2/s) and τ is lifetime of exciton (s). By virtue of longer lifetime, triplet excitons can diffuse significantly longer distance when compared to the singlet excitons which has comparatively shorter lifetime[15]. Thus utilising triplet active material in the solar cells can boost the efficiency of the device significantly, which have been proven in multi-junction organic solar cells[14]. Most of the solar cells utilise the singlet exciton over triplet exciton, due to the fact that the triplet excitons could be trapped by the singlet oxygen which will reduce the efficiency of the solar cell. However, the enhancement due to the longer exciton diffusion of triplet exciton and oxygen free processing of the solar cells will easily overcome the drawback.

1.4.2. Phosphorescent bio-probes

With the rapid development of life science and pathology, research on intracellular active species, cell signal transduction, and apoptosis by fluorescence microscopy imaging has become an important and active field. For biological samples, the target fluorescent signal often suffers from interference with background fluorescence, reducing the target-to-background ratio. An effective strategy to address this problem is to utilize a time-gated technique, which requires long-lived phosphorescence as the target signal and can effectively eliminate the interference from short-lived background fluorescence[16]. This phenomenon is to be successful in the imaging of living cells by using water soluble phosphorescent dyes (Figure 1.5)[17].

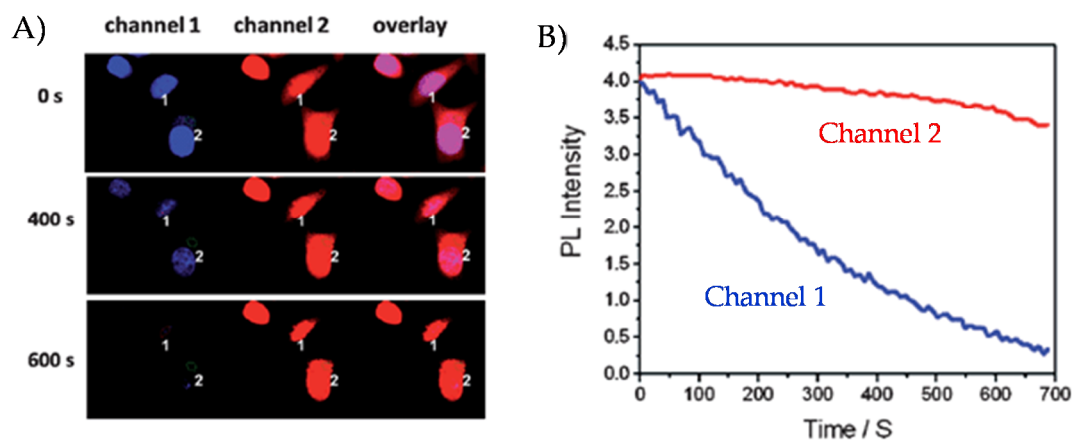


Figure 1. 5. A) Confocal luminescence images of fixed KB cells stained with phosphorescent and fluorescent under same excitation conditions (405 nm) with different laser scan times; B) decay profiles of fluorescent (channel 1) and phosphorescent (channel 2), images (Adapted with permission from ref. 17. Copyright © 2011, Royal Society of Chemistry).

1.4.3. Photodynamic therapy

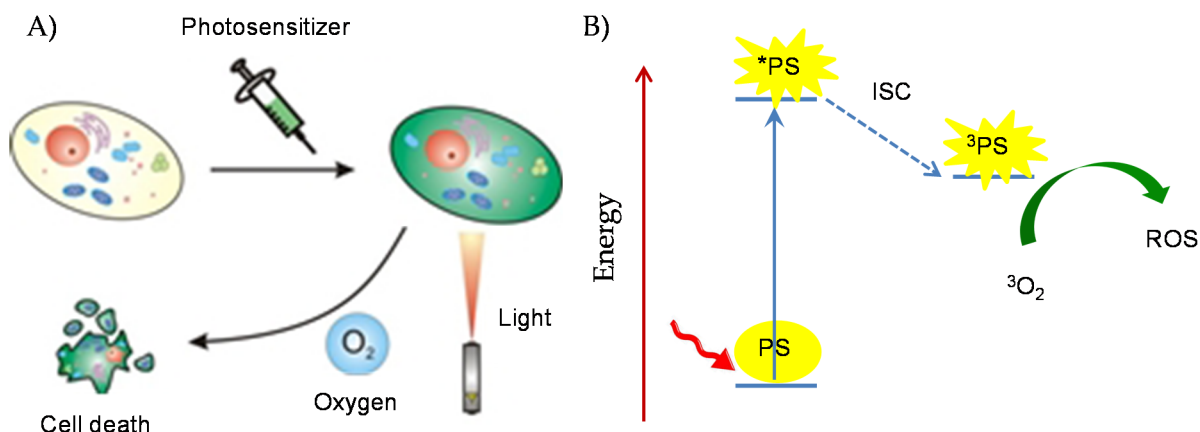


Figure 1. 6. A) Working principle of PDT; B) photophysical processes involved in the formation of reactive oxygen species.

Photodynamic therapy (PDT) is a treatment (Figure 1.6A) that uses photosensitizing agents as drug, along with light to kill cancer cells. PDT employs the photophysical properties of the activated photosensitizer (triplet state), resulting in the production of reactive oxygen species (Figure 1.6B). Upon irradiation with the specific wavelength, the photosensitizing agent can access the triplet excited state which is followed by triplet – triplet energy transfer to generate the reactive oxygen species (ROS)[18].

1.4.4. Phosphorescent displays

Phosphorescent organic light-emitting diodes (PHOLEDs) are now a key part of today's display industry and are also poised to transform solid-state lighting[19]. PHOLEDs use the principle of electro-phosphorescence to convert electrical energy into light in a highly efficient manner with the internal quantum efficiencies of such devices approaching 100%[20]. Due to their potentially high level of energy

efficiency, PHOLEDs are being preferred over other OLEDs for potential use in large-screen displays such as computer monitors or television screens, as well as general lighting needs.

Moreover, organic triplet active materials have received immense attention in the fields of photo-catalysis, triplet-triplet up-conversion and photo-redox reactions. Thus, design and synthesis of long lived triplet active organic molecules is a burgeoning area of research.

1.5. Characterisation of triplet excited state

It is highly essential to have a good understanding of detection techniques to identify the presence of triplet excited state. Triplet excited states can be characterized by following their magnetic, photophysical and photochemical properties.

1.5.1. Electron paramagnetic resonance (EPR)

Systems with $S > 0$ will experience a quantization of spin states when placed in an applied magnetic field and exhibit discrete spin states according to the multiplicity rule $2S + 1$ [21]. When two unpaired electrons are present in a system, the spin state depends upon the alignment of the two electrons as shown in Figure 1.7. If the unpaired electrons are aligned antiparallel, the multiplicity is a singlet ($S=0$), diamagnetic in nature, hence no EPR transition is observed. When the spins are aligned parallel ($S = 1$), in the presence of external magnetic field, system can exhibit three spin states, with spin quantum numbers (M_s) equal to -1, 0 and 1 (Figure 1.7).

The interaction between the spin and the field is described by the Zeeman effect; the energy separation between the spin states increases with the increase of the applied magnetic field according to the expression,

$$E = M_s g_e \mu_B B_0 \quad \text{---(1.6)}$$

$$\Delta E = g_e \mu_B B_0 \quad \text{---(1.7)}$$

where, M_s is spin quantum number; g_e is electronic g factor ($g_e=2.0023$ for free electron); μ_B is Bohr magneton and B_0 is the strength of the applied magnetic field. According to the $\Delta M_s = \pm 1$ selection rule, there are two allowed transitions for triplet excited state in the external magnetic field. The energy separation between the spin states increases with the increase of the applied magnetic field according to the equation 1.7. Thus, electron paramagnetic resonance is the most powerful technique to establish the presence of molecule in its triplet excited state[10].

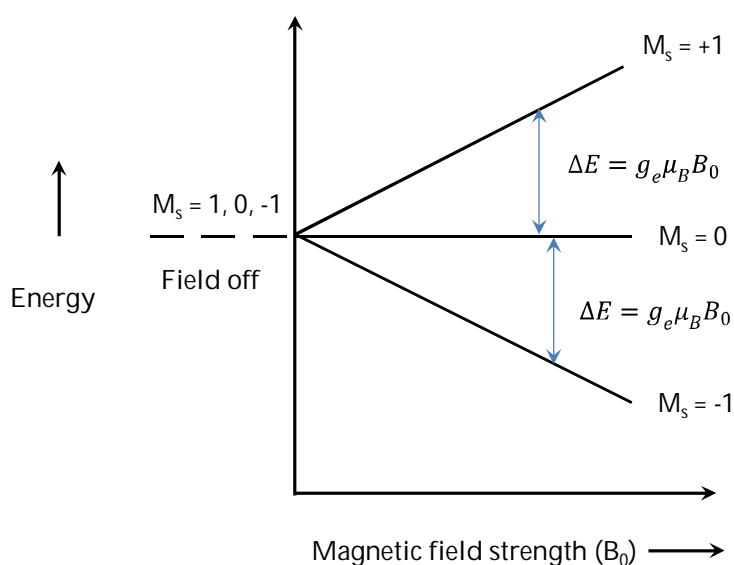


Figure 1. 7. Induction of the spin state energies of triplet excited state as a function of the magnetic field B_0 ; arrows indicate the possible transition in the presence of external magnetic field.

1.5.2. Phosphorescence spectroscopy

Upon excitation to singlet excited state followed by ISC, the molecule can return to the ground state by emission of radiation and this T_1 to S_0 transition is called phosphorescence (Figure 1.8A). As discussed earlier, phosphorescence has long life-time which can vary from 10^{-6} to 10^2 s, depending upon the structure of the molecule. Phosphorescence emission spectra occur at longer wavelengths than fluorescence emission spectra because of the loss in energy which occurs during ISC from the singlet to triplet state (Figure 1.8B)[12]. Because of the long life-times, the molecule has a very high probability of losing its excess energy by non-radiative routes such as internal conversion, bimolecular collision, and photodecompositions. As a result, phosphorescence is not routinely observed in solutions at room temperature. Quenching of the triplet state by oxygen is also effective in preventing phosphorescence, and thorough degassing of the solution is required before

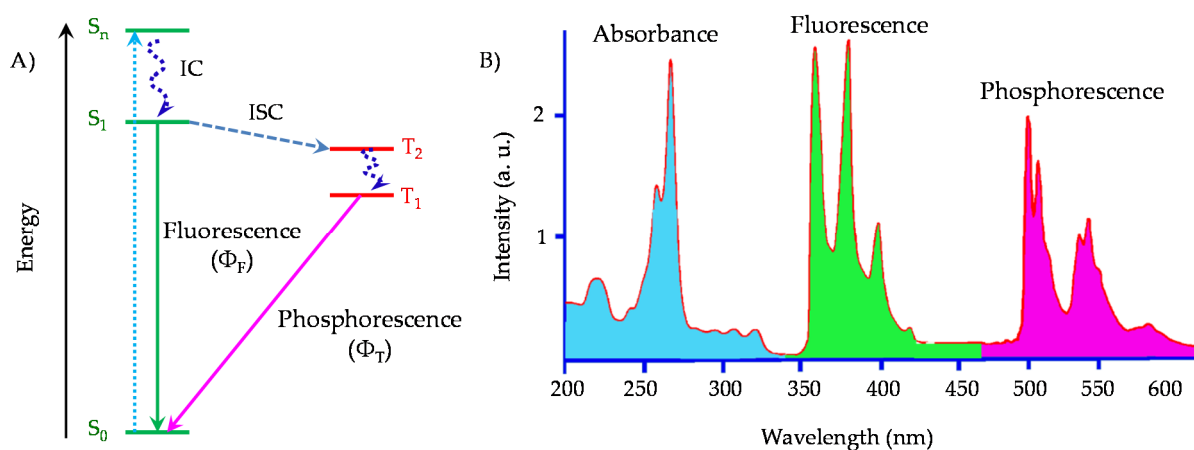


Figure 1. 8. A) Jablonski diagram showing the difference between fluorescence and phosphorescence; B) comparison of absorption, fluorescence and phosphorescence spectra of chrysene.

measurement. Several methods have been used to enable the observation of phosphorescence, in other words, to restrict collisional deactivation. One of the most common techniques is to supercool solutions to a rigid glass state usually at the temperature of liquid nitrogen (77 K). Phosphorescence can also be observed by inserting the analyte into a rigid polymer matrix, although the area of applications is limited. Recent developments have shown that, under certain circumstances, the phosphorescence of polyaromatic hydrocarbons adsorbed on a variety of supports can be observed at room temperature. Amongst these advances, the most important feature is the internal or external addition of heavy atoms improves the efficiency of ISC which enhances the sensitivity of the technique.

1.5.3. Generation of singlet oxygen

Singlet oxygen is the common name of an electronically excited state of molecular oxygen which is less stable than molecular oxygen in the electronic ground state. It is typically generated via energy transfer from the excited state of a photosensitizer to the oxygen molecule (Figure 1.9)[22]. As we discussed in the section 1.4.3, the ability of a molecule to generate singlet oxygen is an evidence for the presence of triplet excited state. Upon illumination, analyte is excited to the excited singlet state (S_1), which crosses to the lower triplet excited state (T_1) via ISC. The excited triplet state can then convert triplet oxygen (3O_2) into singlet oxygen (1O_2) through triplet – triplet energy transfer. The emission at 1270 nm provides a convenient tool to characterize the singlet oxygen in the $^1\Delta_g$ state. The next higher

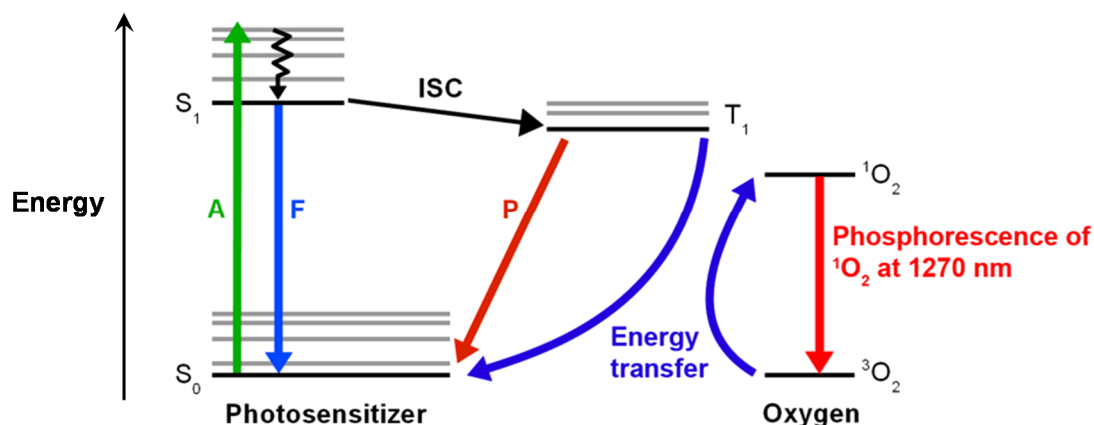


Figure 1. 9. Jablonski diagram showing the triplet – triplet energy transfer process leading to the singlet oxygen (1O_2) population upon excitation.

electronic state is the $^1\Sigma_g$, 37.5 kcal/mol or 13121 cm^{-1} above the ground state. It emits weakly by decay to both the $^1\Delta_g$ state and the ground state.

1.5.4. Transient absorption spectroscopy

Transient absorption spectroscopy helps to study the mechanistic and kinetic details of photophysical processes occurring on the time scales of sub picoseconds to femto seconds (Figure 1.10)[23]. These photophysical events are initiated by an ultrafast laser pulse and are further probed by a probe pulse. With the help of TA measurements, one can look into the relaxation processes of higher electronic states (~femtoseconds), vibrational relaxations (~picoseconds) and intersystem crossing of excited singlet state to triplet excited state (occurs on nanoseconds time scale).

Transient absorption spectroscopy can be used to trace the intermediate states in a photo-chemical reaction; energy, electron transfer process; conformational changes, thermal relaxation, fluorescence or phosphorescence processes, optical gain

spectroscopy of semiconductor laser materials, etc. With the availability of UV-Vis-NIR ultrafast lasers, one can selectively excite a portion of any large molecule to the desired excited states to study the specific molecular dynamics.

In a typical experimental set up, a pump pulse excites the sample and later, a delayed probe pulse strikes the sample. In order to maintain the maximum spectral distribution, two pulses are derived from the same source. The impact of the probe pulse on the sample is recorded and analysed with wavelength/ time to study the dynamics of the excited state. Transient absorption (ΔA or $\Delta O. D.$) records any change in the absorption spectrum as a function of time and wavelength which is, calculated as follows,

$$\text{Transient absorption} = \text{Absorption after probe} - \text{Absorption after pump}$$

Steady state absorption or ground state bleach: Bleaching of ground state refers to depletion of the ground state carriers to excited states ($S_0 \rightarrow S_n$) upon excitation with pump pulse. It is shown by the negative absorption in the transient spectrum.

Transient absorption: Excited electrons are further excited to higher excited states by the probe light (white light). Transient absorption ($S_1 \rightarrow S_n; T_1 \rightarrow T_n$) exhibits positive absorption in the spectrum.

Stimulated emission: Excited species is stimulated to emit light by the probe which follows the fluorescence and /or phosphorescence spectra of the molecule ($S_1 \rightarrow S_0; T_1 \rightarrow S_0$). Stimulated emission shows negative absorption in the transient spectrum.

Depending on the pulse width of the excitation pulse transient absorption

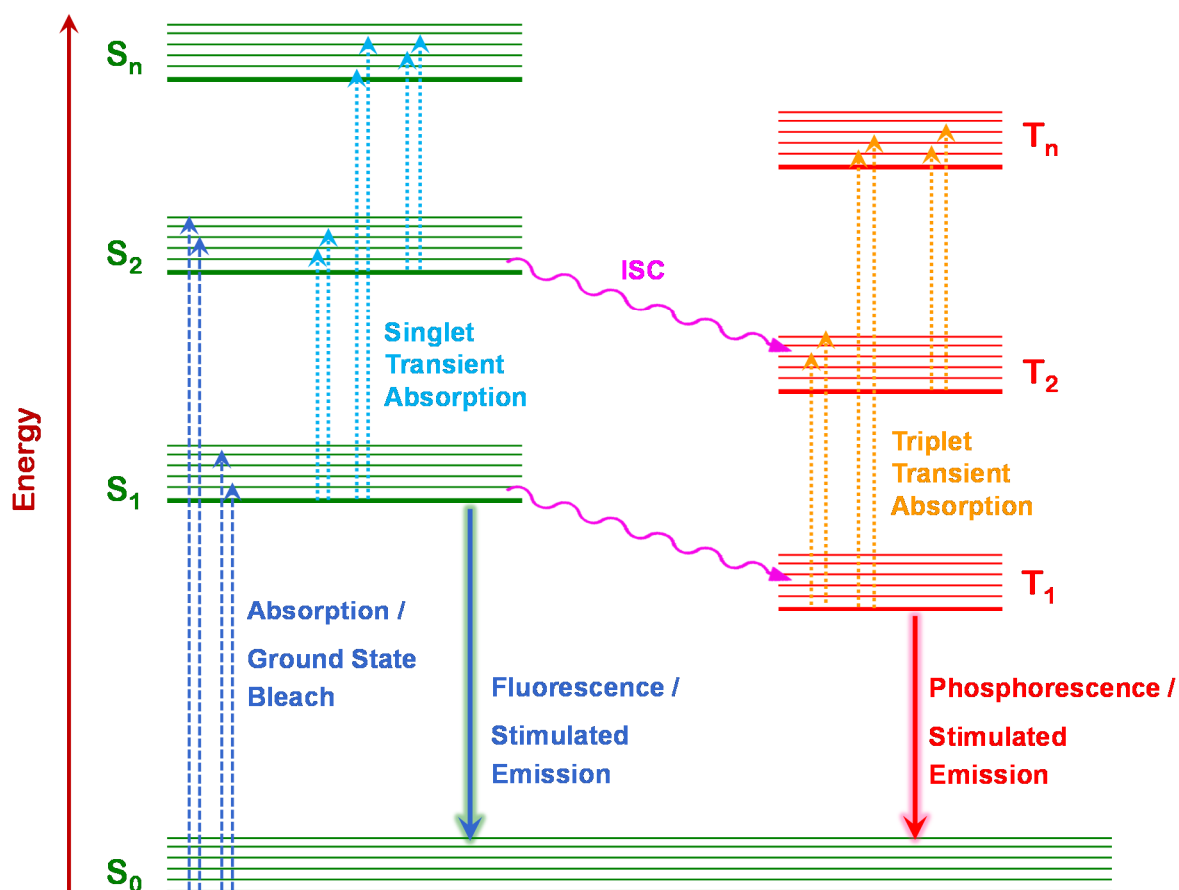


Figure 1. 10. Jablonski diagram showing possible transient absorption of a molecule from the excited state.

spectroscopy is named as 1) attosecond (10^{-18} s); 2) femtosecond (10^{-15} s); 3) picosecond (10^{-12} s) and 4) nanosecond (10^{-9} s) transient absorption spectroscopy. In this thesis, femtosecond and nanosecond spectroscopic techniques are used to characterise and study the excited state properties of various chromophores.

1.6. Triplet excited state in organic molecules

Population of the triplet excited state in the molecule requires a non-radiative transition between two different spin states ($S_n \rightarrow T_n$). Energy and the total angular momentum (orbital and spin) have to be conserved during the transition. The most important interaction that couples two spin states and that provides a means of

conserving the total angular momentum is the coupling of the electron spin with the orbital angular momentum, *i.e.*, the spin-orbit coupling (SOC). In the ocean of organic molecules reported, only handful of molecules has sufficient SOC to exhibit ISC. For example, polyaromatic hydrocarbons such as naphthalene, anthracene, pyrene and chrysene etc.[7] show efficient ISC to populate triplet excited state (Figure 1.11A). Series of reports demonstrates that the ISC properties of organic molecules could be enhanced by introducing various functional groups and atoms as listed below[5].

Chromophores with low-lying $n\text{-}\pi^*$ transitions: Ketones, thiones, and heterocyclic aromatic compounds (Figure 1.11C) are found to show nearly quantitative triplet generation upon excitation. These family of molecules undergo rapid ISC from $n \rightarrow \pi^*$ singlet excited state to an energetically close $\pi \rightarrow \pi^*$ triplet state. According to El-Sayed's selection rule, angular momentum is conserved during the transition, $S_1(n, \pi^*) \rightarrow T_1(\pi, \pi^*)$, hence the transition is allowed[8].

Heavy atom effect: The enhancement of the rate of a spin-forbidden process by the presence of an atom of high atomic number, which is either part of or external to the excited molecular entity, is defined as heavy atom effect. Heavy atom effect is a nuclear-charge effect and scales with Z^4 (Z is the nuclear charge). Heavier nucleus can induce strong SOC as a result, efficiency of ISC is enhanced[24].

Organometallic complexes: Organometallic complexes are the most popular organic phosphors being used currently though they are not purely organic in nature. These

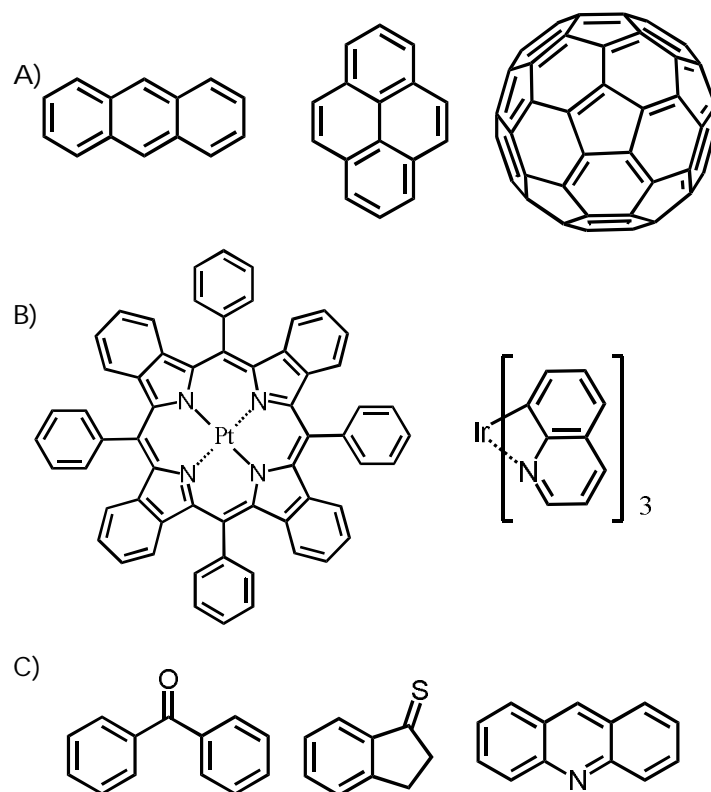


Figure 1. 11. Examples of known organic phosphors; A) polyaromatic hydrocarbon along with fullerene C₆₀; B) organometallic complexes Ir and Pt complexes; C) aromatic ketone, thione and heterocyclic aromatics.

complexes are phosphorescent because of the large metal atom such as Ir, Pt, Ru, Os, Re and Rh etc., which promote SOC (Figure 1.11B). But incorporating precious metals into organic ligands enhances the cost and reduces the flexibility of the material and limit the application.

Halogen substitution: Unlike organometallic complexes, halogen substituted organic molecules are purely organic in nature. Substitution with heavier halogen atoms such as bromine and iodine enhances the SOC of organic molecules significantly. For example ISC properties of naphthalene are enhanced significantly upon substitution with heavier halogen atoms (Figure 1.12)[7].

Molecule	<chem>c1ccc2ccccc2c1</chem>	<chem>Fc1ccc2ccccc2c1</chem>	<chem>Clc1ccc2ccccc2c1</chem>	<chem>Brc1ccc2ccccc2c1</chem>	<chem>Ic1ccc2ccccc2c1</chem>
k_{ISC} (s^{-1})	0.39	0.42	2.35	36.5	310

Figure 1.12. Rate of ISC of naphthalene upon substitution with halogen atoms.

Charge transfer mediated triplet generation: Intramolecular or intermolecular charge transfer (CT) followed by charge recombination can happen through ISC, if the triplet excited state lies below the excited CT state (Figure 1.13)[25]. This phenomenon is observed in various donor – acceptor blends and dyad molecules[8].

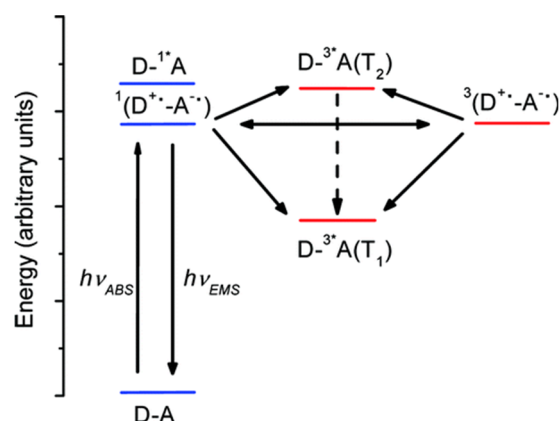


Figure 1.13. Energy level ordering of localised and charge transfer singlet and triplet excited states of donor-acceptor systems (Adapted with permission from ref. 25. Copyright © 2008, American Chemical Society).

Singlet exciton fission: Singlet fission (SF) is a spin allowed process in which a singlet excited molecule shares its energy with the neighboring ground state molecule to generate two triplet excitons (figure 1.14)[26].

This phenomenon has been observed in single crystal, polycrystalline, amorphous solids and concentrated solutions, producing triplet yields as high as

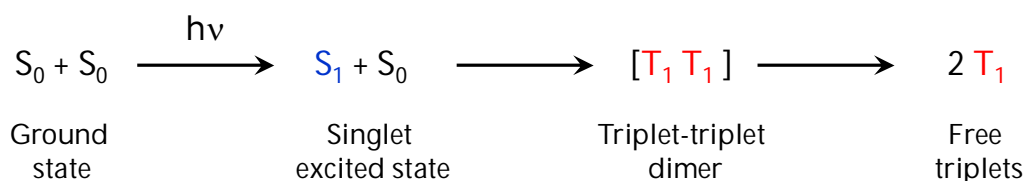


Figure 1.14. Mechanism of singlet exciton fission.

200%. SF has been extensively studied in pentacene and its derivatives. Recently SF mediated triplet generation is gaining more attention due to its ability to enhance the Shockley-Queisser limit of solar cells from 32% to 45%[27].

Till date, SF has been observed in crystalline anthracene[28], tetracene[29], pentacene[30], 1,3-diphenylisobenzofuran[31], rubrene[32], bipentacene[33], carotenoid[34], hexacene[35], TIPS-pentacene[36-37], zeaxanthin[38], terrylene[39], thiophene polymer[40] and perylenediimide[41] having triplet quantum yield ranging from 1-200%. Two pathways for SF where formation of polar transition state followed by triplet generation and a direct single step mechanism have been reported[26]. Wasielewski and coworkers reported significant triplet formation in co-facial/slipped PDI dimers[42-43] through polar transition state and polycrystalline thin films of slipped PDI through single step mechanism[41].

However, despite this great promise, there exist strict limitations to the molecular design of novel phosphorescent materials. The field is restricted, practically, to few families of organic molecules. It is still a challenge to design a triplet active molecule, especially the chromophores without any heavy atoms. This difficulty is mainly due to the lack of established relationships between the ISC and molecular structures.

1.7. Perylenediimide dyes

Perylenediimide dyes are rylene family dyes having two naphthalimides connected through two single bonds (Figure 1.15). In organic materials perylenediimides are among the most stable compounds towards chemical, heat and light. They have been known for nearly 100 years, when Kardos found a way to synthesize perylenediimides in the beginning of 1910s. Several decades later, perylene derivatives have been used as commercial products and they are still recognized as an important class of high-performance pigments. In that market they are primarily applied for the coloration of automotive paint and for the mass coloration of synthetic fiber and engineering resins[44].

The perylene core has twelve functionalizable positions[45], classified into three distinct regions as follows,

- 1) Peri region: 3, 4, 9 and 10th positions
- 2) Bay region: 1, 6, 7 and 12th positions
- 3) Ortho region: 2, 5, 8 and 11th positions

According to the functionalizing positions, there are three important stages for the development of perylenediimides which is referred to as “generations”[44]. In the 1st generation the 3, 4, 9, 10 - diimides substitutions were intensively developed (Figure 1.15). In second generation, bay-decoration with different functional group is being investigated. The third generation PDIs are becoming an interesting direction for research from the recent discovery the ortho-functionalization.

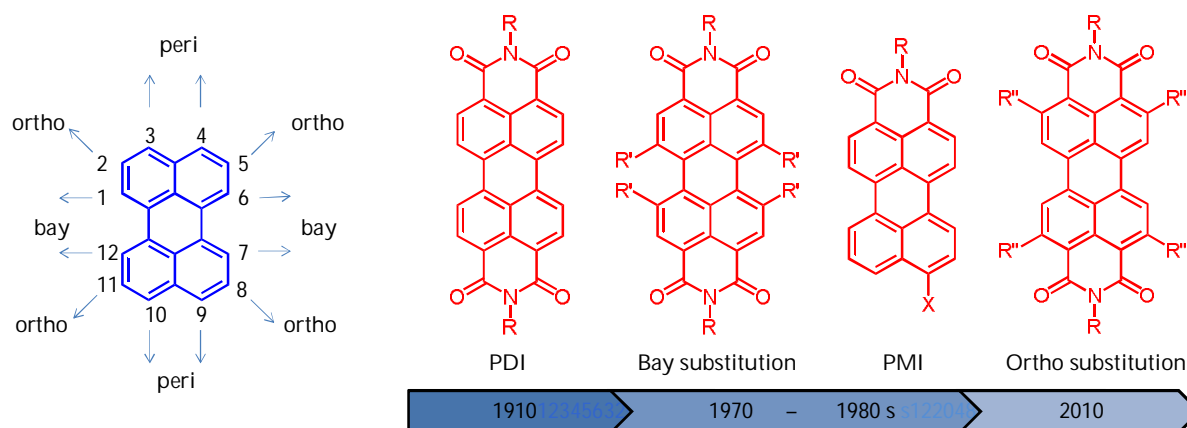


Figure 1. 15. Chemical structure of perylene and its derivative explored during different time period (Adapted with permission from ref. 44. Copyright © 2012, John Wiley and Sons).

1.7.1. Electrochemical properties

PDI dyes exhibit electron deficiency due to the presence of electron withdrawing carbonyl groups. The very typical signature of all PDIs is two reversible redox couples that are located at around -0.6 and -0.8 V vs the Ag/AgCl redox couple in dichloromethane solvent. The oxidative wave is typically irreversible at >1.7 V and at the detection limit for common solvents.

1.7.2. Optical properties

PDIs display vibronic absorption bands at 450, 490 and 530 nm with very high molar absorption coefficient ($\epsilon \approx 75,000$ L mol⁻¹ cm⁻¹) in most of the organic solvents (Figure 1.16A). Density functional theory calculations indicate the transition ($S_0 \rightarrow S_1$) is described as a HOMO to LUMO excitation (Figure 1.16B). The most important feature of this chromophore is its mirror image fluorescence at 535, 580 and 635 nm

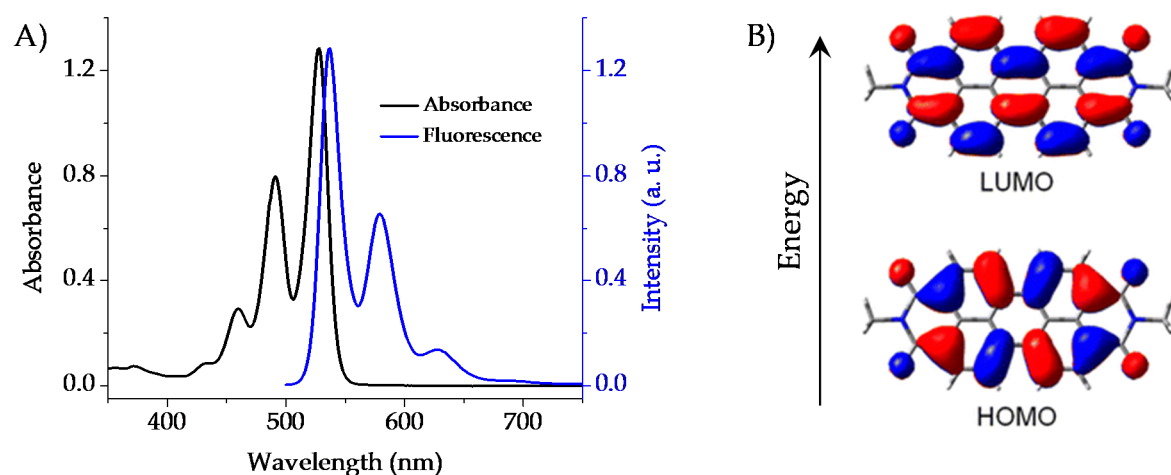


Figure 1. 16. A) absorption and emission spectra of un-substituted PDI in toluene; B) frontier molecular orbitals HOMO and LUMO calculated from B3LYP/6-31++G** (Adapted with permission from ref. 46. Copyright © 2016, American Chemical Society).

(Figure 1.16A) with nearly quantitative ($\Phi_F = 0.98$) fluorescence quantum yield in organic solvent such as toluene, chloroform and dichloromethane.

1.7.3. Applications of PDIs

For several decades, PDIs have been utilized for numerous fundamental studies and in commercial products as well due to their enhanced stability and interesting opto-electronic properties[46]. Supramolecular materials systems of PDI dyes are in particular devoted to conventional and single molecule fluorescence spectroscopy, photo-induced energy and electron transfer processes, and more recently to singlet fission and artificial photosynthesis.

1.7.3.1. Non-fullerene acceptor in solar cells

PDIs are used as n-type semiconductor in optoelectronic devices. Core substituted PDIs are promising candidates as non-fullerene acceptor materials for

organic solar cells. The functionalization of PDIs in the bay positions using chemical groups with different electron donating abilities and with steric hindrance is a versatile tool to modify both the optoelectronic properties and the morphology in the solid state. Very recent report shows PDI based polymeric acceptor exhibit power conversion efficiency of 7.5% in all polymer bulk heterojunction solar cell (Figure 1.17)[47].

1.7.3.2. Artificial photosynthesis

The development of efficient artificial systems for solar energy conversion is important for sustainable energy utilization. Self-assembly of chromophores at specific distances and orientations to provide particular photophysical or redox functions is critical in such applications. PDIs are well known for their spontaneous π -stacked self-assembly (Figure 1.18A)[48], which led the researchers to construct

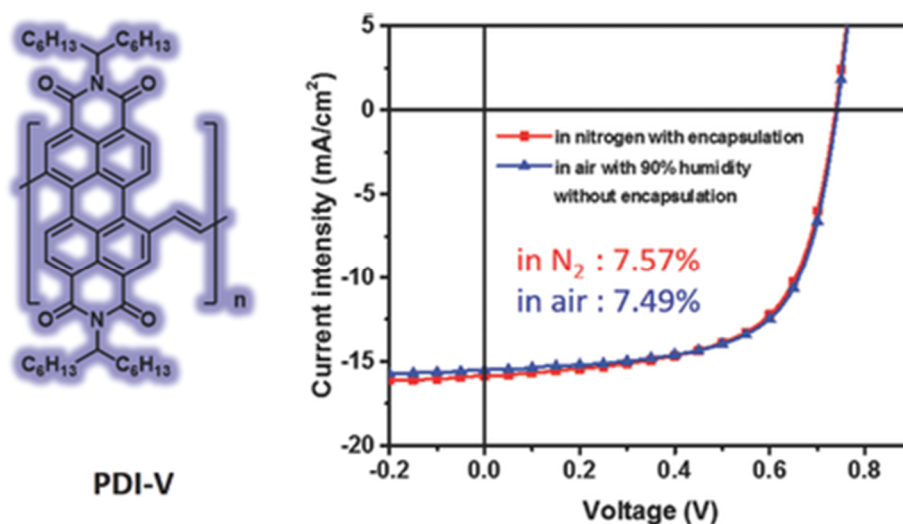


Figure 1. 17. Molecular structure of PDI based polymer and corresponding I-V plot obtained for the polymer bulk heterojunction solar cell (Adapted with permission from ref. 47. Copyright © 2016, John Wiley and Sons).

novel nanostructures with this chromophore. Photoinduced electron transfer (PET) reactions involving PDIs, primarily as electron acceptors, have been widely studied for both intermolecular and intramolecular PET between PDI-based acceptors and electron donors in monomeric and self-assembly. The ability to self-assemble identical or very similar chromophores, demonstrating energy funnelling and electron transfer can greatly simplify the design of an artificial reaction center (Figure 1.18B)[49].

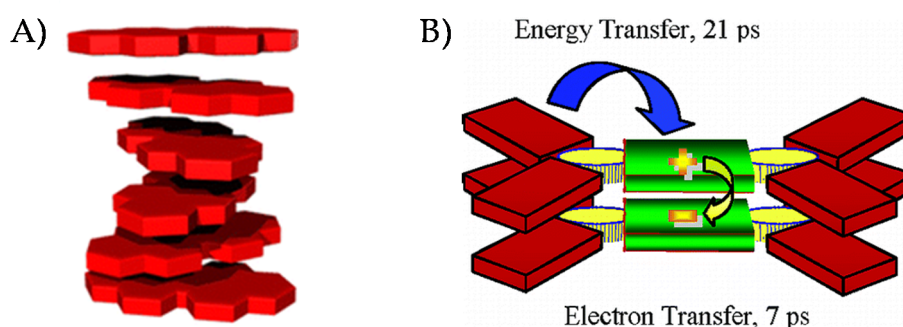


Figure 1. 18. A) Model for the columnar PDI aggregates (Adapted with permission from ref. 32. Copyright © 2012, Royal Society of Chemistry); B) self-assembled artificial photosynthetic system based PDI chromophore (Adapted with permission from ref. 49. Copyright © 2004, American Chemical Society)

1.7.4. Disadvantages of PDI

Despite being well-explored for photo-functional applications, PDIs lack desirable features such as access to triplet state and solid-state fluorescence.

Negligible ISC: Perylene and perylene based chromophores exhibit very poor ability to undergo ISC from the singlet excited state. Organic triplet excited states are getting more attention due to their longer lifetime and paramagnetic properties.

Unfortunately, PDI dyes exhibit negligible intersystem crossing ($\Phi_{ISC} < 0.01$) due to the lack of significant SOC in the molecule.

Quenched fluorescence in solid state: Though PDIs exhibit desirable photophysical properties in the solution state, stacking nature leads to severely quenched emission which has greatly hindered the exploitation of their properties and further applications in the solid state[50].

1.7.5. Strategies reported in the literature

Literature survey shows that various strategies have been adopted to access the long-lived triplet excited state in the perylenediimide chromophores. Ford et. al. reported bimolecular sensitisation mediated triplet generation of PDI by triplet-triplet energy transfer[51]. Tilley et. al. reported thionation of the carbonyl groups in PDI resulted in ultrafast intersystem crossing in the chromophore[52]. Wasielewski[53], Castellano[54], Würthner[55] and co-workers have shown the heavy metal incorporation promotes the ISC in the metal-PDI complexes. Torres[56], Janssen[43] and co-workers have reported the charge transfer mediated triplet generation of PDI in D-A dyad and triad systems. Unprecedented triplet generation was reported by Flamigni and co-workers in the asymmetrically substituted PDI derivatives[57].

1.8. Objective of the thesis

Though PDIs are well explored for the photo-functional applications, most of the applications of PDIs focus on the photophysical properties arising from the

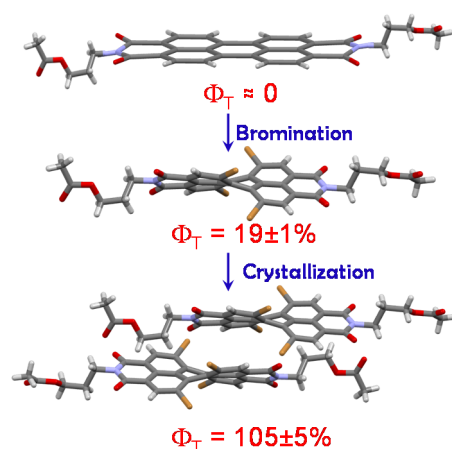
singlet excited state; investigations dedicated to their triplet excited state are rather limited. Although PDIs consist of 4 carbonyl groups in the peri region, no significant ISC is observed in the molecule upon excitation. Triplet excited states are surprisingly important due their crucial role in photocatalysis, high performance solar cells, bio-imaging and photovoltaics. Reported methods to access triplet excited state in PDIs include bimolecular sensitization, metal induced heavy atom effect, upgrading carbonyl to thionyl functionality and bay imidisation. Designing of heavy atom free, PDI systems for efficient ISC is still burgeoning area of research. This dissertation is devoted to study the novel strategies to enhance the efficiency to ISC in core-twisted PDI based chromophores.

Chapter 2

Access to Triplet Excited State in Core-Twisted Perylenediimides

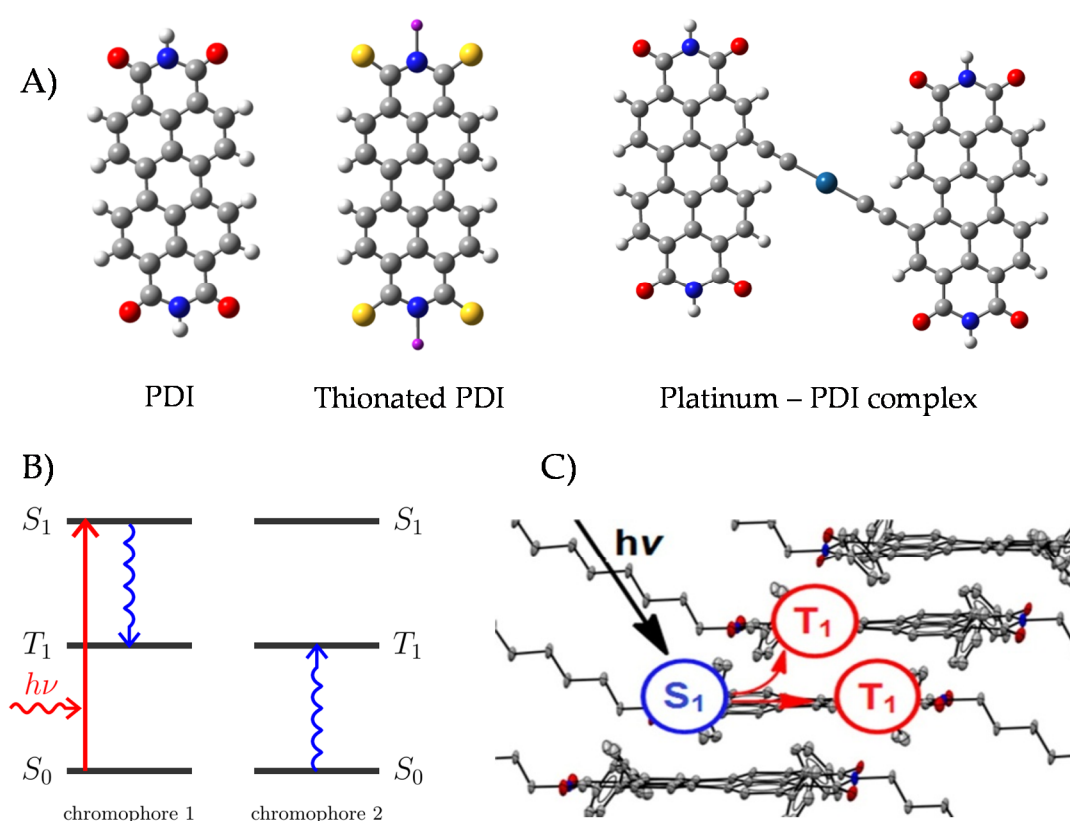
Abstract

Solvent-free crystal structure of N,N-bis(propylacetyl)-1,6,7,12-tetrabromoperylene-3,4:9,10-bis(dicarboximide), PDI-Br₄, obtained by X-ray diffraction reveals the core-twisted perylene motif having π - π stacks at an interplanar separation of 3.7Å. Slip-stacked arrangement of PDI units in PDI-Br₄ arises due to the presence of bulky bromine atoms. Femtosecond pump-probe measurements of monomeric PDI-Br₄ in toluene reveal ultrafast intersystem crossing ($\tau_{ISC} < 110$ fs) when excited at 400 nm. Triplet quantum yield (Φ_T) of $19 \pm 1\%$ and $105 \pm 5\%$ for PDI-Br₄ in toluene and vapour annealed polycrystalline 60 nm thick film respectively are estimated from nanosecond transient absorption measurements. Quantum chemical calculations show that the combined effects of heavy atom and core-twist in PDI-Br₄ can activate the intersystem crossing by altering the singlet-triplet energy gap. Enhanced quantum yield accounts for the singlet fission mediated generation of triplet excited state in the PDI-Br₄ thin film.



2.1. Introduction

Perylenediimide (PDI) chromophore received immense attention in materials and biological applications due to remarkable photo-, thermal- and chemical stability[58-60]. Despite being well-explored for photo-functional applications[50, 61-68], PDIs lack essential features such as solid-state fluorescence and access to triplet state. Reported methods to access triplet state of PDI (Scheme 2.1A) makes use of bimolecular triplet sensitization[51],



Scheme 2.1. A) chemical structure of PDI, thionated PDI and Pt-PDI complex; B) energy level diagram for singlet exciton fission between two interacting chromophores 1 and 2 (Adapted with permission from ref. 27. Copyright © 2009, American Chemical Society); C) schematic of singlet fission in polycrystalline thin film of slip-stacked PDI (Adapted with permission from ref. 41. Copyright © 2009, American Chemical Society).

incorporation of sulphur[52] and heavy metals such as Ir[53], Pt[54], Ru[55] that promote intersystem crossing (ISC). Unprecedented triplet state of perylenediimide was observed in unsymmetrically substituted PDIs[57]. Though the triplet excited state is achieved in monomeric form, most of the organic molecules undergo triplet-triplet annihilation and lose their triplet excited state properties upon formation of assembly. Retention/generation of the triplet excited state in assembled/solid-state is still a challenging task in organic materials.

Generation of triplet excited state in assembled chromophoric systems through singlet exciton fission (SF) process is an emerging topic of interest (Scheme 2.1B). SF is a spin allowed process whereby a singlet excited chromophore is energetically down-converted into two triplet excitons. SF mediated formation of two triplet excitons per photon can, in principle, increase the Shockley-Queisser limit for power conversion efficiency from 32% to 44% in solar cells[27, 69-71]. Till date, SF has been observed in crystalline anthracene[28], tetracene[29], pentacene[30], 1,3-diphenylisobenzofuran[31], rubrene[32], bipentacene[33], carotenoid[34], hexacene[35], TIPS-pentacene[36-37], zeaxanthin[38], terrylene[39], thiophene polymer[40] and perylenediimide[41] having triplet quantum yield ranging from 1-200%. SF was also observed in concentrated solution of TIPS-pentacene[72] and very dilute solution of bipentacene[73] with quantitative triplet yield. Recently, crystal packing and crystallite size dependence on the rate of SF is reported in tetracene polymorphs[70, 74]. Two pathways for SF where formation of polar transition

state followed by triplet generation and a direct single step mechanism have been reported[26]. Wasielewski and coworkers reported significant triplet formation in co-facial/slip-stacked PDI dimers[42-43] through polar transition state and polycrystalline thin films of slip-stacked PDI (Scheme 2.1C) through single step mechanism[41]. State-of-the-art theory supports that slip-stacked co-facial arrangement of molecular pairs is a prerequisite for singlet fission[75-76].

Access to triplet excited states in monomeric/aggregate/single crystalline PDI based chromophores continues to possess immense interest[77]. Our ongoing interest towards the twisted chromophoric structures[78-81], for promising excited state properties, encouraged us to investigate the influence of core-twist in generating the triplet excited state in monomeric and crystalline PDI. Here we report the first example of the heavy atom and core-twist induced triplet formation in monomeric PDI-Br₄[82]. Interestingly, slip-stacked arrangement of PDI-Br₄ exhibits combination of spin-orbit (SO) coupling and SF mediated triplet generation in polycrystalline thin film.

2.2. Synthesis, characterisation and crystal structure of PDI-Br₍₀₋₄₎

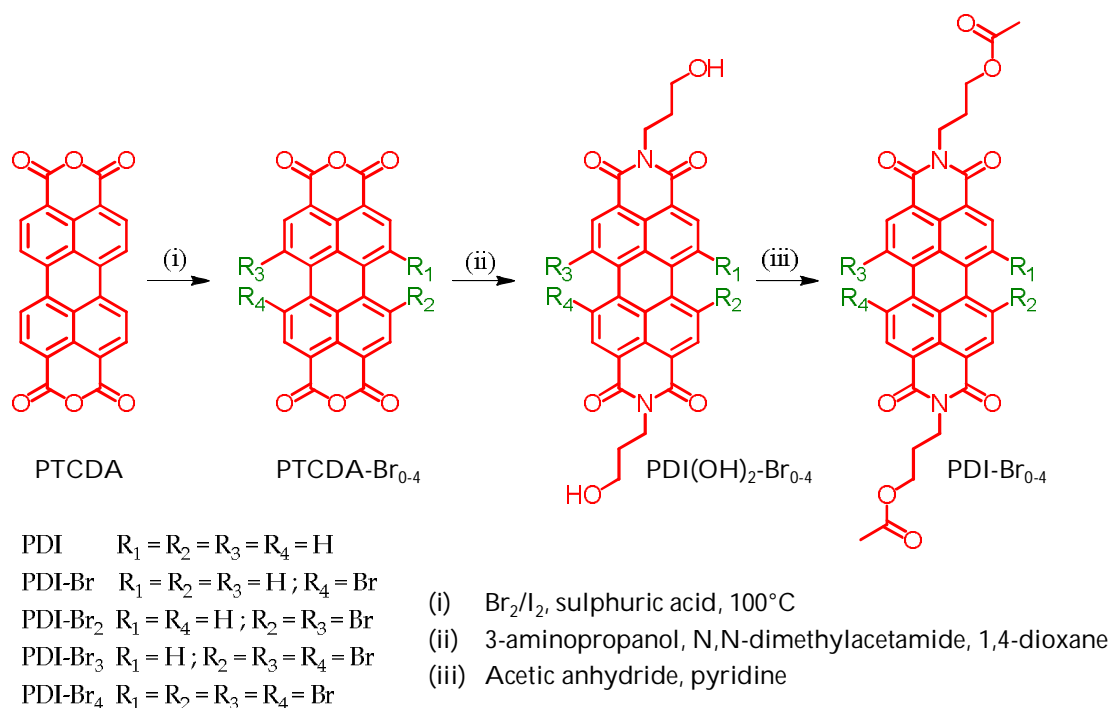
Brominated perylenediimide derivatives PDI-Br₍₁₋₄₎ were synthesised and characterised as per the reported procedure (Scheme 2.2)[83]. Except for PDI-Br₃, synthesis of PDI-Br₁₋₂/PDI-Br₄ has been reported[84-87]. Würthner and co-workers have explored the extent of core-twist upon halogenation of PDI at bay-positions[88]. X-ray structure of crystalline solvated PDI-Br₄[88] and crystalline solvent-free PDI-

Br₂[84] are well-documented, however, crystalline solvent-free PDI-Br₄ are yet to be reported. Slow evaporation from different ratios of dichloromethane/hexane mixture offered fluorescent crystals of PDI-Br₂₋₄ in triclinic space group *P*-1 (Table 2.1). π - π

Table 2.1. Crystallographic data and refinement parameters for the derivatives PDI-Br₂₋₄.

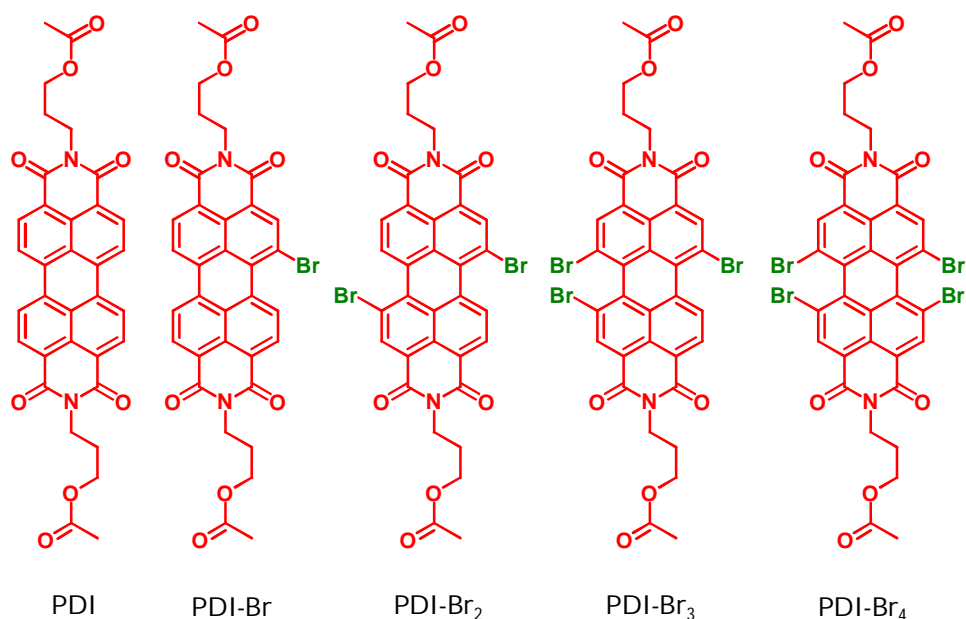
	PDI-Br₂	PDI-Br₃	PDI-Br₄
formula	C ₃₄ H ₂₄ Br ₂ N ₂ O ₈	C ₃₄ H ₂₃ Br ₃ N ₂ O ₈	C ₃₄ H ₂₂ Br ₄ N ₂ O ₈
formula wt.	748.3710	827.2610	906.1631
colour, shape	Red, Needle	Red, Block	Red, Block
crystal system	Triclinic	Triclinic	Triclinic
space group	<i>P</i> -1	<i>P</i> -1	<i>P</i> -1
<i>a</i> , Å	4.8146(7)	11.4678(6)	10.800(5)
<i>b</i> , Å	9.1602(14)	12.2449(6)	11.197(5)
<i>c</i> , Å	17.672(3)	12.6152(6)	13.581(5)
α , degree	76.925(5)	84.037(2)	81.322(5)
β , degree	84.870(5)	82.349(2)	77.257(5)
γ , degree	75.057(5)	70.582(2)	89.597(5)
<i>V</i> , Å ³	733.11(19)	1652.44(14)	1582.9(12)
temp, K	296	296	296
<i>d</i> _{calcd} , g/cm ⁻³	1.694	1.820	1.900
no. of reflections collected	10852	5794	5384
no. of unique reflections	4884	4441	3956
2 θ _{max} , degree	50	50	50
no. of parameters	218	433	435
R1, wR2 (<i>I</i> > 2 σ (<i>I</i>))	0.0443, 0.1260	0.0985, 0.3155	0.0305, 0.0719
R1, wR2 (all data)	0.0596, 0.1463	0.1217, 0.3374	0.0563, 0.1038
goodness of fit	1.142	1.116	1.083
CCDC number	1402604	1402605	1402606

interactions between the neighboring PDI units appear unimpeded due to solvation in crystalline PDI-Br₃ (vide infra). The present study focuses on the impact of core-twist in the photophysical properties of PDI-Br₀₋₄ (Scheme 2.3) in monomeric (solution) vs. crystalline state.



Scheme 2.2. Synthesis scheme for PDI-Br₀₋₄.

The dihedral angle between the two identical halves (long axis) is found to be 2.4°, 39° in PDI-Br₂ and PDI-Br₄, respectively. PDI-Br₃ exhibits dihedral angle of 27.9° and 37.8° between the two non-identical halves due to asymmetry, suggesting varying degree of core-twisting nature of PDI on successive bromination at the bay region. In the solvent-free single crystals of PDI-Br₂, face to face π -surfaces are found at a distance of 3.51 Å along with the transverse shift of 2.93 Å and longitudinal shift of 1.0 Å (Figure 2.1A and D). Adjacent π - π surfaces are found at the distance of 3.54 Å along with the transverse shift of 2.39 Å and longitudinal shift of 4.23 Å in PDI-Br₃



Scheme 2.3. Molecular structures of the derivatives under study.

crystals (Figure 2.1B and E). Solvent free single crystals of PDI-Br₄ exhibit nearest π surfaces at the distance of 3.66 Å along with the transverse shift of 2.40 Å and longitudinal shift of 5.64 Å (Figure 2.1C and F). On increasing the number of bromine atoms at the bay region, perylenediimide exhibits a gradual increase in the distance and the longitudinal shift between the adjacent PDI units in the crystalline state. Orbital overlap between adjacent perylenediimide units in PDI is estimated from X-ray crystal structure to be 46%[59]. Percentage overlap between the vicinal PDI π -surfaces in crystalline state is found to be 22.1% for PDI-Br₂, 16.8% for PDI-Br₃ and 9.5% for PDI-Br₄ (Figure 2.1D-F). Quantum theory of atoms in molecules analysis suggests the presence of C=O... π [89-90] interaction at a distance of 3.10 Å between the neighboring PDI units in crystalline PDI-Br₄. PDI-Br₃ displays C-H... π [91] interaction at a distance of 2.76 Å along with the C-Br... π [92-93] interaction at a distance of 3.48 Å.

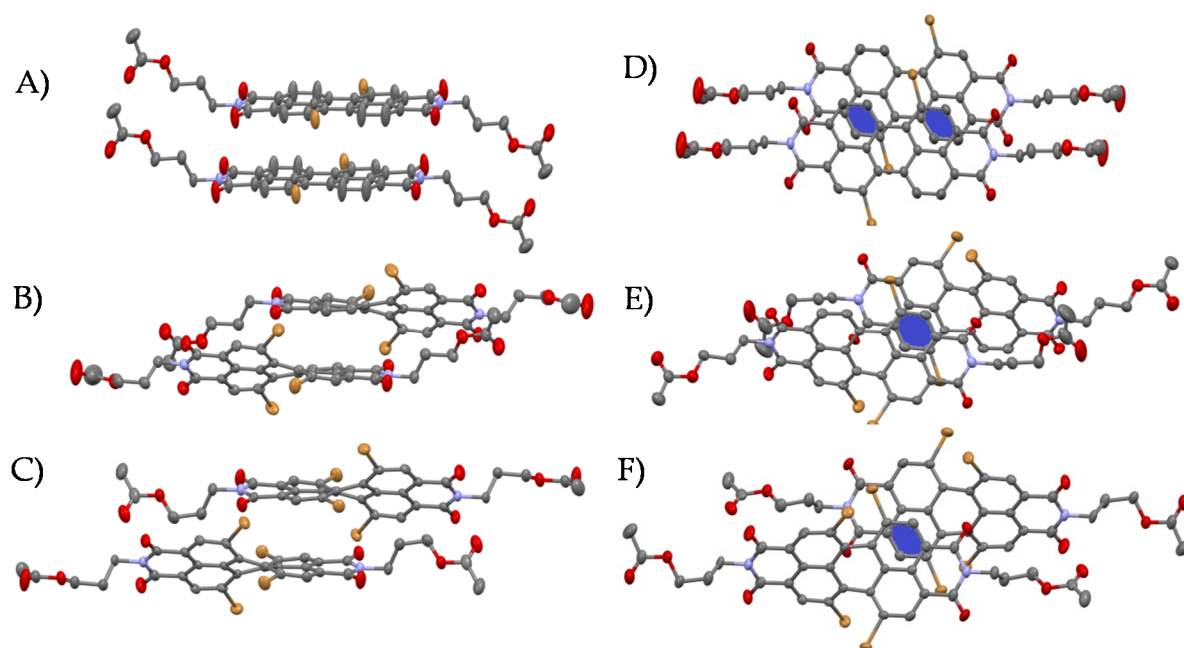


Figure 2.1. Crystal packing of the derivatives PDI-Br₂₋₄. A), B) and C) side view of the dimers in PDI-Br₂, PDI-Br₃ and PDI-Br₄ respectively; D), E) and F) corresponding top view (coloring show the area of π overlap; Reprinted with permission from ref. 82. Copyright © 2016, American Chemical Society).

2.3. Results and discussions

2.3.1. Electrochemical studies

Cyclic voltammetry measurement of PDI in DCM (Figure 2.2A) shows two reversible reduction peaks (-0.547 V and -0.728 V) with reference to Ag/AgCl electrode, characteristic of PDI, as reported[94]. On successive increase in number of electron releasing bromine atoms per PDI unit, reversible reduction potential (Figure 2.2B) is significantly decreased to -0.319 V and -0.528 V for PDI-Br₄. Decrease in the reduction potential of PDI-Br₄ when compared to the PDI could arise from the presence of additional bromine atoms in PDI-Br₄.

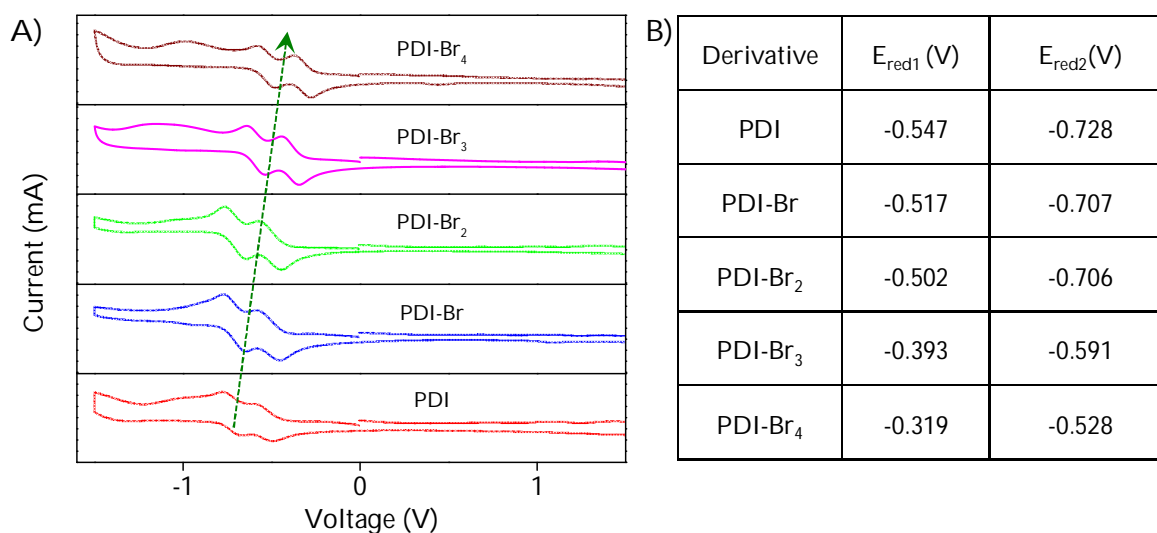


Figure 2.2. A) Cyclic voltammogram of the derivatives (1 mM) PDI-Br₀₋₄ in dichloromethane in the presence of tetrabutylhexafluoroammoniumphosphate (100 mM) with respect to Ag/Ag⁺ electrode; and B) Tabulation of the first and second reduction potential of the derivatives PDI-Br₀₋₄ in dichloromethane with respect to the Ag/Ag⁺ reference electrode.

2.3.2. Photophysical studies in solution state

UV-Vis absorption spectra of PDI-Br₀₋₂ in toluene (Figure 2.3A) exhibit three distinct bands corresponding to S₀→S₁ transition, oriented along the longitudinal axis[95]. Red-shifted absorption maxima with the increase of bromine atoms is fully consistent with the decreasing trend of S₀→S₁ transition energy evaluated at time dependent density functional theory (TD-DFT) method. Whereas S₀→S₂ transition is symmetry forbidden in planar PDIs (i.e. PDI-Br₀₋₂), significant absorbance at 425-440 nm in PDI-Br₃₋₄ arises due to core-twist, consistent with earlier reports[95-96]. Oscillator strength calculated from TD-DFT method for S₀→S₂ transition shows gradual increase from PDI (0.00) to PDI-Br₄ (0.11), in agreement with our experimental data. Steady state fluorescence spectrum (Figure 2.3B) of PDI in

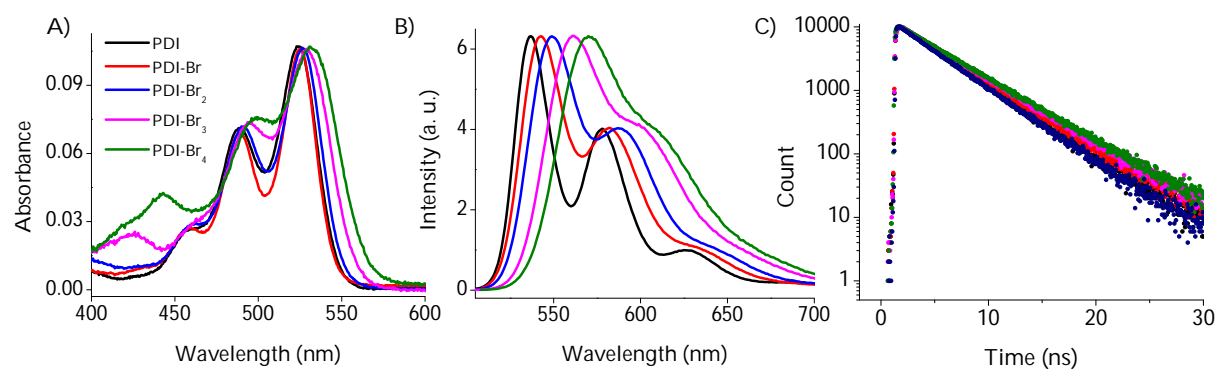


Figure 2.3. A) absorption; B) emission ($\lambda_{ex} = 480$ nm) and C) time-dependent fluorescence studies ($\lambda_{ex} = 480$ nm and monitored at their emission maxima) of the derivatives PDI-Br₀₋₄ in toluene Reprinted with permission from ref. 80. Copyright © 2016, American Chemical Society).

toluene shows vibronic bands at 536, 577 and 627 nm as reported[51]. On increasing the number of bromine atoms per PDI unit, fluorescence quantum yield (Table 2.2) is reduced from $\Phi_F = 97\%$ (for PDI) to 64% (for PDI-Br₄). Similar to UV-Vis absorption,

Table 2.2. Photophysical properties of derivatives PDI-Br₀₋₄ in toluene solution.

	Solution (Toluene)						
	λ_{abs} , nm	ϵ_{molar} , L mol ⁻¹ cm ⁻¹	λ_{em} , nm	τ_F , ns	Φ_F , %	Φ_T , %	ΔE (S ₁ -T ₂), eV
PDI	459, 490, 525	71000	536, 577, 627	4.17	97 (99)*	< 1	0.2923
PDI-Br	459, 490, 526	60088	543, 582, 630	4.49	97 (97)*	< 1	0.2702
PDI-Br ₂	460, 491, 526	51587	550, 588, 640	4.73	94 (96)*	1	0.2444
PDI-Br ₃	425, 462, 494, 530	39801	561, 603	4.89	85 (83)*	5	0.1792
PDI-Br ₄	440, 465, 499, 532	26743	570, 610	4.13	64 (64)*	18	0.1171

*Quantum yield determined in 1, 2-dibromoethane confirms the absence of external heavy atom effect imparted by bromine atoms.

emission maxima also exhibit red-shift with increase in number of bromine atoms (Table 2.1). Similar Φ_F for PDI-Br₀₋₄ in dibromoethane and toluene suggests the lack of external heavy atom effect in promoting ISC. Upon excitation at 439 nm, picosecond time-resolved fluorescence measurement shows the singlet excited state lifetime of PDI-Br₀₋₄ in the range of 4.1-4.9 ns (Figure 2.3C) by monitoring at the respective emission maximum.

2.3.3. Transient absorption measurement in solution

2.3.3.1. Femtosecond transient absorption spectroscopy

Femtosecond transient absorption (fTA) measurements were performed on PDI-Br₀₋₄ in toluene to investigate the influence of core-twist on the excited state properties. Upon excitation at 400 nm, using 110 fs laser pulse, PDI-Br₀₋₄ in toluene exhibit ground state recovery at 500–600 nm and a positive band around 600-680 nm as reported for bay substituted PDIs (Figure 2.4)[97]. Singular value decomposition (SVD) followed by global analyses of ΔA versus time and wavelength based three dimensional map of PDI-Br₀₋₄ were carried out to understand the principal components responsible for the absolute spectra. Decay associated difference spectra (DADS) of PDI-Br₀₋₂ (Figure 2.4A-C and F-H) displayed two principal components: i) ground state depletion ($S_0 \rightarrow S_n$)/stimulated emission ($S_1 \rightarrow S_0$; $\tau \sim 4$ ns) and ii) positive absorption due to $S_1 \rightarrow S_n$ transitions[97]. DADS (Figure 2.4D, E, I and J) of PDI-Br₃₋₄ exhibited three principal components that are attributed to i) ground state depletion ($S_0 \rightarrow S_n$)/stimulated emission ($S_1 \rightarrow S_0$) and positive absorptions due to ii) $S_1 \rightarrow S_n$ and iii) $T_1 \rightarrow T_n$ transitions[53]. A representative fTA and SVD spectra corresponding to

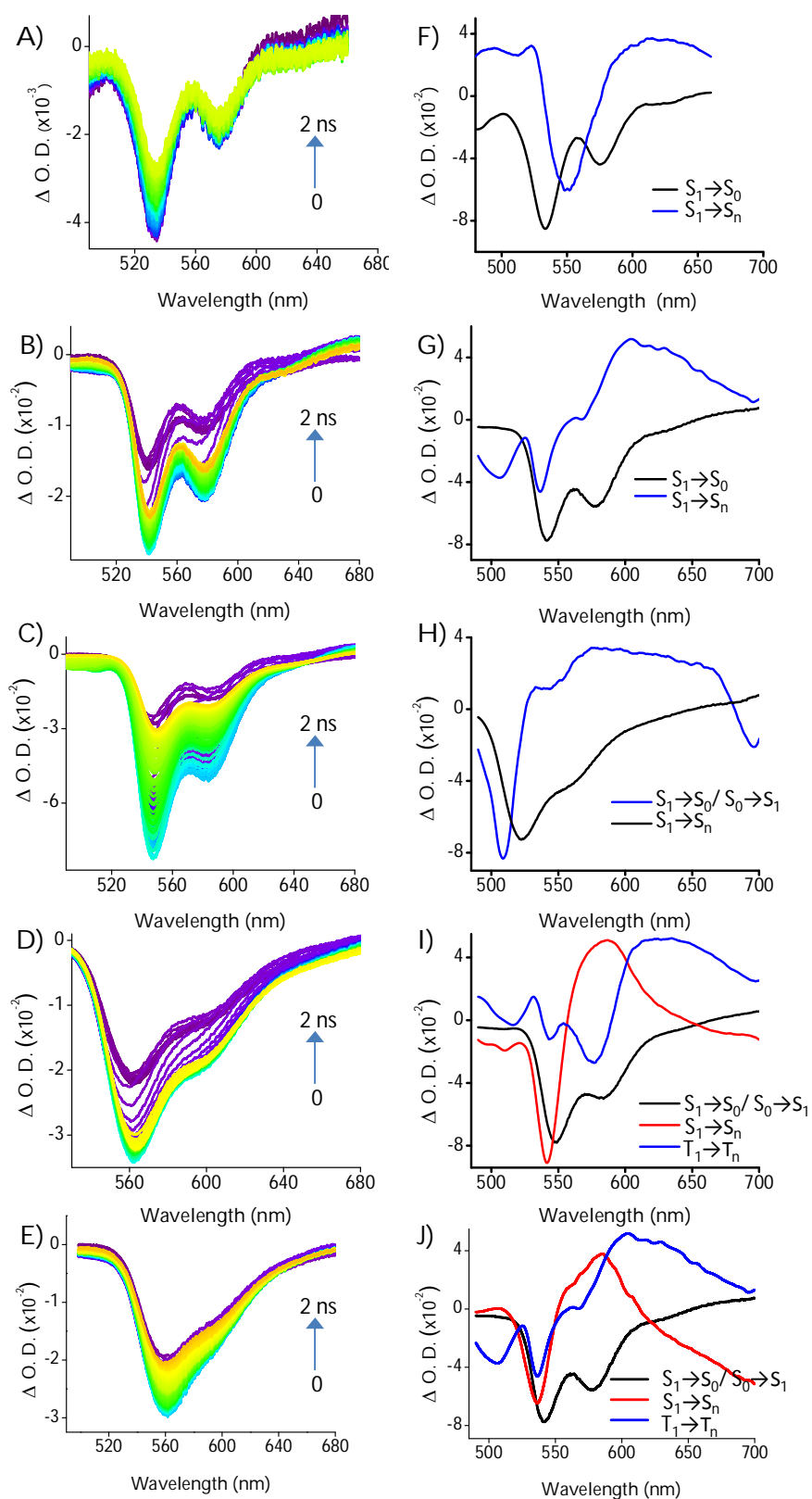


Figure 2.4. A), B), C), D) and E) fTA spectra of the derivatives PDI, PDI-Br, PDI-Br₂, PDI-Br₃ and PDI-Br₄ respectively; F), G), H), I) and J) corresponding decay associated difference spectra obtained from SVD analysis.

PDI-Br₄ in toluene is explained in detail. Right singular vector at 500-680 nm ($\tau \sim 4$ ns) corresponds to i) $S_0 \rightarrow S_n$ (500-570 nm) and ii) $S_1 \rightarrow S_0$ (550-600 nm) transitions, respectively. Right singular vectors at 550-650 nm and 600-680 nm correspond to $T_n \rightarrow T_1$ ($\tau > 4$ ns) and $S_n \rightarrow S_1$ ($\tau < 0.1$ ns) transitions, respectively, consistent with the earlier reports[41].

2.3.3.2. Nanosecond transient absorption spectroscopy

To further characterize the long-lived triplet excited state of PDI-Br₃₋₄, nanosecond transient absorption (nTA) measurements were performed. nTA measurements of PDI-Br₀₋₄ in toluene were carried out upon excitation of the samples with 10 ns, 355 nm and 532 nm laser. Photoexcited PDI shows weak signal corresponding to triplet excited state as a consequence of poor ISC ($\Phi_T \sim 0.3\%$)[51]. Substitution of one/two bromine atoms at the bay region of PDI resulted in slight increase of ISC ($\Phi_T \leq 1\%$), estimated using triplet-triplet energy transfer method upon photoexcitation at 532 nm[51]. Ultrafast inherent fluorescence vs. slower ISC could be attributed to the lack of heavy atom effect in PDI-Br₁₋₂, which is in good agreement with reported perylene based chromophoric systems[98].

Upon excitation at 532 nm, PDI-Br₃₋₄ in toluene exhibit strong absorption bands at 370 nm and 575 nm in addition to ground state depletion at 440, 490 and 530 nm (Figure 2.5). Observed nTA spectra of PDI-Br₄ in toluene is similar to the reported spectra obtained from indirect excitation of PDI using anthracene as triplet sensitizer[51]. Due to the stronger bleach at 450-550 nm, positive absorption at 480

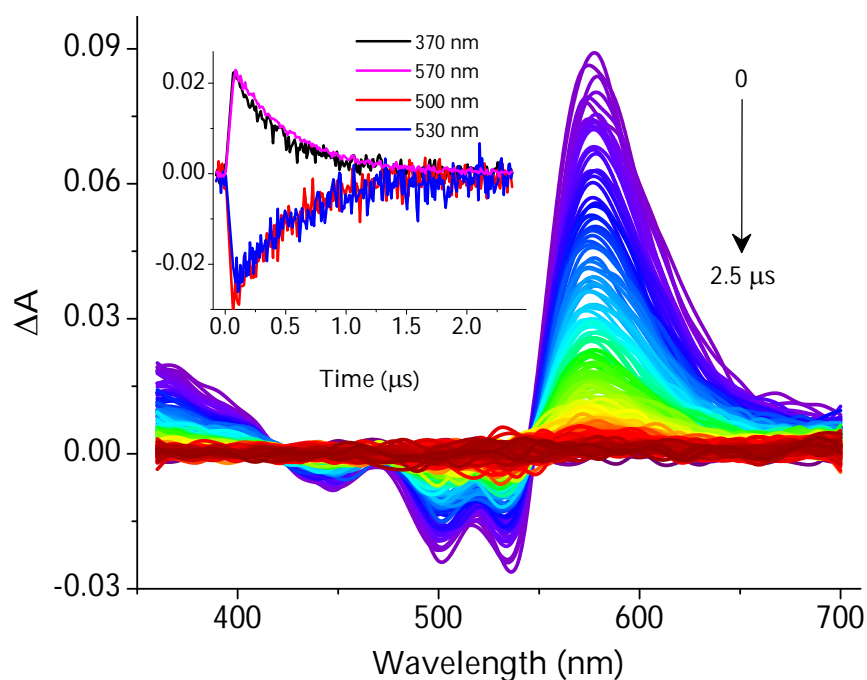


Figure 2.5. *nTA spectra of PDI-Br₄ in toluene upon excitation with 532 nm laser. Inset shows the kinetics of bleach recovery and triplet decay monitored at respective wavelength (Reprinted with permission from ref. 80. Copyright © 2016, American Chemical Society).*

nm and 500 nm is diminished in the spectra as compared to the reported spectra. Φ_T of PDI-Br₃ and PDI-Br₄ are calculated to be $5\pm 1\%$ and $18\pm 1\%$, respectively, which is significantly higher when compared to PDI-Br₀₋₂. Identical rate constants ($k_T \sim 2.5 \times 10^6 \text{ s}^{-1}$) for the decay of positive absorption band at 570 nm and the recovery of bleach at 530 nm in PDI-Br₂₋₄ suggests that the triplet decay quantitatively regenerates the ground state. It is also found that the rate of decay of the triplet excited state remains independent of degree of bromination in PDI-Br₂₋₄. Non-linear increase in the core-twist angle and Φ_T of PDI-Br₀₋₄ with the increase in number of bromine atoms suggest the dominant role of core-twist[99] in facilitating the triplet generation. Importance of twist angle to facilitate ISC in chromophoric systems was comprehensively established by Caldwell and co-workers[99].

Triplet energy level of PDI-Br₄ in toluene ($E_T = 31 \pm 3$ kcal/mol) is experimentally obtained through triplet-triplet energy transfer between PDI-Br₄ and an appropriate standard triplet energy donor/acceptor using Sandros method[51]. Low-lying triplet energy levels for PDI-Br₀₋₄ were calculated from TD-DFT method using the B3LYP/6-311G+(d, p)[100-101] basis set to understand the driving force for enhanced ISC. Calculated triplet energy level of PDI-Br₄ ($E_T = 29.7$ kcal/mol) is in good agreement with the experiment. Enhanced ISC in PDI-Br₃₋₄ could arise as a consequence of i) core-twist promoted asymmetry in the molecule and ii) close lying singlet and triplet (ΔE_{S-T}) energy levels (Table 2.2). To understand the role of higher excited state population, nTA measurements of PDI-Br₄ toluene solution was carried out exciting at different wavelengths. Observed similar quantum yield of triplet formation upon excitation at 355 nm ($\Phi_T = 19 \pm 1\%$) and 532 nm ($\Phi_T = 18 \pm 1\%$) suggests that the rate of $S_n \rightarrow S_1$ internal conversion is faster than the rate of $S_n \rightarrow T_n$ intersystem crossing as reported earlier[53].

2.3.4. Optical properties of PDI-Br₀₋₄ in polycrystalline thin film

Thin films of PDI-Br₀₋₄ were prepared by spin-coating the chloroform solution on quartz plate. The films were dried in the vacuum and stored in nitrogen atmosphere prior to the experiments. PDI-Br₄ thin film thickness was measured to be 60 ± 5 nm using profilometry (Veeco Dektak 150 surface profiler; Figure 2.6B). Resemblance between experimental and simulated powder X-ray diffractogram indicates the polycrystalline nature (Figure 2.6A) of PDI-Br₄ thin film. Continuous-

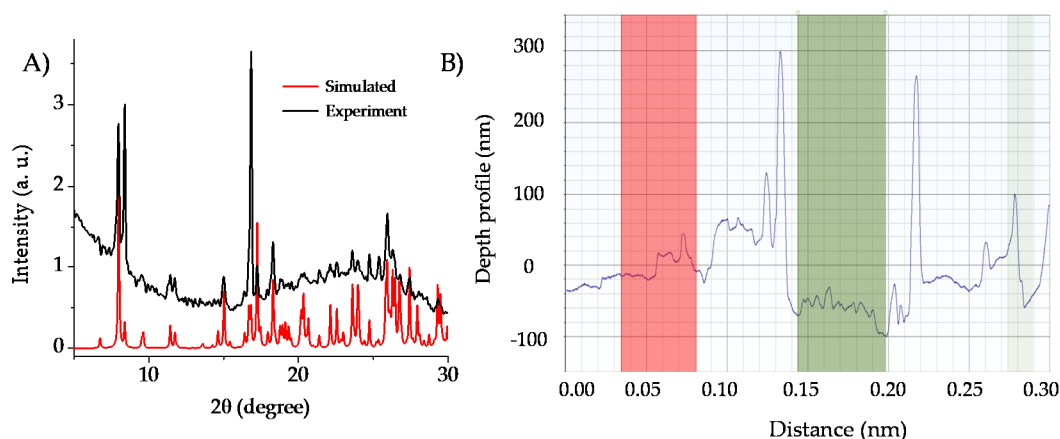


Figure 2.6. A) Powder XRD pattern of polycrystalline thin film of PDI-Br₄ along with the simulated P-XRD pattern obtained from single crystal; B) profilometric traces of PDI-Br₄ polycrystalline thin film (thickness is 60±10 nm).

wave resonance Raman spectroscopic measurements of PDI-Br₄ in solution (monomeric) and thin film (polycrystalline) state were performed to investigate the structural integrity (Figure 2.6A). PDI-Br₄ in toluene exhibits Raman bands at 1332, 1380, 1586, 1606 and 1735 cm⁻¹ as reported earlier[102]. Observed considerable change in the intensities of corresponding bands of PDI-Br₄ thin film compared to solution state is attributed to the crystal packing effects (vide supra).

UV-Vis spectrum of PDI thin film (Figure 2.7A) shows broad band at 390, 470, 500, 540, and 590 nm. Upon successive bromination, vibronic band intensity ratio ($A_{500\text{ nm}}/A_{540\text{ nm}}$) indicates weak exciton interactions in core-twisted PDI-Br₃₋₄ when compared to strong exciton interactions in planar PDI-Br₀₋₂[65]. Dissimilar degrees of exciton interactions between the neighbouring chromophoric units in core-twisted vs. planar PDIs is consistent with the extent of π - π overlap evaluated from the X-ray crystal structures. Upon excitation at 450 nm, PDI thin film exhibits very weak and

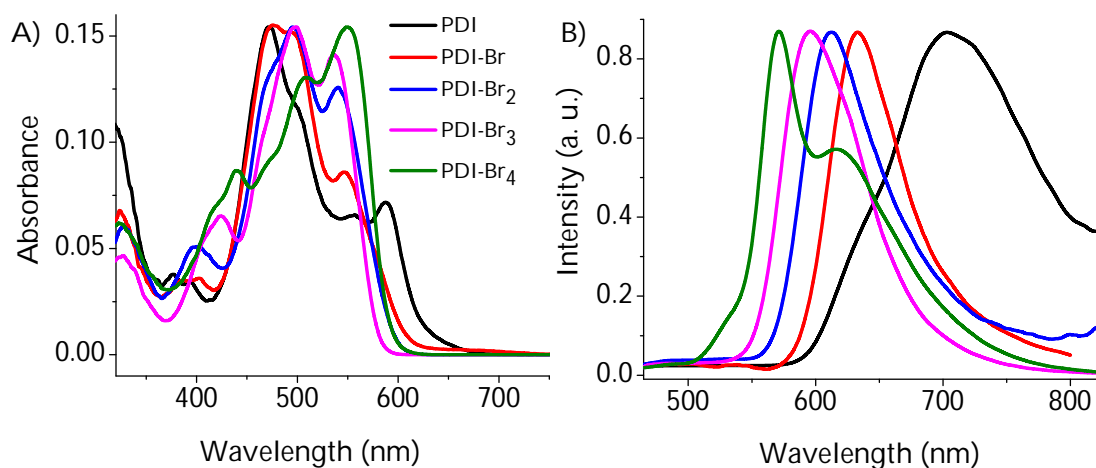


Figure 2.7. A) absorption and B) emission ($\lambda_{ex}= 480$ nm) spectra of the derivative PDI-Br₀₋₄ in polycrystalline thin film state.

broad emission ($\Phi_F < 1\%$) around 600-800 nm (Figure 2.7B, Table 2.3). On successive bromination, gradual blue-shift in the emission maximum could be attributed to the systematic decrease in the extent of exciton interaction in PDI-Br₁₋₄ thin film. Core-twisting the PDI chromophore in PDI-Br₁₋₄ resulted in a gradual increase of fluorescence quantum yield ($\Phi_F = 2\pm 0.4\%$ for PDI-Br; $\Phi_F = 12\pm 1\%$ for PDI-Br₄) in thin film state (Table 2.3). Decrease in the extent of adjacent PDI-PDI orbital overlap,

Table 2.3. Photophysical properties of derivatives PDI-Br₀₋₄ in polycrystalline thin film.

	λ_{abs} , nm	λ_{em} , nm	Φ_F , %
PDI	390, 470, 500, 555, 590	650-800 (bs)	0.01
PDI-Br	400, 475, 495, 545	635	0.02
PDI-Br ₂	400, 500, 540	610	0.03
PDI-Br ₃	425, 500, 535	595	0.07
PDI-Br ₄	440, 505, 550	570, 620	0.12

upon successive bay-halogenation, could be attributed to the core-twist dependent decrease in the free energy for self-assembly[95].

Picosecond time-resolved fluorescence measurements of PDI-Br₍₃₋₄₎ aggregates in thin film reveal significantly shorter lifetime ($\tau_f^a \leq 2.0$ ns) when compared to the characteristic lifetime ($\tau_f^m \sim 4.0$ ns) of monomeric PDI chromophore in solution. An increase in the rate of radiative decay of PDI-Br₃₋₄ in thin film ($k_r^a = 5 \times 10^{10} \text{ s}^{-1}$) when compared to that in solution ($k_r^m = 2.5 \times 10^{10} \text{ s}^{-1}$) confirms J-type aggregation in thin film state. Slip angles calculated from crystal structure analysis of PDI-Br₃ ($\theta = 45^\circ$) and PDI-Br₄ ($\theta = 43^\circ$) further confirms the existence of J-aggregate ($\theta \leq 54^\circ$) in twisted PDIs[103].

2.3.5. Transient absorption measurement in polycrystalline thin film

Nanosecond transient absorption measurements of polycrystalline thin film of PDI-Br₀₋₄ were performed upon exciting with 10 ns, 355 and 532 nm laser. Upon exciting at 532 nm, PDI-Br₀₋₄ exhibit ground state depletion at 500–580 nm along with the positive absorption at 460 and 590 nm. nTA spectra of PDI-Br₀₋₄ thin film is in good agreement with the nTA spectra of polycrystalline thin films of N,N bis(n-octyl)-2,5,8,11-tetraphenyl-PDI reported earlier[41]. Absence of positive absorption at 540 nm of PDI when compared to the reported nTA spectra[41] could be corroborated to the stronger bleach at 500-600 nm[51]. Detailed characterization of long-lived triplet excited state observed at 460 nm and 590 nm, was further carried out for thin film of PDI-Br₄ as a representative case (Figure 2.8). Observed lifetime

($\tau_T^a \sim 700$ ns) of ^3PDI in thin film is significantly longer when compared to that in solution ($\tau_T^m \sim 400$ ns).

2.3.6. Singlet exciton fission in polycrystalline thin film

Linear dependence of ΔA from nTA spectra on the laser intensity suggests that the singlet-singlet annihilation do not kinetically compete with the triplet formation in PDI-Br₄ thin film. Unlike the ultrafast appearance of ^3PDI in polycrystalline thin

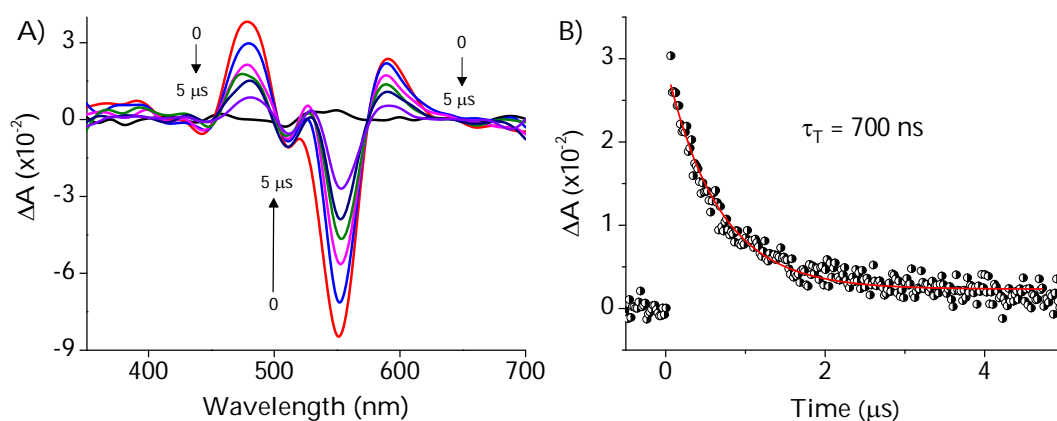


Figure 2.8. A) nTA spectra of PDI-Br₄ in polycrystalline thin film upon excitation at 532 nm; B) corresponding kinetics profile of the triplet decay monitored at 600 nm.

film of N,N bis(n-octyl)-2,5,8,11-tetraphenyl-PDI through dominant SF mechanism ($\Phi_T = 140 \pm 20\%$), PDI-Br₄ under similar conditions could exhibit via SO coupling and/or SF. Upon photoexcitation at 532 nm, Φ_T in thin film of PDI-Br₄ was determined employing the method reported by Wasielewski and co-workers[41]. For PDI-Br₄, the triplet yield measured in 60 nm thick film is found to be $79 \pm 5\%$ (Figure 2.9) when compared to 18% in monomeric PDI-Br₄ in toluene. Enhanced Φ_T in polycrystalline thin film compared to monomeric PDI-Br₄ suggests the generation of

triplet excited state via SF. Singlet and triplet energy level calculation (Figure 2.9A) show the possibility for endogonic SF from S_1 ($S_1 \leq 2T_1$) and exergonic SF from S_m ($S_m \geq 2T_1$; $m \geq n$). Based on the TD-DFT calculations, observed low yield of SF on 532 nm excitation could be due to the endogonic nature of the process ($S_1 \leq 2T_1$). By exciting to higher excited state, yield of SF mediated triplet generation could be improved due to exergonic nature ($S_n \geq 2T_1$). To explore the existence of exergonic SF from higher excited state, PDI-Br₄ in polycrystalline thin film was excited with 355 nm laser. PDI-Br₄ in polycrystalline thin film exhibits enhanced triplet generation (105±5%, Figure 2.10B), when compared to endogonic SF process (79±5%), which is in agreement with the TD-DFT calculations (Figure 2.9). Involvement of higher singlet excited state followed by exergonic SF process in polycrystalline pentacene has been recently reported by Friend and coworkers[33, 72]. Slip-stacked arrangement and favourable singlet-triplet energy levels [$E(S_m) \geq 2E(T_n)$; where $m \geq n$]

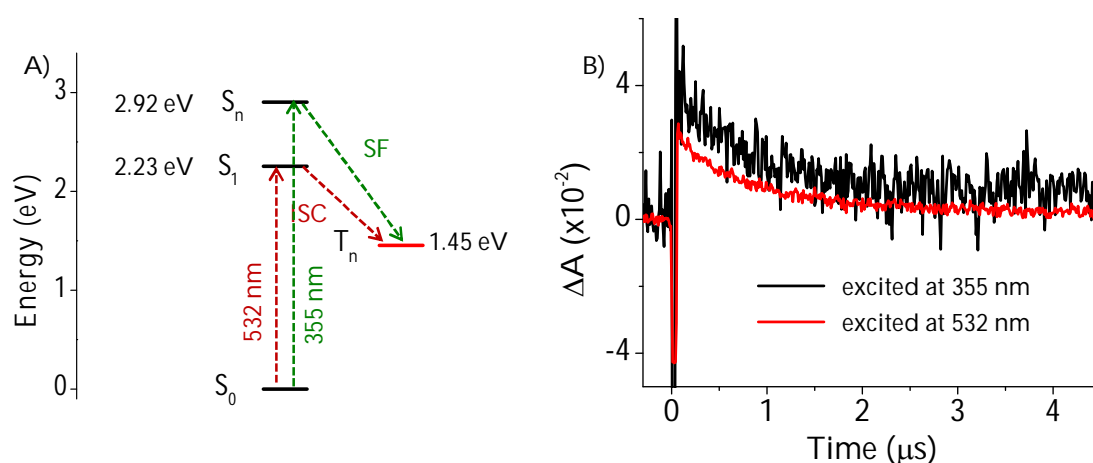


Figure 2.9. A) calculated singlet and triplet energy levels (ISC- intersystem crossing; SF- singlet fission); B) triplet state decay kinetics of PDI-Br₄ in polycrystalline thin film monitored at 600 nm upon excitation with 355 and 532 nm.

may promote SF mediated triplet population in thin film of PDI-Br₄. Absence of quantitative SF in PDI-Br₄ thin film could arise due to i) less efficient SF and/or ii) significant triplet-triplet annihilation process as reported earlier[74]. fTA measurements in polycrystalline thin film of PDI-Br₄ could not identify the existence of charged intermediates ruling out the possibility of triplet formation via charge recombination, consistent with the polycrystalline thin film of N,N bis(n-octyl)-2,5,8,11-tetraphenyl-PDI reported by Wasielewski and coworkers[26, 41].

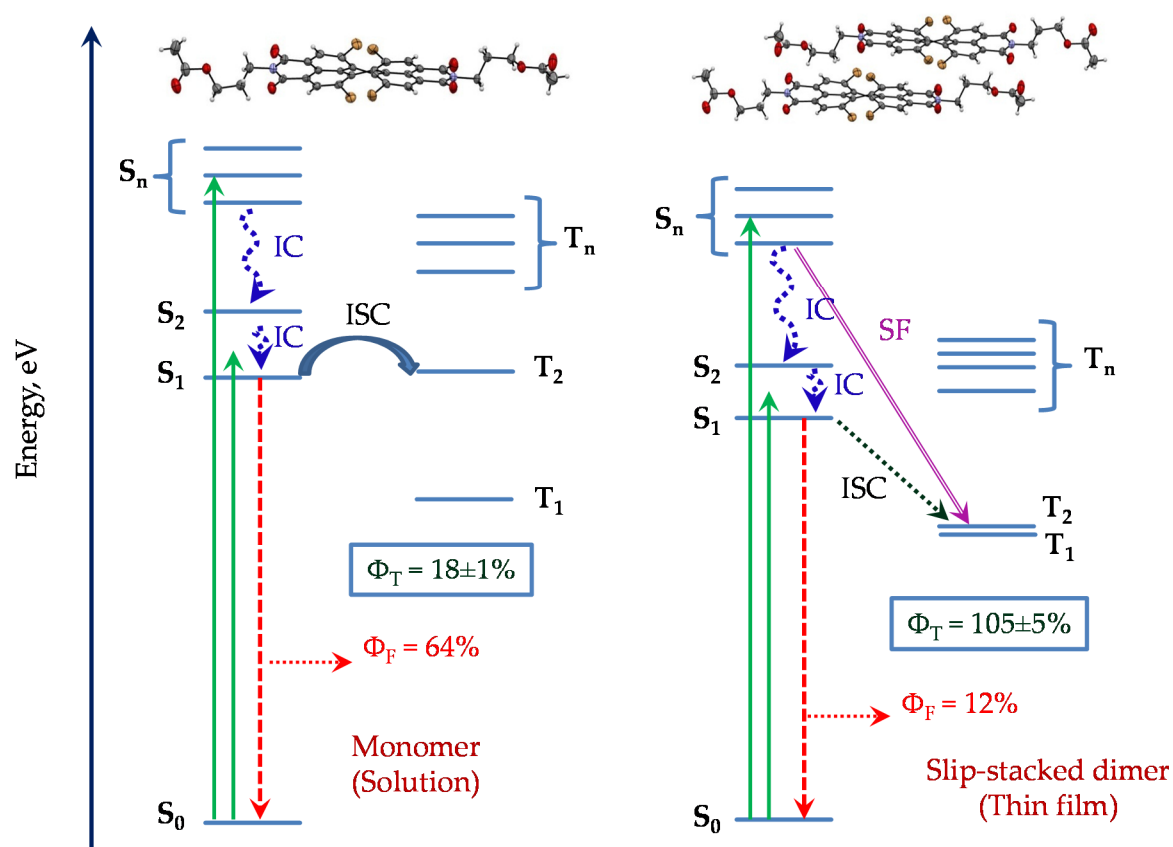


Figure 2.10. Plausible Jablonski diagram of PDI-Br₄ in monomer and polycrystalline thin film; energy levels are calculated from TDDFT (B3LYP/LANL2dz) method. (IC - internal conversion; ISC - intersystem crossing; SF - singlet fission; Φ_F - fluorescence quantum yield; Φ_T - triplet quantum yield; Reprinted with permission from ref. 82. Copyright © 2016, American Chemical Society).

To further confirm the existence of SF process, qualitative estimation of triplet generation in optically matched neat and polymethylmethacrylate (PMMA) blend thin films were carried out. nTA spectra of PMMA blend PDI-Br₄ film exhibits reduced triplet generation when compared to the neat film. Marginally longer lifetime ($\tau_{T(\text{PMMA})}=850$ ns) of PDI-Br₄ triplet in blend film when compared to the neat film ($\tau_T=700$ ns) could arise from the stabilization of triplet excited state in PMMA matrix, as reported earlier[104]. In the presence of PMMA, decrease in triplet generation could be attributed to the frustration of the interaction of the PDI-Br₄ chromophores in the blend film, thereby reducing the efficiency of SF mediated triplet generation.

2.4. Conclusions

In conclusion, we have studied the effect of bromination at the bay region on the photophysical properties of PDI in solution (monomeric) and polycrystalline state. We observed a triplet quantum yield of $19\pm 1\%$ for core-twisted PDI-Br₄ monomer (Figure 2.10A). Core-twist induced asymmetry in the molecular geometry and energetically accessible T_n levels are attributed to the observed triplet generation. Existence of slip stacked arrangement and suitable singlet-triplet energy levels [$E(S_m) \geq 2E(T_n)$; where $m \geq n$] resulted in SO and SF mediated triplet generation ($\Phi_T = 105\pm 5\%$) in polycrystalline PDI-Br₄ thin-film (Figure 2.10). Higher excited state population facilitates exergonic SF mediated triplet generation in polycrystalline thin-film of core-twisted PDI-Br₄. Core-twisted PDI could be a potential candidate

for energy conversion devices due to its retention/generation of triplet excited state in polycrystalline thin-film state.

2.5. Experimental section

2.5.1. Synthesis and characterisation

Synthesis of PTCDA-Br₁₋₄: 7.5 g of perylene-3,4,9,10-tetracarboxylic dianhydride (PTCDA) was stirred with 80 mL of concentrated sulphuric acid for 4 hours. 500 mg of elemental iodine was added and the reaction mixture was heated to 110°C. 1/ 2/ 3 or 4 equivalents of elemental bromine was added drop wise to synthesise mono, di, tri and tetra bromo PTCDA. The reaction mixture was refluxed for 24 hours. After 24 hours, the product was precipitated by pouring the reaction mixture into 200 mL of ice water. The product (PTCDA-Br₁₋₄) was filtered and dried in hot air oven. Owing to the insolubility of the compounds, they were taken for next step of synthesis without any characterisation.

Synthesis of PDI-Br₀₋₄: 7.5 g of PTCDA/PTCDA-Br₁₋₄ was taken in 75 mL of N,N-dimethylacetamide and 75 mL of 1,4-dioxane and stirred for 30 minutes. 2.2 equivalents of 3-aminopropanol was added dropwise into the reaction mixture at 80°C. The reaction mixture was refluxed at 110 °C for 2 hours. After 2 hours, the reaction mixture was cooled to room temperature and poured into 200 mL of ice water. Precipitated product was filtered and dried in hot air oven. The imidisation was confirmed by IR spectroscopic technique by monitoring the C=O stretching. IR (KBr, cm⁻¹): 3397, 1694, and 1651. The dried product was acetylated by treating with excess equivalent of acetic anhydride in dried pyridine. The final products PDI-Br₀₋₄ were purified by column chromatography. All the products have been characterised by spectroscopic and analytical techniques.

PDI (yield = 50 %). M.p. > 300 °C. ¹H NMR [500 MHz, CDCl₃, δ]: 8.58 (d, J= 7.50 Hz, 4H), 8.49 (d, J = 7.50 Hz, 4H), 4.28 (t, J = 6.5 Hz, 4H), 4.16 (t, J = 6.15 Hz, 4H), 2.08 (m,

4H), 1.99 (s, 6H). ^{13}C NMR [125 MHz, CDCl_3 , δ]: 170.22, 159.51, 135.84, 131.20, 131.05, 129.42, 126.36, 124.65, 60.73, 39.34, 26.27, 20.92. IR (KBr, cm^{-1}): 1732, 1694 and 1657. Elemental analysis: calcd. value for $\text{C}_{34}\text{H}_{26}\text{N}_2\text{O}_8$: 69.15% C, 4.44% H and 4.74% N; found: 69.05% C, 4.50% H and 4.65% N. HRMS (ESI) m/z calculated for $\text{C}_{34}\text{H}_{26}\text{N}_2\text{O}_8$ $[\text{M}]^+$: 590.5788, found: 590.6107.

PDI-Br (yield = 30 %). M.p. > 300 °C. ^1H NMR [500 MHz, CDCl_3 , δ]: 9.69 (d, J = 8.00 Hz, 1H), 8.81 (s, 1H), 8.60 (m, 3H), 8.48 (d, J = 8.00 Hz, 2H), 4.27 (m, 4H), 4.15 (m, 4H), 2.08 (m, 4H), 1.99 (s, 6H). ^{13}C NMR [125 MHz, CDCl_3 , δ]: 170.48, 159.67, 140.45, 135.70, 133.20, 131.86, 131.24, 131.08, 129.47, 128.17, 127.33, 126.82, 124.71, 124.04, 60.85, 39.42, 26.43, 20.84. IR (KBr, cm^{-1}): 1735, 1693 and 1653. Elemental analysis: calcd. value for $\text{C}_{34}\text{H}_{25}\text{BrN}_2\text{O}_8$: 61.00% C, 3.76% H and 4.18% N; found: 61.15% C, 3.68% H and 4.14% N. HRMS (ESI) m/z calculated for $\text{C}_{34}\text{H}_{25}\text{BrN}_2\text{O}_8$ $[\text{M}]^+$: 669.4749, found: 669.5005.

PDI-Br₂ (yield = 70 %). M.p. > 300 °C. ^1H NMR [500 MHz, CDCl_3 , δ]: 9.41 (d, J = 8.20 Hz, 2H), 8.84 (s, 2H), 8.62 (d, J = 8.20 Hz, 2H), 4.25 (t, J = 7.1 Hz, 4H), 4.11 (t, J = 6.10 Hz, 4H), 2.04 (m, 4H), 1.95 (s, 6H). ^{13}C NMR [125 MHz, CDCl_3 , δ]: 171.09, 162.40, 138.11, 133.16, 132.98, 130.16, 129.31, 128.61, 126.98, 123.04, 122.62, 120.90, 62.20, 37.86, 27.34, 20.95. IR (KBr, cm^{-1}): 1733, 1698 and 1670. Elemental analysis: calcd. value for $\text{C}_{34}\text{H}_{24}\text{Br}_2\text{N}_2\text{O}_8$: 54.57% C, 3.23% H and 3.74% N; found: 54.68% C, 3.29% H and 3.61% N. HRMS (ESI) m/z calculated for $\text{C}_{34}\text{H}_{24}\text{Br}_2\text{N}_2\text{O}_8$ $[\text{M}]^+$: 748.3710, found: 748.3754.

PDI-Br₃ (yield = 60 %). M.p. > 300 °C. ^1H NMR [500 MHz, CDCl_3 , δ]: 9.37 (d, J = 8.05 Hz, 1H), 8.85 (s, 1H), 8.75 (d, J = 1.50 Hz, 2H), 8.64 (d, J = 8.05 Hz, 1H), 4.26 (m, 4H), 4.13 (m, 4H), 2.06 (m, 4H), 1.99 (s, 3H), 1.98 (s, 3H). ^{13}C NMR [125 MHz, CDCl_3 , δ]: 170.05, 159.14, 136.27, 132.67, 130.81, 130.25, 129.04, 128.55, 128.32, 127.50, 124.24, 123.57, 60.44, 39.13, 25.78, 20.46. IR (KBr, cm^{-1}): 1738, 1701 and 1662. Elemental analysis: calcd. value for $\text{C}_{34}\text{H}_{23}\text{Br}_3\text{N}_2\text{O}_8$: 49.36% C, 2.80% H and 3.39% N; found:

49.18% C, 2.92% H and 3.30% N. HRMS (ESI) m/z calculated for $C_{34}H_{23}Br_3N_2O_8$ $[M]^+$: 827.2610, found: 827.2967.

PDI-Br₄ (yield = 35 %). M.p. > 300 °C. ¹H NMR [500 MHz, CDCl₃, δ]: 8.75 (s, 4H), 4.26 (t, J = 7.05 Hz, 4H), 4.13 (t, J = 6.25 Hz, 4H), 2.04 (m, 4H), 1.8 (s, 6H). ¹³C NMR [125 MHz, CDCl₃, δ]: 171.06, 162.20, 136.21, 131.81, 131.45, 124.05, 122.55, 62.09, 37.99, 27.36, 20.93, IR (KBr, cm⁻¹): 3041, 1675 and 1249. Elemental analysis: calcd. value for $C_{34}H_{22}Br_4N_2O_8$: 45.07% C, 2.45% H and 3.09% N; found: 45.18% C, 2.60% H and 3.05% N. HRMS (ESI) m/z calculated for $C_{34}H_{22}Br_4N_2O_8$ $[M]^+$: 906.1631, found: 906.1724.

2.6. Appendix

2.6.1. Materials and methods:

All chemicals were obtained from commercial suppliers and used as received without further purification. All reactions were carried out in oven-dried glassware prior to use and wherever necessary. All reactions were performed under dry nitrogen in dried, anhydrous solvents using standard gastight syringes, cannulae, and septa. Solvents were dried and distilled by standard procedures. TLC analyses were performed on precoated aluminum plates of silica gel 60 F254 plates (0.25 mm, Merck) and developed TLC plates were visualized under short and long wavelength UV lamps. Column chromatography was performed using silica gel of 200-400 mesh employing a solvent polarity correlated with the TLC mobility observed for the substance of interest. Yields refer to chromatographically and spectroscopically homogenous substances. Melting points were obtained using a capillary melting point apparatus and are uncorrected. IR spectra were recorded on a Shimadzu IRPrestige-21 FT-IR spectrometer as neat thin films between NaCl plates in case of liquids and as KBr pellets in the case of solids. ¹H and ¹³C NMR spectra were measured on a 500 MHz and 125 MHz Bruker advanced DPX spectrometer respectively. Internal standard used for ¹H and ¹³C NMR is 1,1,1,1-tetramethyl silane (TMS). All CHN analyses were carried out on an Elementar vario MICRO cube

Elemental Analyzer. All values recorded in elemental analyses are given in percentages. High Resolution Mass Spectra (HRMS) were recorded on a Agilent 6538 Ultra High Definition (UHD) Accurate-Mass Q-TOF-LC/MS system using either atmospheric pressure chemical ionization (APCI) or electrospray ionization (ESI) mode. Thin film samples were prepared by spin-coating saturated chloroform solution of PDI-Br_{0.4} on quartz plate.

2.6.2. X-ray crystallography:

High-quality specimens of appropriate dimensions were selected for the X-ray diffraction experiments. Crystallographic data collected are presented in the supplementary information. Single crystals were mounted using oil (Infineum V8512) on a glass fibre. All measurements were made on a CCD area detector with graphite monochromated Mo K α radiation. The data was collected using Bruker APEXII detector and processed using APEX2 from Bruker. All structures were solved by direct methods and expanded using Fourier techniques. The non-hydrogen atoms were refined anisotropically. Hydrogen atoms were included in idealized positions, but not refined. Their positions were constrained relative to their parent atom using the appropriate HFIX command in SHELXL-97. The full validation of CIFs and structure factors of PDI-Br_{2.4} were performed using the CheckCIF utility and found to be free of major alert level. 3D structure visualization and the exploration of the crystal packing of PDI-Br_{2.4} were carried out using Mercury 3.1. Percentage (%) overlap was calculated from area of overlapped moieties of perylenediimide aromatic rings in the crystal structures. Percentage of overlapped aromatic surface area to total aromatic surface area gives the % overlap[105].

2.6.3. Spectral measurements:

Absorption spectra were recorded in Shimadzu UV-3600 UV-Vis-NIR while emission (fluorescence/phosphorescence) and excitation spectra were performed in

Horiba Jobin Yvon Fluorolog spectrometer. All spectroscopic experiments were performed by using standard quartz cuvettes of path length 1cm for solution in dried and distilled solvents. The solution state fluorescence quantum yields were determined by using optically matched solutions. Fluorescein dissolved in ethanol ($\Phi_{fl} = 79\%$)[106] was used as the standard. The fluorescence quantum yield was calculated as follows,

$$\Phi = \Phi_R \times \frac{I}{I_R} \times \frac{A_R}{A} \times \frac{\eta^2}{\eta_R^2} \quad \text{---(2.1)}$$

Phosphorescence measurement was performed in Quartz tube in chloroform/ethyl iodide solid glasses at 77K in Horiba Jobin Yvon Fluorolog spectrometer. During the measurement, time per flash was 61 and delay after the flash was 0.05 ms.

The solid state quantum yield of model derivative PDI and PDI-Br₁₋₄ were measured using an integrating sphere for which the accuracy was verified using tris(8-hydroxyquinolate)aluminium (Alq₃) as a standard and is determined to be $37 \pm 4 \%$ (reported quantum yield $\Phi_{fl} = 40\%$)[107]. Fluorescence decay measurements were carried out in an IBH picosecond single photon counting system. The excitation laser used was 439 nm with a pulse width of less than 100 ps. The fluorescence decay profiles were deconvoluted using IBH data station software version 2.1 and fitted, minimizing the χ^2 values of the fit to 1 ± 0.05 .

2.6.4. Femtosecond transient absorption measurement (fTA):

Spectra-physics Tsunami Oscillator (80 MHz, 800 nm) was used as seed for a Spectra-Physics Spitfire Regenerative amplifier (1 KHz, 4 mJ). A fraction of the amplified output was used to generate 400 nm pump pulse. Residual 800 nm pulse was sent through a delay line inside an ExciPro pump-probe spectrometer from CDP Systems. A rotating CaF₂ plate (2 mm thickness) was used to generate continuum of white light from the delayed 800 nm pulses. The continuum of white light was split

into two and the streams were used as probe and reference pulses. Transient absorption spectra were recorded using a dual diode array detector with a 200 nm detection window. Sample solutions were prepared in a rotating sample cell with 400 μm path length. IRF was determined by solvent (10% Benzene in Methanol) two photon absorption and was found to be approximately 130 fs at about 530 nm. Energy per pulse incident on the sample is attenuated employing 80% neutral density filter when required. Toluene solution of the derivatives PDI-Br₁₋₄ and the model derivative PDI were pumped with 400 nm laser and probed by the white light[108].

2.6.5. Nanosecond transient absorption measurement (nTA):

Laser flash photolysis experiments of the argon purged solutions were carried out in an Applied Photophysics Model LKS-60 laser kinetic spectrometer using the second and third harmonic (355 nm and 532 nm, pulse duration ≈ 10 ns) of a Quanta Ray INDI-40-10 series pulsed Nd:YAG laser. Triplet states of the PDI-Br₀₋₄ in toluene were confirmed using the measurement of oxygen purged solutions through nanosecond flash photolysis studies. Triplet quantum yields[51] upon direct photoexcitation (532 nm) were determined by using [Ru(bpy)]C₁₂ in methanol as standard ($\Phi_T = 100\%$), with non-saturating laser intensities. Equal volume of 0.2 m solution of β -carotene was added to optically matched solutions of reference and the sample. The equation for the triplet quantum yield is given by,

$$\Phi_T^S = \Phi_T^{Ref} \times \frac{\Delta A^S}{\Delta A^{Ref}} \times \frac{k_{obs}^S}{k_{obs}^S - k_0^S} \times \frac{k_{obs}^{Ref} - k_0^{Ref}}{k_{obs}^{Ref}} \quad \text{---(2.2)}$$

Where, Φ_T^S and Φ_T^{Ref} denote the triplet quantum yield of the sample and reference respectively; ΔA^S and ΔA^{Ref} are transient absorption intensity of β -carotene in sample and reference respectively; k_{obs}^S and k_0^S are decay rate of sample transient species before and after the addition of β -carotene. k_{obs}^{Ref} and k_0^{Ref} are decay rate of reference transient species before and after the addition of β -carotene.

The triplet energy of the PDI-Br₄ was estimated from rate constants for triplet energy transfer by using the Sandros relation[109] given in the following equation,

$$k_Q = k_{diff} (1 / (1 + \exp(-\frac{\Delta E_T}{kT}))) \quad \text{---(2.3)}$$

where k_Q is the bimolecular rate constant for energy transfer, k_{diff} is the diffusion-limited value of k_Q , and ΔE_T is the triplet energy difference between the donor and acceptor. The values of k_Q were obtained from the slopes of the pseudo-first-order decay rate constant (k_{obs}) of the donor triplet versus the concentration of acceptor according to the following equation

$$k_{obs} = k_0 + k_Q(\text{acceptor}) \quad \text{---(2.4)}$$

where k_0 is the first-order rate constant for decay of the donor triplet in the absence of acceptor. β -carotene and Ru(bpy)₃Cl₂ were used as triplet energy acceptor whereas anthracene, phenanthrene and coronene were used as triplet energy donor in the study with PDI-Br₄.

2.6.5.1. Relative triplet yield calculation in solution:

Triplet quantum yield on exciting at 532 nm = 18±1%

Transient absorption on exciting at 355 nm = 0.03

Transient absorption on exciting at 532 nm = 0.1444

Ground state absorption at 355 nm = 0.0199

Ground state absorption at 532 nm = 0.21

$$\varphi_{T(355\text{ nm})} = \varphi_{T(532\text{ nm})} \times \frac{\Delta A_{355\text{ nm}}}{\Delta A_{532\text{ nm}}} \times \frac{A_{532\text{ nm}}}{A_{355\text{ nm}}}$$

$$\varphi_{T(355\text{ nm})} = ((18\pm 1) \times 0.03 \times 0.1444) / (0.21 \times 0.0199) = 19\pm 1\%$$

2.6.5.2. Triplet yield calculation for singlet fission:

Film thickness : 60±5 nm,

Spot size : 0.785 cm²

Unit cell volume: 1583 Å³

Formula units/cell: 2

Excitation wavelength: 532 nm

Excitation pulse energy: 2±0.1 mJ

Absorbance at 532 nm: 0.195±0.004

Absorbance maximum: 0.240±0.004 @ 550 nm

$$\xi = \frac{E \cdot \lambda \cdot K \cdot (1-10^{-A})}{l \cdot a} \quad \text{---(2.5)}$$

$$\xi = \frac{0.002 \text{ J} \cdot 532 \text{ nm} \cdot 5.034 \times 10^{15} \text{ J}^{-1} \text{ nm}^{-1} \cdot (1 - 10^{-0.195})}{60 \times 10^{-7} \cdot 0.785 \text{ cm}^2}$$

$$\xi = (4.1132 \pm 0.05) \times 10^{20}$$

Number of density = 2 molecules / 1.583 x 10⁻²¹ cm³ = 1.263 x 10²¹

ξ / no. of density = 0.3256± 0.01

Expected bleach = -(0.3256± 0.01) x (0.240 ± 0.004) = -0.0782±0.002

Observed bleach = 0.0616±0.004

Number of ground state molecule lost = 0.0616 / 0.0782 = 79±5 %

2.6.5.3. Relative triplet yield calculation in polycrystalline thin film:

Triplet quantum yield on exciting at 532 nm = 79±5%

Transient absorption on exciting at 355 nm = 0.01

Transient absorption on exciting at 532 nm = 0.028

Ground state absorption at 355 nm = 0.0371

Ground state absorption at 532 nm = 0.1386

$$\varphi_{T(355 \text{ nm})} = \varphi_{T(532 \text{ nm})} \times \frac{\Delta A_{355 \text{ nm}}}{\Delta A_{532 \text{ nm}}} \times \frac{A_{532 \text{ nm}}}{A_{355 \text{ nm}}}$$

$$\varphi_{T(355 \text{ nm})} = ((79 \pm 5) \times 0.01 \times 0.1386) / (0.028 \times 0.0371) = 105 \pm 5\%$$

2.6.6. Computational methods:

2.6.6.1. Gaussian calculations

Ground-state optimised structure and harmonic oscillator frequencies were computed using density functional theory (DFT) at the Becke's three parameter functional in combination with the Lee-Yang-Parr correlation functional (B3LYP) and 6-31+G(d,p) basis set. Vertical excitation energies and oscillator strengths were calculated employing time dependent DFT (TD-DFT) at the B3LYP/6-311+G(d,p) level of theory. Vertical excitation energy and oscillator strength for the slip stacked dimer were calculated from TD-DFT at the B3LYP/LANL2dz level of theory. All computations were performed with the Gaussian 09 program suite[110].

2.6.6.1. Quantum theory of atoms in molecules (QTAIM):

The wave function for the derivative PDI-Br₃₋₄ are obtained employing the geometries taken from the crystal structure using Gaussian set of codes at B3LYP/6-31+G(d,p) level. Quantum theory of atoms in molecules (QTAIM) analysis aims at understanding the description of interatomic interaction in the single crystal X-ray structure. A bond is defined along the bond line between two nuclei, called a bond path, along which electron density is concentrated. In a three dimensional space there are four types of critical points, corresponding to non-degenerate points: termed (3, -3), (3, -1), (3, +1) and (3, +3). The (3, -3) and (3, +3) types represent a maximum (which corresponds to a nuclear position) and a minimum, respectively. While (3, -1) and (3, +1) types represent saddle points called bond critical points and the ring critical points, respectively. The bond critical point (BCP) is a point along the bond path at the interatomic surface, where the shared electron density reaches a minimum. The physical characteristics of the BCPs [the electron density at BCP, $\rho(r_{BCP})$, and its Laplacian, $\nabla^2\rho(r_{BCP})$] reveal the approximate measure of the amount of electron density built up in the bonding region and as such could be taken as characteristic of the bond. When $\nabla^2\rho(r_{BCP}) < 0$ and is large in magnitude, $\rho(r_{BCP})$ is also large which means that there is a concentration of electronic charge in

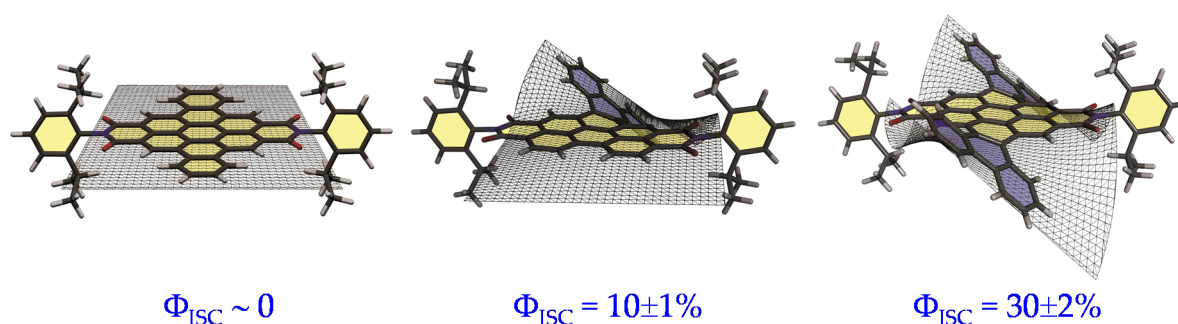
the internuclear region. This is also an indication of a sharing of electronic charge between both nuclei that defines the covalent (polar) bond. When $\nabla^2\rho(r_{\text{BCP}}) < 0$ there is a depletion of electronic charge in the internuclear region. Using the AIM 2000 software package, the electron density was integrated over atomic basins according to the quantum theory of atoms in molecules using PROAIM, and thus the BCP data and the molecular graphs were obtained.

Chapter 3

Enhanced Intersystem Crossing in Core-Twisted Aromatics

Abstract

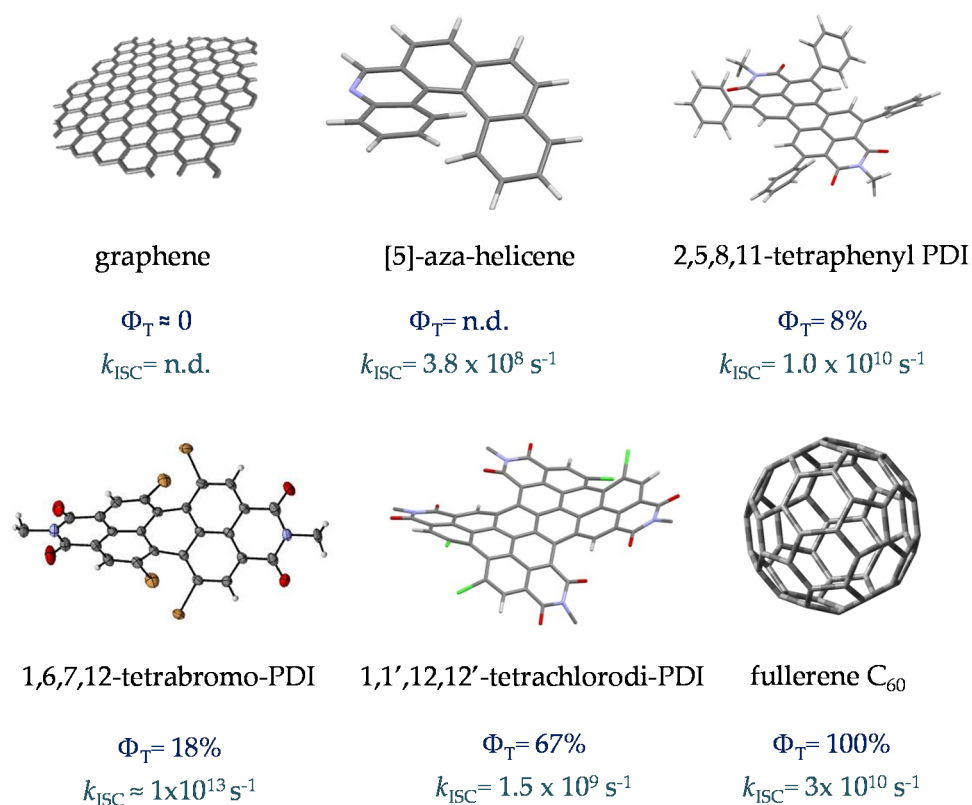
We describe the design, bottom-up synthesis and X-ray single crystal structure of systematically twisted aromatics 1c and 2d for efficient intersystem crossing. Steric congestion at the core region creates nonplanar geometry that induces significant yield of triplet excited state in the electron poor polyaromatic hydrocarbons 1c and 2d. A systematic increase in the number of twisted regions in 1c and 2d exhibits a concomitant enhancement in the rate and yield of intersystem crossing, as monitored using femtosecond and nanosecond transient absorption spectroscopy. Twist-induced spin-orbit coupling via activated out-of-plane C-H/C=C vibrations can facilitate the formation of triplet excited state in twisted aromatics 1c and 2d, in contrast to negligible intersystem crossing in planar analog 3c. The ease of synthesis, high solubility, access to triplet excited state and strong electron affinity make such imide functionalized core-twisted aromatics as a desirable material for organic electronics.



3.1. Introduction

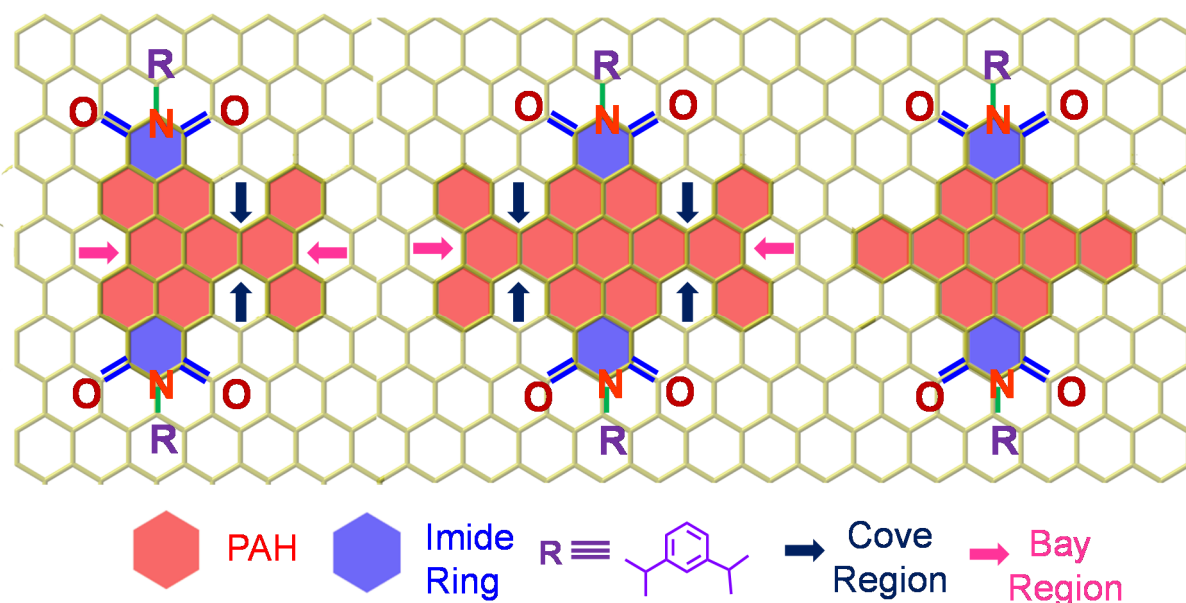
Carbon based contorted nanostructures[111] are emerging as vital components for optoelectronic devices[112], drug-delivery[113], catalysis[114] and sensors[115]. Planar nanostructures of carbon continue to attract immense interest for diverse applications[116]. Albeit low singlet-triplet energy gap, weak spin-orbit coupling (SOC) diminishes intersystem crossing (ISC) in graphene[117]. Enhancement of SOC in graphene was achieved by dilute hydrogenation[118], fluorination[119], or proximity with WS₂[120]. Graphene grown on Cu, gold intercalated graphene grown on Ni[121] and Pb intercalated graphene grown on Ir[122] show strong SOC (ca. 20-100 meV). Heavy adatoms (with partially filled p orbitals) deposited on the graphene lattice, also induce large intrinsic SOC[123]. Hydrogenation of graphene generates non-planar sp³ sites that are responsible for the induced SOC whereas other adatoms exhibit heavy atom effect in promoting the ISC in graphenoid structures. Interestingly, curvature dependent excited state properties such as ISC were observed in fullerene derivatives[124]. State-of-the-art theoretical and experimental investigations validate the importance of twist/nonplanarity in enhancing the SOC in graphenoid structures[125-126]. Systematic incorporation of twist in heavy atom free[127] sp² hybridized graphenoid structure[128] (Scheme 3.1) to activate ISC has received less attention[117, 129].

Our on-going interest with core-twisted[82] organic chromophores[78, 81] prompted us to study the role of twist in the triplet formation. Recent efforts from



Scheme 3.1. Molecular Structure of non-planar chromophores studied for efficient ISC along with the carbon allotropes graphene and fullerene C₆₀; Efficiency and the rate of ISC are mentioned in the scheme.

our group on heavy atom substituted core-twisted perylene diimide showed enhancement in triplet generation[82]. To isolate the influence of twist from heavy atom effect, it is imperative to impart heavy atom free twist in the chromophoric structure. Bottom-up approach to synthesize contorted aromatics[130-134], that include hexabenzocoronene[135], hexabenzoovalene[136], dibenzotetrathienocoronene[137], octabenzocircumbiphenyl[138], dimeric[77] and oligomeric perylene diimide[139] is still an emerging area. Hydrogen-hydrogen repulsion induced steric congestion at the cove region of extended perylene diimide chromophore offered core-twisted nanographenes 1c and 2d (Scheme 3.2) having π



Scheme 3.2. Molecular Structure the core-twisted derivative 1c and 2d along with the model derivative 3c; arrows indicate cove and bay regions in the derivatives.

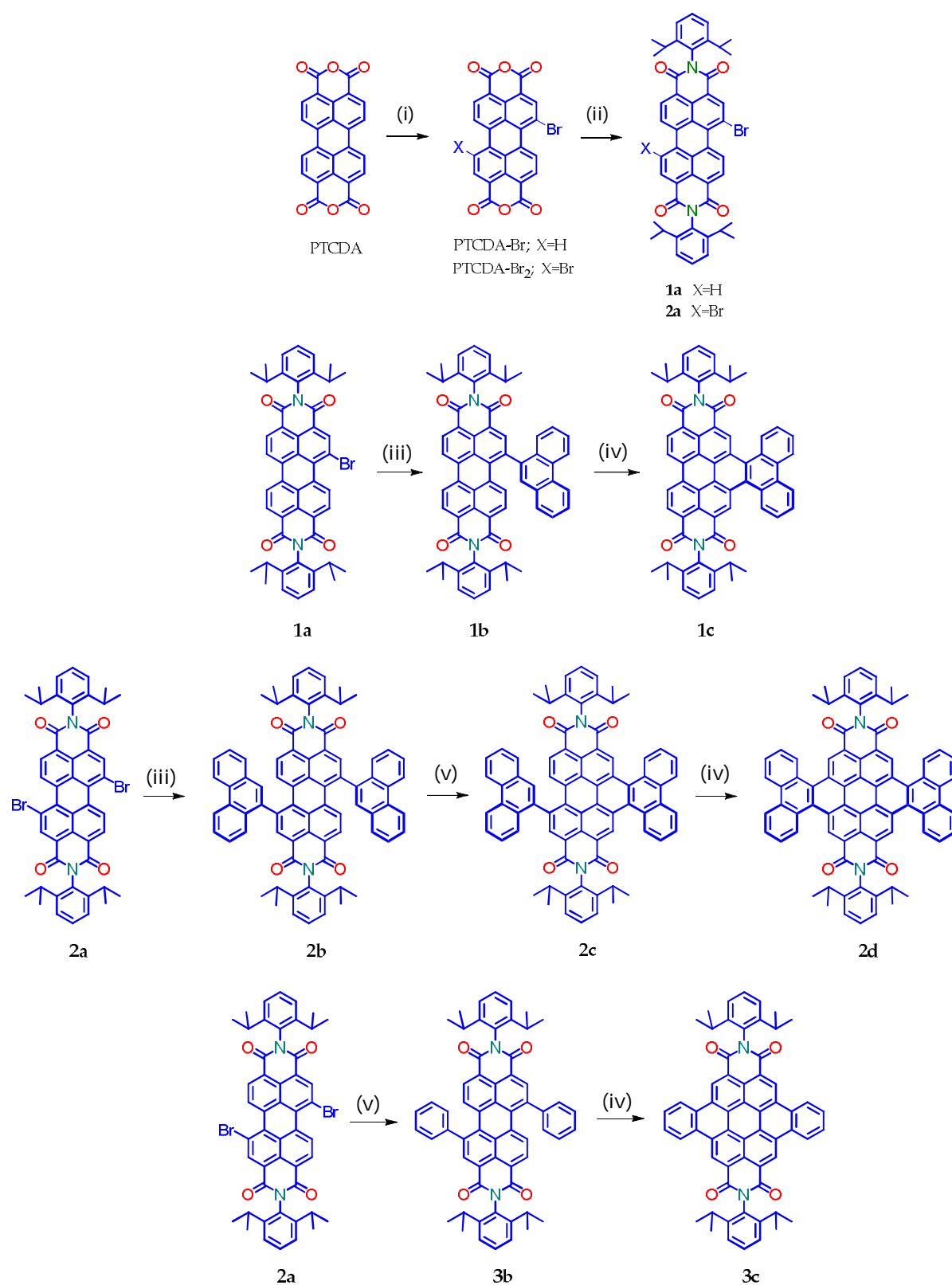
extension length of 1.1-1.6 nm. Presence of imide in the nonplanar derivatives 1c and 2d improves i) electron affinity[140], ii) access to precisely functionalized edges[141] and ii) chemical/thermal/photochemical stability[142]. We herein report the first systematic investigation on “twist-only” induced intersystem crossing ($k_{isc} = 1 \times 10^9 \text{ s}^{-1}$ for 1c and $k_{isc} = 4 \times 10^{10} \text{ s}^{-1}$ for 2d) in imide functionalized core-twisted aromatics[143]. Time-resolved absorption spectroscopic measurements display enhanced triplet quantum yield ($\Phi_T = 10 \pm 1\%$ for 1c and $\Phi_T = 30 \pm 2\%$ for 2d) in twisted aromatics when compared to negligible $\Phi_T (< 1\%)$ in the planar analog 3c.

3.2. Synthesis, characterisation and crystal structure of twisted aromatics

Synthesis: Compounds 1c and 2d were synthesized by Suzuki coupling of one and two phenanthrene units respectively with perylenediimide (PDI) followed by the metal catalyzed Scholl dehydrogenation reaction (Scheme 3.3). Bromination and

imidisation of 1 were performed by following the procedure reported elsewhere[19]. 1a and 2a were treated with one and two equivalents of 9-phenanthreneboronic acid to yield 1b and 2b respectively. Upon irradiation with sunlight in the absence and presence of iodine resulted in low yield of cyclized products (<1%). Upon exposure to 450 Watt Xenon lamp for 30 seconds at 40 °C, dilute solution (ca. 1 μ M) of 1b and 2b in toluene offered 1c and 2c respectively. At higher reactant concentration (1b and 2b), 450 Watt Xenon lamp light induced cyclization was not efficient even at elevated temperature (40-80°C). Further, 1b and 2b were subjected to Scholl reaction with FeCl₃ in dry DCM/CH₃NO₂ solution under nitrogen flow. Between 0-30 °C, cyclized products from 1b and 2b were formed in low yield (<1%). At higher temperature (40 °C), desired products 1c and 2d were obtained in 50% and 40% yield respectively under continuous nitrogen flow. Intermediate 2c (5% yield) was also isolated during the reaction and characterized by spectroscopic methods (Scheme 3.3). Model planar derivative 3c was synthesized via Suzuki coupling of two benzene units with 1,7-dibromo PDI (2a) followed by Scholl dehydrogenation reaction. Red fluorescent single crystals of 1c and 2d were obtained from chloroform and toluene solution respectively.

Crystal Structure: Compound 1c crystallized in tetragonal space group P-43 containing 4 molecules per unit cell (Table 3.1). Repulsion between H1', H8' atoms of phenanthrene unit and H2, H11 atoms of PDI unit, at the cove region (Figure 3.1) twist the chromophore 1c. The splay angles at the two cove regions of the compound



(i) Br₂/I₂, H₂SO₄, 85°C; (ii) 2,6-diisopropylaniline, imidazole, 130°C; (iii) 9-phenanthrenylboronic acid, Pd(PPh₃)₄, K₂CO₃, THF, H₂O; (iv) FeCl₃, CH₃NO₂, dichloromethane, 40°C; (v) phenylboronic acid, Pd(PPh₃)₄, K₂CO₃, THF, H₂O.

Scheme 3.3. Synthesis of the core-twisted derivatives **1c**, **2d** and the model derivative **3c**.

Table 3.1. Single crystal analysis parameter of the derivatives 1c and 2d.

	1c	2d
formula	C ₆₂ H ₄₈ N ₂ O ₄	C ₇₆ H ₅₄ N ₂ O ₄
formula wt	885.0555	1059.2530
colour, shape	Red, block	Red, Block
crystal system	Tetragonal	Triclinic
space group,	<i>P</i> -4 ₃	<i>P</i> -1
a, Å	13.9364(2)	11.4627(5)
b, Å	13.9364(2)	11.8704(5)
c, Å	34.5285(7)	15.6450(6)
α, deg	90	76.067(2)
β, deg	90	89.834(2)
γ, deg	90	72.770(10)
V, Å ³	6706.2(2)	1968.03(14)
temp, K	296	296
d _{calcd} , g/cm ⁻³	1.348	1.205
no. of reflections collected	11487	7652
no. of unique reflections	9920	3794
2 θ _{max} , deg	50	50
no. of parameters	803	472
R1, wR2 (I > 2 σ (I))	0.1013, 0.0730	0.1469, 0.0694
R1, wR2 (all data)	0.2326, 0.2046	0.2099, 0.1717
goodness of fit	1.022	1.025
CCDC number	1402604	1402605

1c are found to be 44.3° and 40.7° (Figure 3.1A and B). Compound 2d possessing wagging conformation crystallizes in triclinic space group *P*-1, having one molecule per unit cell (Table 3.1). Repulsion between H1', H8' atoms of phenanthrene units

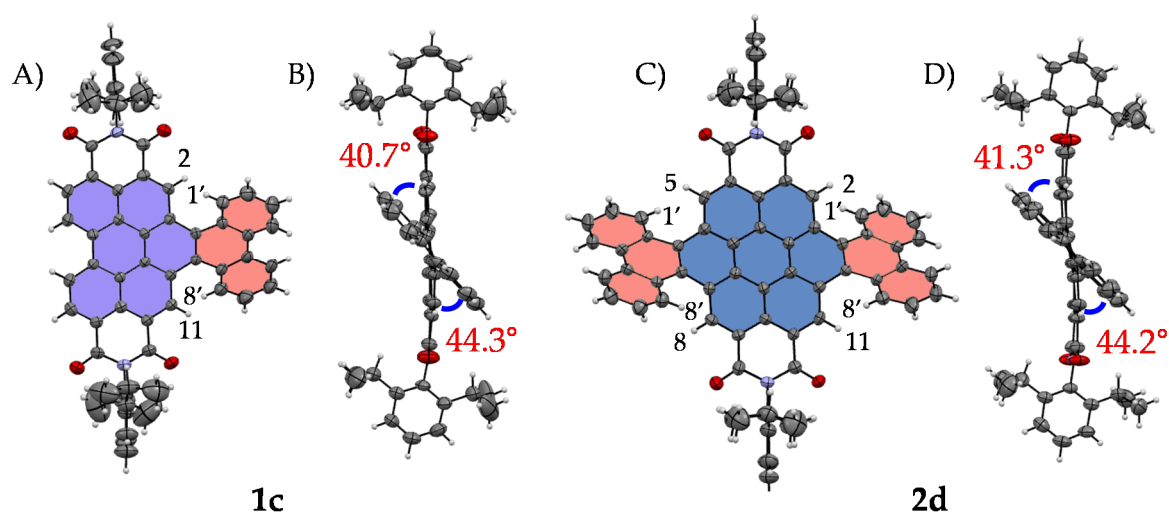


Figure 3.1. A) and C) crystal structure of the core-twisted derivatives 1c and 2d; B) and D) corresponding side view.

and the pery region hydrogen atoms (H2, H5, H8 and H11) of PDI (Figure 3.1) at the 4 core regions twist the chromophore 2d with splay angle of 44.2° and 41.3° (Figure 3.1C and D). To evaluate the thermodynamic stability between the helical vs.wagging conformation of the derivative 2d (Figure 3.2), we conducted density functional theory (DFT) calculations at the B3LYP/6-311G++(d, p) level. From the

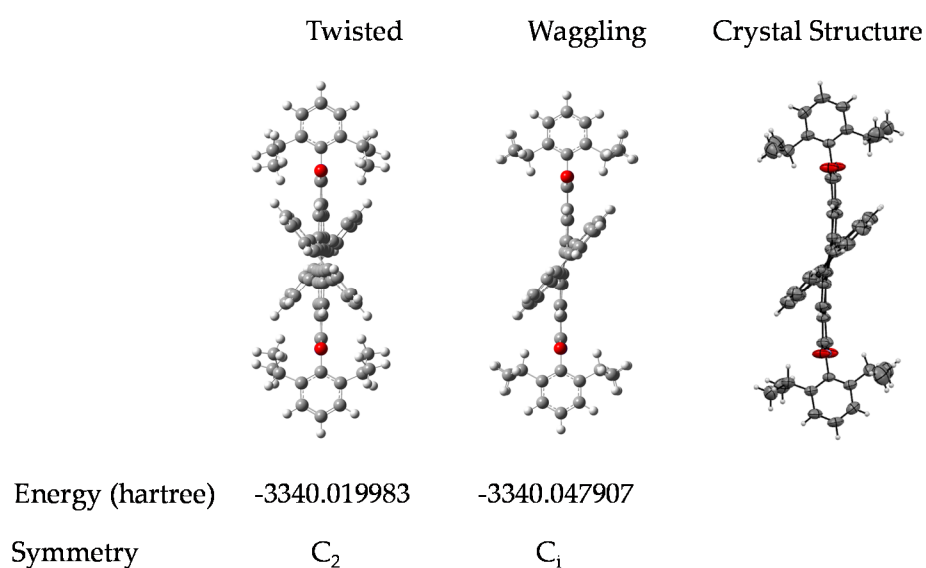


Figure 3.2. Energy optimized twisted and wagging conformation of the derivative 2d along with the corresponding crystal structure.

DFT calculations, it is estimated that the wagging conformer of 2d is thermodynamically more stable than the helical conformer by 17.5 kcal mol⁻¹ (Figure 3.2). Single crystal X-ray structure analysis of 1c and 2d revealed a contorted polycyclic skeleton having 9 and 13 aromatic rings respectively.

3.3. Results and discussions

3.3.1. Electrochemical studies

Cyclic voltammogram (0.1 M, *n*Bu₄NPF₆ in DCM) exhibited reversible reduction peaks (Figure 3.3A) at -0.69 and -0.92 V for 1c; -0.77 and -1.01 V for 2d. The reduction potential of the derivatives 1c and 2d are more negative than those of the model derivative 3c (-0.55 and -0.79 V), indicating that the 1c and 2d derivatives are significantly weaker electron acceptors. Highest occupied molecular orbital (HOMO) distribute over the whole π system of the derivatives 1c, 2d and the model derivative 3c (Figure 3.3B). In contrast, lowest unoccupied molecular orbital (LUMO) spreads only at the coronenediimide core, due to the presence of electron withdrawing imide group.

3.3.2. Photophysical characterisation in solution state

By virtue of the twisted nature, derivatives 1c and 2d with large π -surface dissolve well in common organic solvents like chloroform, dichloromethane and toluene. UV-Visible absorption spectrum (Figure 3.4A) of 1c in toluene shows peaks centered at 475, 505 and 545 nm corresponding to $\pi \rightarrow \pi^*$ (HOMO \rightarrow LUMO) transition (Figure 3.4A). Derivative 2d in toluene exhibits $\pi \rightarrow \pi^*$ transition at i) 582 and 539 nm

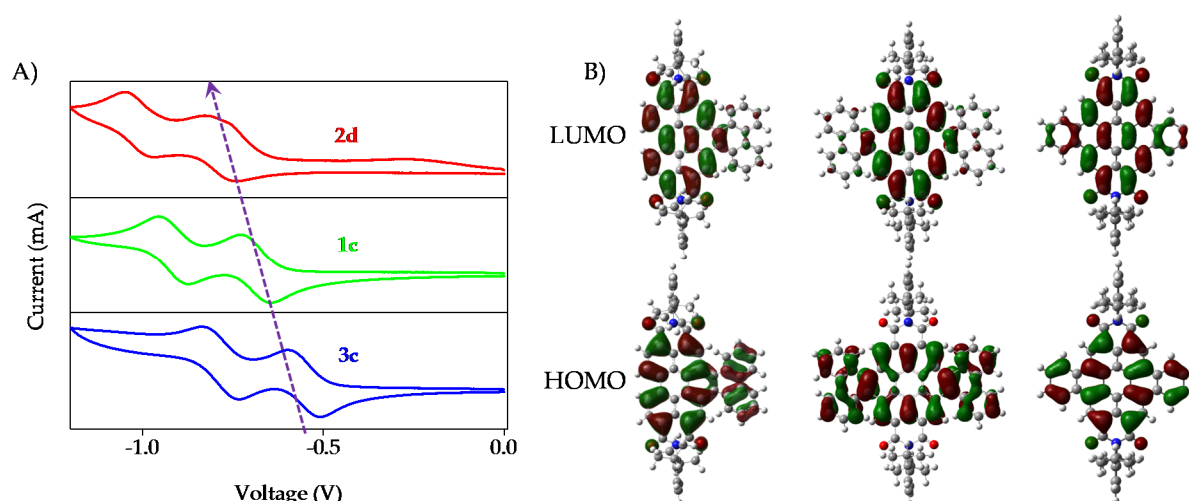


Figure 3.3. A) Cyclic voltammogram analysis of the derivatives (1 mM) 1c, 2d and 3c in dichloromethane in the presence of tetrabutylhexafluoroammoniumphosphate (100 mM) with respect to Ag/Ag⁺ electrode; B) FMO analysis obtained from the TD-DFT calculations.

corresponding to $S_0 \rightarrow S_1$ (HOMO \rightarrow LUMO); ii) 475, 445 and 416 nm due to $S_0 \rightarrow S_2$ (HOMO-1 \rightarrow LUMO); iii) 385 nm corresponding to $S_0 \rightarrow S_n$ (HOMO \rightarrow LUMO+1), in agreement with the DFT calculations (Figure 3.4A). Model derivative 3c exhibits peak centered at 460 and 490 nm corresponding to $\pi \rightarrow \pi^*$ (HOMO \rightarrow LUMO) transition as reported earlier[144]. Upon excitation at 480 nm, 1c shows vibronically resolved emission (Figure 3.4B) centered at 555, 597 and 652 nm with the fluorescence quantum yield (Φ_F) of $70 \pm 2\%$. Temperature dependent emission ($\lambda_{ex}=480$ nm) and excitation ($\lambda_{em}=600$ nm) spectra of 1b in toluene indicated the evolution of a new species having emission features identical to that of 1c (Figure 3.5A). Spectroscopic analysis confirms the photocyclization of 1b in toluene (ca. 1 μ M) at higher temperature to yield 1c. When compared to 1c, derivative 2d exhibits red-shifted emission centered at 586, 635 and 696 nm with Φ_F of $40 \pm 2\%$. Model derivative 3c show vibronically resolved emission centered at 510, 550 and 580 nm

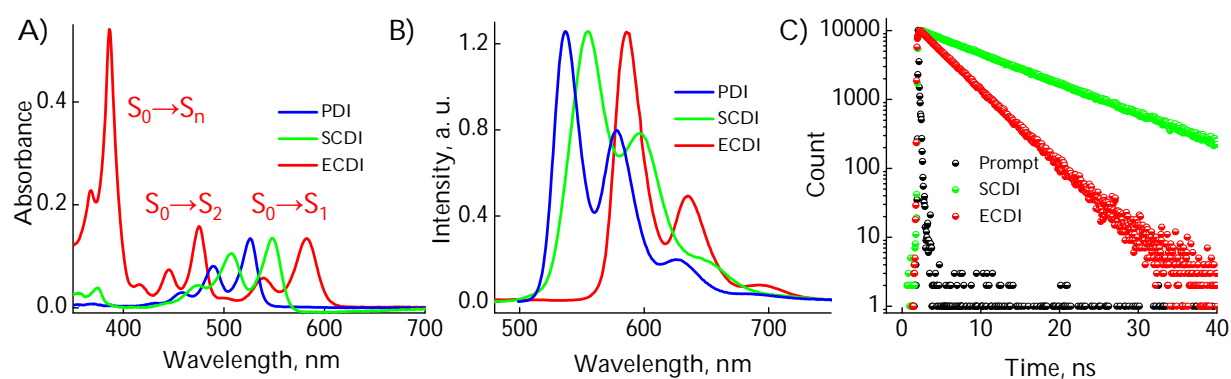


Figure 3.4. A) absorption; B) emission spectra ($\lambda_{ex} = 480$ nm); C) time dependent emission spectra ($\lambda_{ex} = 480$ nm and monitored at their emission maxima) of the derivatives 1c, 2d and 3c in toluene.

with Φ_F of $85 \pm 2\%$ (Figure 3.4B). Partial reduction in the Φ_F of 1c and 2d when compared 3c could be attributed to the non-radiative decay pathways arising from nonplanar nature of the chromophores 1c and 2d[125]. Upon excitation at 480 nm, derivative 1c and 2d in toluene exhibit fluorescence lifetime (Figure 3.4C) of 10 and 5.4 ns respectively. Model derivative 3c in toluene shows monoexponential fluorescence lifetime of 5.5 ns upon excitation with 480 nm.

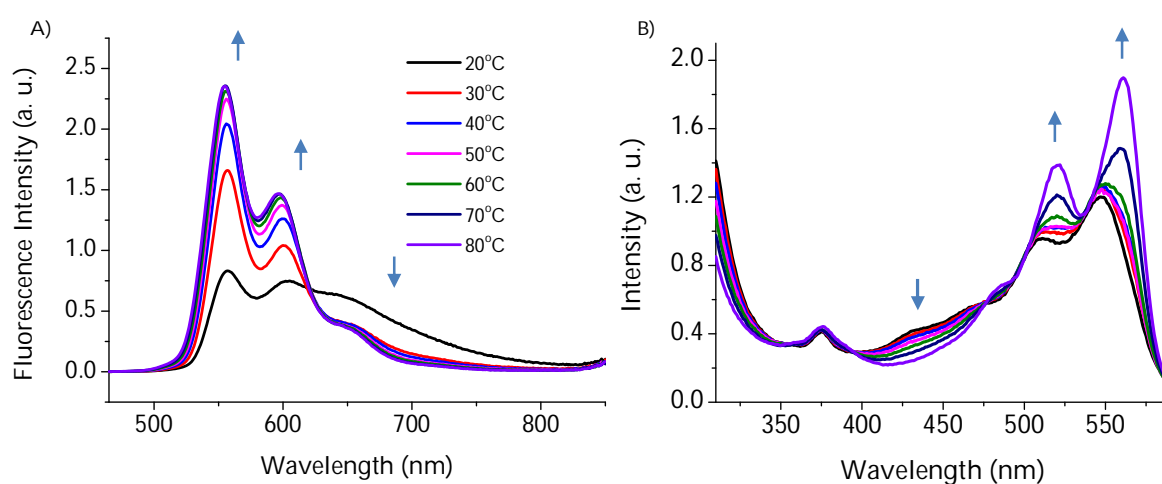


Figure 3.5. Temperature dependent A) emission ($\lambda_{ex} = 480$ nm) and B) excitation spectra ($\lambda_{em} = 600$ nm) of the derivative 1b in toluene.

3.3.3. Transient absorption measurements

3.3.3.1. Nanosecond transient absorption measurements

Further insights into the excited state deactivation in core-twisted derivatives came from nanosecond and femtosecond transient absorption measurements. Upon excitation at 355 nm, 10 ns laser pulse, 1c in toluene (Figure 3.6A) exhibited the negative absorption peaks centered at 380, 470 and 510 nm corresponding to ground state depletion ($S_0 \rightarrow S_n$). Observed twin absorption centered at 400 and 580 nm with the single exponential decay lifetime of 3.7 μs (Figure 3.6B) is attributed to triplet excited state in 1c. Compound 2d in toluene (Figure 3.6C) showed ground state

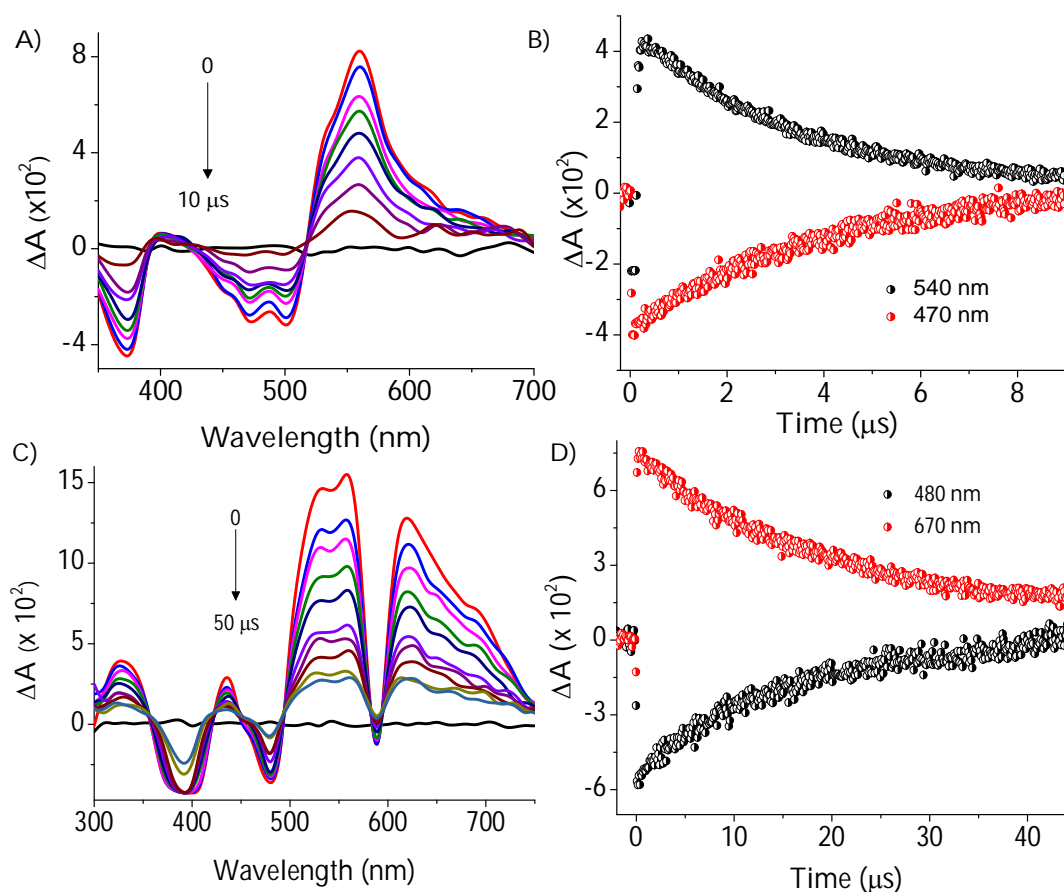


Figure 3.6. A) and C) nTA spectra of the core-twisted derivatives 1c and 2d respectively; B) and D) kinetics profile of the transient species (triplet decay and bleach recovery) in the derivatives 1c and 2d respectively in toluene upon excitation with 355 nm, 10 ns laser pulse.

depletion at 390, 480 and 590 nm, consistent with the UV-Vis absorption spectrum. Transient absorption corresponding to triplet excited state is observed at 340, 420, 560 and 610 nm with the lifetime of 19.6 μ s (Figure 3.6D). The existence of triplet excited state in 1c and 2d were further confirmed by the quenching of the transient spectra by oxygen purging.

In contrast, planar derivative 3c in toluene exhibited negligible transient absorption upon excitation at 355 nm. Triplet quantum yield (Φ_T) of 1c and 2d were calculated to be 10 \pm 1% and 30 \pm 2% respectively employing triplet-triplet energy transfer method[82]. Significant enhancement in the Φ_T of 1c and 2d when compared to the model derivative 3c is attributed to the twist induced SOC as reported earlier[129]. However, ISC was reported by Flamigni and coworkers in unsymmetrically substituted planar perylene derivatives which could be attributed to the $n\pi^*$ to $\pi\pi^*$ transition arising from the bay imidisation[57, 145].

3.3.3.2. Femtosecond transient absorption measurements

To unravel the kinetics of intersystem crossing, core-twisted derivatives 1c and 2d in toluene were excited with 110 fs, 300 nm laser pulse. Femtosecond transient absorption (fTA) spectra of 1c and 2d showed a sharp negative absorption at 600 nm, corresponding to the second harmonic of the pump laser ($2\lambda_{ex} = 600$ nm). Photoexcitation of 1c at 300 nm displayed (Figure 3.7A) negative absorption at 505 and 545 nm along with the positive absorption peaks centered at 510, 550, 630, 680 and 720 nm. Negative absorption observed at 505 and 545 nm could be attributed to

ground state depletion consistent with UV-Vis absorption spectrum. Singular value decomposition (SVD) of ΔA versus time and the wavelength based three-dimensional map of **1c** followed by global analysis yielded three principle components. Negative absorption centered at 560 nm with the lifetime of 9.5 ns is ascribed to stimulated emission. Positive absorption centered at 720 nm corresponds to $S_1 \rightarrow S_n$ transitions that decay with a lifetime of 70 ps ($k_{IC} = 0.14 \times 10^{11} \text{ s}^{-1}$) (Figure 3.7B). The rise time of emerging positive absorption peak at 630 nm is estimated to be 1 ns ($k_{ISC} = 1 \times 10^9 \text{ s}^{-1}$) and is ascribed to $T_1 \rightarrow T_n$ transition (Figure 3.7B). Upon

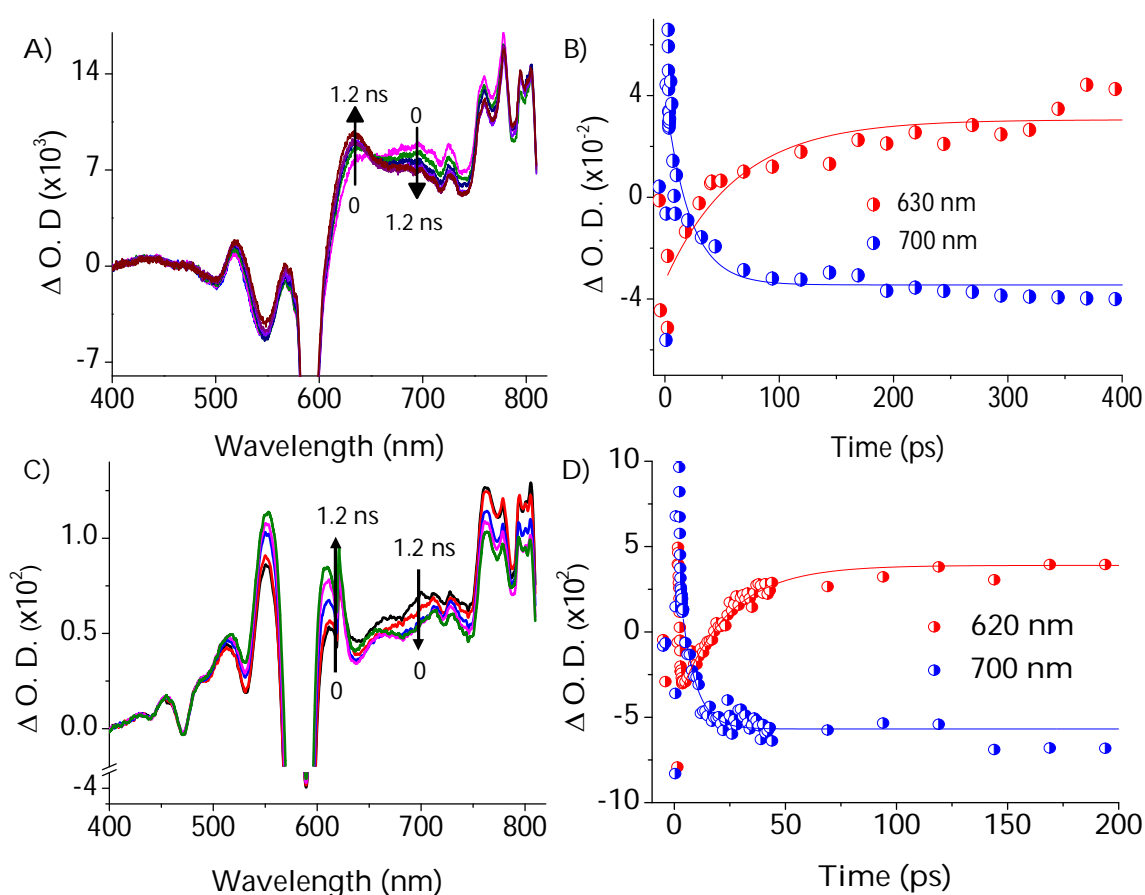


Figure 3.7. A) and C) fTA spectra of the core-twisted derivatives **1c** and **2d** respectively; B) and D) kinetics profile of the transient species (triplet and singlet decay) in the derivatives **1c** and **2d** respectively in toluene upon excitation with 300 nm, 110 fs laser pulse.

excitation at 300 nm, 2d in toluene (Figure 3.7C) showed ground state depletion at 475, 532 and 585 nm, consistent with the ground state absorption spectrum. SVD followed by global analyses of the positive absorption bands centered at 455, 516, 552 and 610-800 nm consist of three principal components. Negative absorption centered at 600 nm, with the lifetime of 5.1 ns is attributed to stimulated emission. The right singular vector at 720 nm decays with a lifetime of 6.5 ps ($k_{IC} = 1.54 \times 10^{11} \text{ s}^{-1}$) that corresponds to $S_1 \rightarrow S_n$ transition (Figure 3.7C). During the decay centered at 720 nm, concomitant appearance of a new band at 630 nm is observed (Figure 3.7D). Emerging band at 630 nm with a rise time (τ_{ISC}) of 25 ps ($k_{ISC} = 4 \times 10^{10} \text{ s}^{-1}$) is attributed to $T_1 \rightarrow T_n$ transition in the derivative 2d. According to the rates of internal conversion (k_{IC}) and intersystem crossing (k_{ISC}), the efficiency of ISC ($\phi_{ISC} = k_{ISC}/k_{IC}$) is calculated to be 7.1% and 26% for 1c and 2d respectively which is in agreement with the Φ_T calculated from the triplet-triplet energy transfer method. Quantum chemical calculations (Figure 3.8) indicate that out of plane C=C and C-H vibrations (ν_{op}) can allow efficient ISC from a $\pi\pi^*$ type singlet to $\pi\pi^*$ type triplet driven by Herzberg-Teller vibronic coupling[146].

3.4. Conclusions

In conclusion, we report the design and synthesis of solution processable electron deficient core-twisted aromatics 1c and 2d. Femtosecond and nanosecond transient absorption measurements revealed “twist-only” induced ultrafast ISC in the non-planar derivatives 1c and 2d. Enhanced out of plane C=C and C-H

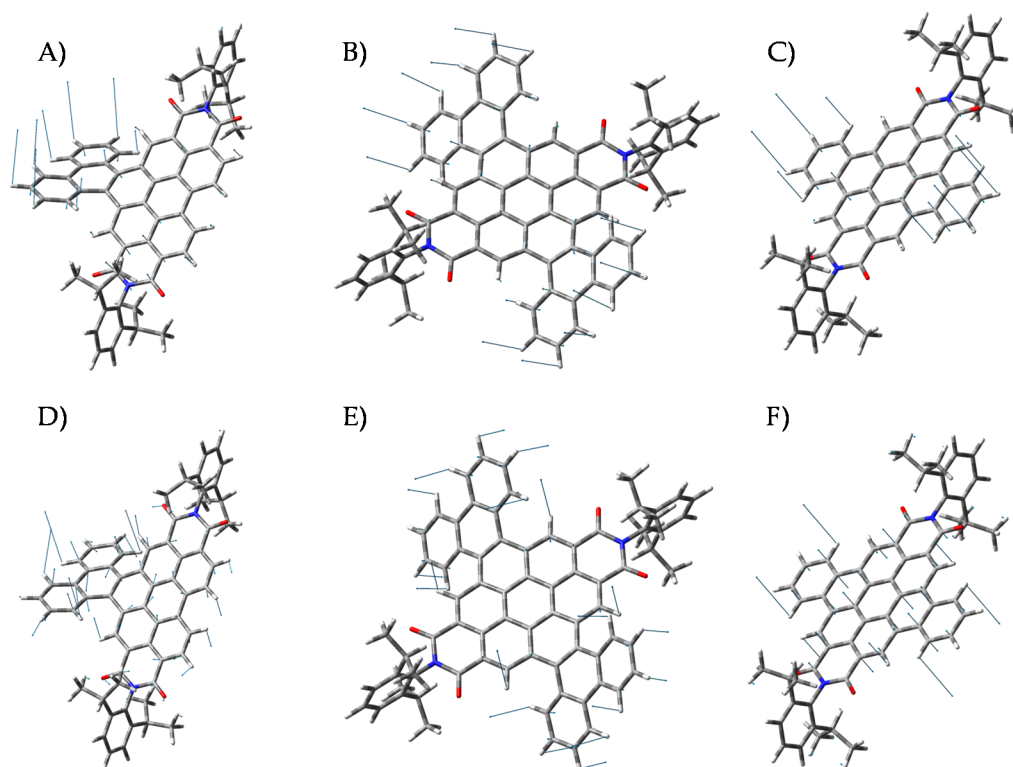


Figure 3.8. A), B) and C) out-of-plane mode C-H vibration; D), E) and F) out-of-plane mode C=C vibration in the derivatives 1c, 2d and 3c respectively (obtained from DFT calculation, Gaussian 09).

vibrations facilitate efficient ISC with Φ_T of $10 \pm 1\%$ and $30 \pm 2\%$ in the derivatives 1c and 2d respectively, driven by Herzberg–Teller vibronic coupling. Higher k_{ISC} of $4 \times 10^{10} \text{ s}^{-1}$ for doubly twisted 2d when compared to k_{ISC} of $1 \times 10^9 \text{ s}^{-1}$ for singly twisted 1c clearly establishes the role of nonplanarity in facilitating ISC. Ease of solution processability and activated triplet excited state in the twisted aromatics 1c and 2d are beneficial for photovoltaic device applications. Current efforts in our laboratory are directed towards developing twisted chromophores for high performance optoelectronic devices.

3.5. Experimental section

3.5.1. Synthesis and characterisation

3.5.1.1. Synthesis of 1a and 2a

7.5 g of PTCDA (1) was stirred with 80 mL of concentrated sulphuric acid for 4 hours. 500 mg of elemental iodine was added and the reaction mixture was heated to 85°C. 1 or 2 equivalents of elemental bromine was added drop wise to synthesise 1-bromo and 1,7-dibromo (PTCDA-Br₍₁₋₂₎) respectively. The reaction mixture was refluxed for 24 hours. After 24 hours, the product was precipitated by pouring the reaction mixture into 200 mL of ice water. The product (PTCDA-Br₍₁₋₂₎) was filtered and dried in hot air oven. Since, the product was insoluble in any solvent, subjected to imidisation reaction without further purification. 1 g PTCDA-Br₍₁₋₂₎ of were mixed with 4 g of imidazole and 3 equivalents of 2,6-diisopropylaniline under nitrogen atmosphere. Reaction mixture was refluxed at 140 °C for 12 hours. After completion of the reaction, reaction mixture is poured into the solution of 60 % ethanol and 40 % 1N HCl. Red coloured precipitate was filtered and dried in hot air oven. 1a and 2a were purified by silica column chromatographic technique using dichloromethane/petroleum ether mixture (50:50) as the eluent.

1a (yield = 30 %). M.p. > 300 °C. ¹H NMR [500 MHz, CDCl₃, δ]: 9.69 (d, J= 8.00 Hz, 1H), 8.81 (s, 1H), 8.60 (m, 3H), 8.48 (d, J= 8.00 Hz, 2H), 7.50 (m, 2H), 7.33 (m, 4H), 2.72 (m, 2H), 2.56 (m, 2H) 1.12 (m, 6H), 1.10 (m, 6H), 1.06 (m, 6H), 1.05 (m, 6H). ¹³C NMR [125 MHz, CDCl₃, δ]:170.4, 159.6, 140.4, 135.7, 133.0, 131.8, 131.2, 131.0, 129.4, 128.7, 127.3, 126.8, 124.7, 124.0, 60.8, 39.4, 26.4, 20.8. IR (KBr, cm⁻¹): 1735, 1693 and 1653. Elemental analysis: calcd. value for C₄₈H₄₁BrN₂O₄: 61.00% C, 3.76% H and 4.18% N; found: 61.15% C, 3.68% H and 4.14% N. HRMS (EI) m/z calculated for C₄₈H₄₁BrN₂O₄ [M]⁺: 669.4749, found: 669.4735.

2a (yield = 70 %). M.p. > 300 °C. ¹H NMR [500 MHz, CDCl₃, δ]: 9.41 (d, J= 8.20 Hz, 2H), 8.84 (s, 2H), 8.62 (d, J= 8.20 Hz, 2H), 7.52 (m, 2H), 7.35 (m, 4H), 2.60 (m, 4H), 1.06

(m, 24H). ^{13}C NMR [125 MHz, CDCl_3 , δ]: 171.09, 162.40, 138.11, 133.16, 132.98, 130.16, 129.31, 128.61, 126.98, 123.04, 122.62, 120.90, 62.20, 37.86, 27.34, 20.95. IR (KBr, cm^{-1}): 1733, 1698 and 1670. Elemental analysis: calcd. value for $\text{C}_{48}\text{H}_{40}\text{Br}_2\text{N}_2\text{O}_4$: 54.57% C, 3.23% H and 3.74% N; found: 54.68% C, 3.29% H and 3.61% N. HRMS (EI) m/z calculated for $\text{C}_{48}\text{H}_{40}\text{Br}_2\text{N}_2\text{O}_4$ $[\text{M}]^+$: 748.3710, found: 748.3704.

3.5.1.2. Synthesis of 1b

0.2 mmol of 1-bromoperylenediimide (1a) was dissolved in dry THF and 10 mL of 2 M potassium carbonate was added. Reaction mixture was purged with nitrogen for 15 minutes. 0.02 mmol of tetrakis(triphenylphosphine)palladium(0) and 0.25 mmol of 9-phenanthreneboronic acid were added under nitrogen atmosphere. Reaction mixture was refluxed at 65 °C under nitrogen atmosphere. After completion of the reaction, product was extracted in dichloromethane and purified by column chromatography using dichloromethane/petroleum ether mixture (60:40) as eluent. Red coloured solid was obtained as product (1b) in 50 % yield. M.p. > 300 °C. ^1H NMR [500 MHz, CDCl_3 , δ]: 8.82 (m, 4H), 8.73 (s, 2H), 8.66 (s, 1H), 8.02 (d, 1H), 7.85 (m, 3H), 7.66 (m, 4H), 7.40 (m, 3H), 7.28 (t, 2H), 7.19 (d, 2H), 2.73 (m, 2H), 2.56 (m, 2H), 1.15 (m, 6H), 1.13 (m, 6H), 1.06 (m, 6H), 1.05 (m, 6H). ^{13}C NMR [125 MHz, CDCl_3 , δ]: 163.67, 163.56, 163.29, 163.23, 145.71, 145.62, 145.50, 139.98, 139.12, 137.53, 135.57, 135.06, 134.96, 134.27, 131.83, 131.71, 131.62, 131.49, 131.44, 130.50, 130.47, 130.39, 129.75, 129.69, 129.07, 128.97, 128.22, 127.76, 127.71, 127.58, 127.55, 127.41, 127.13, 126.56, 125.55, 124.16, 124.07, 123.83, 123.40, 123.34, 123.05, 122.98, 122.48, 122.41, 31.94, 29.71, 29.27, 29.24, 29.13, 29.11, 24.07, 24.00, 23.97, 23.92, 23.91, 22.71. IR (KBr, cm^{-1}): 2960, 1705, 1668, 1591, 1497, 1458, 1339 and 1250. Elemental analysis: calcd. value for $\text{C}_{62}\text{H}_{50}\text{N}_2\text{O}_4$: 83.95% C, 5.68% H and 3.16% N; found: 84.05% C, 5.50% H and 3.15% N. HRMS (EI) m/z calculated for $\text{C}_{62}\text{H}_{50}\text{N}_2\text{O}_4$ $[\text{M}]^+$: 886.3771, found: 886.3762.

3.5.1.3. Synthesis of 1c

100 mg of 1b was dissolved in 500 mL of dry dichloromethane and heated to 40 °C under nitrogen atmosphere. A solution of 8 equivalents ferric chloride in 10 mL dry nitromethane was added dropwise into the reaction mixture under continuous nitrogen purging. The reaction mixture was refluxed at 40 °C for 1 hour. Reaction temperature was limited by the boiling point of dichloromethane. Completion of the reaction is monitored through thin layer chromatographic (TLC) technique. Then methanol was poured into the reaction mixture to stop the reaction. Reddish orange coloured product was precipitated. 1c was purified by silica column chromatographic technique using dichloromethane/petroleum ether (60:40) mixture as eluent. Yield obtained was 50 %. Compound 1c crystals were obtained from the slow evaporation of chloroform solution. M.p. > 300 °C. ¹H NMR [500 MHz, CDCl₃, δ]: 10.30 (s, 2H), 9.41 (d, 2H), 9.15 (d, 2H), 8.77 (d, 2H), 8.64 (d, 2H), 7.78 (m, 4H), 7.46 (t, 2H), 7.32 (d, 4H), 2.83 (m, 4H), 1.16 (m, 24H). ¹³C NMR [125 MHz, CDCl₃, δ]: 164.20, 164.15, 145.77, 134.95, 134.11, 131.70, 131.03, 130.82, 129.83, 129.68, 128.75, 128.54, 128.47, 128.07, 127.64, 126.68, 124.93, 124.74, 124.15, 123.43, 122.46, 122.00, 53.41, 29.70, 29.32, 24.09, 24.05. IR (KBr, cm⁻¹): 2960, 1709, 1670, 1595, 1458, 1327 and 1248. Elemental analysis: calcd. value for C₆₂H₄₈N₂O₄: 84.14% C, 5.47% H and 3.17% N; found: 84.28% C, 5.39% H and 3.21% N. HRMS (EI) m/z calculated for C₆₂H₄₈N₂O₄ [M]⁺: 884.3614, found: 884.3604.

3.5.1.4. Synthesis of 2b

0.2 mmol of 1,7-dibromoperylene-1,10-diimide (2a) was dissolved in dry THF and 10 mL of 2 M potassium carbonate was added. Reaction mixture was purged with nitrogen for 15 minutes. 0.02 mmol of tetrakis(triphenylphosphine)palladium(0) and 0.50 mmol of 9-phenanthreneboronic acid were added under nitrogen atmosphere. Reaction mixture was refluxed at 65 °C under nitrogen atmosphere. After completion of the reaction, product was extracted in dichloromethane and purified

by column chromatography using dichloromethane/petroleum ether mixture (65:35) as eluent. Red coloured solid was obtained as product (2b) in 45 % yield. M.p. > 300 °C. ^1H NMR [500 MHz, CDCl_3 , δ]: 8.84 (m, 2H), 8.78 (m, 2H), 8.68 (d, 2H), 8.15 (d, 1H), 8.01 (d, 1H), 7.94 (m, 3H), 7.88 (m, 2H), 7.81 (m, 3H), 7.73 (m, 4H), 7.63 (m, 2H), 7.54 (t, 1H), 7.46 (t, 1H), 7.36 (t, 2H), 7.20 (m, 4H), 2.62 (m, 4H), 1.04 (m, 24H). ^{13}C NMR [125 MHz, CDCl_3 , δ]: 163.69, 163.66, 163.39, 163.33, 145.63, 145.60, 145.50, 139.98, 139.12, 137.53, 135.57, 135.06, 134.96, 134.27, 131.83, 131.71, 131.62, 131.49, 131.44, 130.50, 130.47, 130.39, 129.75, 129.69, 129.07, 128.97, 128.22, 127.76, 127.71, 127.58, 127.55, 127.41, 127.13, 126.56, 125.55, 124.16, 124.07, 123.83, 123.40, 123.34, 123.05, 122.98, 122.48, 122.41, 31.94, 29.71, 29.27, 29.24, 29.13, 29.11, 24.07, 24.00, 23.97, 23.92, 23.91, 22.71 (KBr , cm^{-1}): 2960, 1732, 1694 and 1657. Elemental analysis: calcd. value for $\text{C}_{76}\text{H}_{58}\text{N}_2\text{O}_4$: 85.85% C, 5.50% H and 2.63% N; found: 85.88% C, 5.40% H and 2.65% N. HRMS (EI) m/z calculated for $\text{C}_{76}\text{H}_{58}\text{N}_2\text{O}_4$ $[\text{M}]^+$: 1062.4397, found: 1062.4367.

3.5.1.5. Synthesis of 2d

100 mg of 2b was dissolved in 500 mL of dry dichloromethane and heated to 40 °C under nitrogen atmosphere. A solution of 8 equivalents ferric chloride in 10 mL dry nitromethane was added dropwise into the reaction mixture under continuous nitrogen purging. The reaction mixture was refluxed at 40 °C for 1 hour. Aliquot of the reaction mixture was poured into methanol to stop the reaction. Red coloured precipitate was filtered and dried in hot air oven. One side cyclised product 2c was purified by column chromatographic technique using dichloromethane/petroleum ether (65:35) and characterised by ^1H NMR spectroscopy. M.p. > 300 °C. ^1H NMR [500 MHz, CDCl_3 , δ]: 10.82 (s, 2H), 8.99 (m, 2H), 8.93 (m, 2H), 7.90 (m, 4H), 7.63 (m, 3H), 7.49 (m, 4H), 7.38 (m, 3H), 7.22 (m, 4H), 7.20 (m, 2H), 7.12 (m, 2H), 3.64 (m, 2H), 2.97 (m, 2H), 1.24 (m, 24H). IR (KBr , cm^{-1}): 1748, 1709 and 1665. HRMS (EI) m/z calculated for $\text{C}_{76}\text{H}_{56}\text{N}_2\text{O}_4$ $[\text{M}]^+$: 1060.4240, found: 1060.4167. Since, very little material was isolated, further studies were not performed on this molecule. We focused to synthesise both side cyclised poly

aromatic imides. Rest of the reaction mixture was refluxed under nitrogen atmosphere for 4 more hours. Then the reaction mixture was poured into methanol and red coloured precipitate was filtered and dried. Product 2d was purified by silica column chromatographic technique using dichloromethane/petroleum ether (65:35) mixture as eluent. Yield obtained was 40 %. 2d crystals were obtained from the slow evaporation of toluene solution. M.p. > 300 °C. ^1H NMR [500 MHz, CDCl_3 , δ]: 10.86 (s, 4H), 8.99 (m, 4H), 8.89 (m, 4H), 7.86 (m, 8H), 7.50 (t, 2H), 7.37 (d, 4H), 2.98 (m, 4H), 1.21 (d, 24H). ^{13}C NMR [125 MHz, CDCl_3 , δ]: 164.95, 145.87, 131.81, 131.69, 130.77, 129.67, 128.97, 128.43, 128.35, 128.16, 126.88, 124.26, 124.18, 121.25, 29.41, 24.15. IR (KBr, cm^{-1}): 1738, 1701 and 1662. Elemental analysis: calcd. value for $\text{C}_{76}\text{H}_{54}\text{N}_2\text{O}_4$: 86.18% C, 5.14% H and 2.64% N; found: 86.08% C, 5.12% H and 2.50% N. HRMS (EI) m/z calculated for $\text{C}_{76}\text{H}_{54}\text{N}_2\text{O}_4$ $[\text{M}]^+$: 1058.4084, found: 1058.4067.

3.5.1.6. Synthesis of 3b

0.2 mmol of 1,7-dibromoperylene-1,4,9,16-tetracarboxylic diimide (2a) was dissolved in dry THF and 10 mL of 2 M potassium carbonate was added. Reaction mixture was purged with nitrogen for 15 minutes. 0.02 mmol of tetrakis(triphenylphosphine)palladium(0) and 0.50 mmol of phenylboronic acid were added under nitrogen atmosphere. Reaction mixture was refluxed at 65 °C under nitrogen atmosphere. After completion of the reaction, product was extracted in dichloromethane and purified by column chromatography using dichloromethane/petroleum ether mixture (65:35) as eluent. Red coloured solid was obtained as product (3b) in 45 % yield. M.p. > 300 °C. ^1H NMR [500 MHz, CDCl_3 , δ]: 8.66 (s, 2H), 8.15 (d, 2H), 7.87 (d, 2H), 7.57 (m, 4H), 7.46 (m, 8H), 7.27 (d, 4H), 2.84 (m, 4H), 1.12 (d, 24H). ^{13}C NMR [125 MHz, CDCl_3 , δ]: 163.10, 162.50, 144.64, 141.12, 140.44, 134.83, 134.37, 132.01, 129.46, 129.30, 128.99, 128.63, 128.07, 127.79, 127.43, 123.09, 121.34, 120.96, 28.17, 23.04, 22.97. IR (KBr, cm^{-1}): 2960, 1732, 1694 and 1657. Elemental analysis: calcd. value for $\text{C}_{60}\text{H}_{50}\text{N}_2\text{O}_4$: 83.50% C, 5.84% H and 3.25% N; found: 83.62% C, 5.60% H and 3.35% N. HRMS (EI) m/z calculated for $\text{C}_{60}\text{H}_{50}\text{N}_2\text{O}_4$ $[\text{M}]^+$: 862.3771, found: 862.3777.

3.5.1.7. Synthesis of 3c

100 mg of 3b was dissolved in 500 mL of dry dichloromethane and heated to 40 °C under nitrogen atmosphere. A solution of 8 equivalents ferric chloride in 10 mL dry nitromethane was added dropwise into the reaction mixture under continuous nitrogen purging. The reaction mixture was refluxed at 40 °C for 1 hour. Reaction temperature was limited by the boiling point of dichloromethane. Completion of the reaction is monitored through thin layer chromatographic (TLC) technique. Then methanol was poured into the reaction mixture to stop the reaction. Orange coloured product was precipitated. 3c was purified by silica column chromatographic technique using dichloromethane/petroleum ether (60:40) mixture as eluent. Yield obtained was 50 %. M.p. > 300 °C. ¹H NMR [500 MHz, CDCl₃, δ]: 10.68 (s, 4H), 9.56 (m, 4H), 8.17 (m, 4H), 7.53 (t, 2H), 7.40 (d, 4H), 2.94 (m, 4H), 1.15 (d, 24H). ¹³C NMR [125 MHz, CDCl₃, δ]: 164.20, 146.47, 131.70, 130.12, 129.83, 129.75, 129.37, 125.30, 125.20, 124.90, 124.82, 124.40, 124.06, 122.65, 29.75, 24.19. IR (KBr, cm⁻¹): 2950, 1715, 1680, 1596 and 1458. Elemental analysis: calcd. value for C₆₀H₄₆N₂O₄: 83.89% C, 5.40% H and 3.25% N; found: 83.98% C, 5.29% H and 3.21% N. HRMS (EI) m/z calculated for C₆₂H₄₈N₂O₄ [M]⁺: 858.3458, found: 858.3444.

3.6. Appendix

3.6.1. Materials and methods

As discussed in the Chapter 2.

Spectral measurements: As discussed in the Chapter 2.

Transient absorption measurements: As discussed in the Chapter 2.

Efficiency of intersystem crossing (Φ_{isc}) could be estimated from the rates of internal conversion (k_{ic}) and intersystem crossing (k_{isc}) as follows,[77]

$$\phi_{ISC} = \frac{1}{\tau_{ISC}} \bigg/ \frac{1}{\tau_{IC}} \quad \text{---(3.1)}$$

Where, τ_{ISC} – rate of intersystem crossing and τ_{IC} – rate of internal conversion; extracted from the fTA spectra analysis.

X-ray crystallography: As discussed in the Chapter 2.

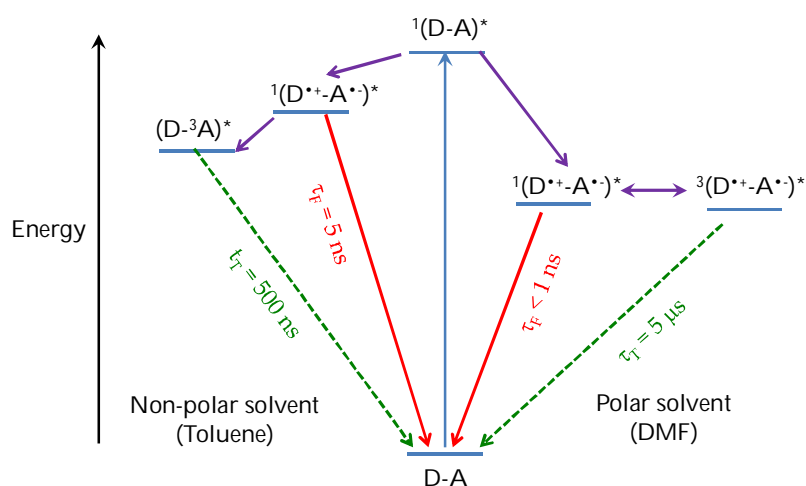
Computational methods: Ground-state optimised structure and harmonic oscillator frequencies were computed using density functional theory (DFT) at the Becke's three parameter functional in combination with the Lee-Yang-Parr correlation functional (B3LYP) and 6-311+G(d,p) basis set. Vertical excitation energies and oscillator strengths were calculated employing time dependent DFT (TD-DFT) at the B3LYP/6-311G++(d,p) level of theory. All computations were performed with the Gaussian 09 program suite[110].

Chapter 4

Charge-Transfer Facilitated Triplet Generation in Perylenediimide based Orthogonal Dyads and Triads

Abstract

Near-orthogonal donor-acceptor (D-A) dyads and triads (D-A-D) containing anthracene (AN) / pyrene (PY, electron donor) and perylenediimide (PDI, electron acceptor) show a low-energy CT absorption band. Lippert-Mataga analysis established the CT character of the emitting singlet states in dyad and triads employing the solvatochromic shift in the position of the fluorescence spectra. Furthermore, the Rehm–Weller relation based exploration of the thermodynamic feasibility of electron transfer, suggests a favourable change in free energy for the electron transfer from the singlet excited state of AN/PY to PDI unit ($\Delta G = -1.1$ eV for AN; $\Delta G = -1.4$ eV for PY). Upon excitation ($\lambda_{\text{ex}} = 355$ nm), excited (high energy) charge transfer intermediate leads to solvent polarity dependent intersystem crossing to generate localised triplet ($^3A^*$) and/or triplet charge transfer $^3(D^{+\cdot}-A^{\cdot-})^*$ state. Solvent dependent nTA spectra of the dyads and triads show that non-polar solvent like toluene facilitate the formation of $^3A^*$ while long lived triplet charge separated state $^3(D^{+\cdot}-A^{\cdot-})^*$ is formed in polar solvents such as DMF. The present chapter offers the correlation between solvent polarity vs. excited state photophysical properties in near-orthogonal D-A dyads and D-A-D triads.



4.1. Introduction

Photoinduced electron transfer (PET) processes are widely studied in electron donor (D) – acceptor (A) systems to understand the factors that affect the rate and efficiency of charge transfer[147]. The research on PET primarily focuses on mimicking the natural photosynthetic systems where the photoexcitation is followed by sequential energy and electron transfer processes which lead to a long lived charge separated state with very high yield[148-149]. Reported literature encompasses a large extent of multichromophoric systems[150] including molecular dyad, triads[151-152], tetrads[153] and pentads[154-155] to mimic the multistep charge/electron transfer processes occurring in natural photosynthesis[156]. However, the lifetime of the charge separated states is not significantly increased due to the rapid geminate charge recombination. Mimicry of some other aspects of photosynthetic reaction centers has proven less facile. A particularly interesting aspect of primary photosynthesis is the back electron-transfer reaction that produces a triplet state of the initial bacteriochlorophyll or chlorophyll donors in green plant photosystem II reaction centers[157-158]. Long lived charge separation has been observed in artificial photosynthetic systems where the donor- acceptor system can access an excited state triplet character $(D^+-A^-)^*$ [159-160]. Charge recombination leading to the formation of the triplet state has been successfully realized in many donor–spacer-acceptor systems[161]. The formation of locally excited triplet state $(D-{}^3A)^*$ / $({}^3D-A)^*$ and charge transfer triplet excited state $({}^3(D^+-A^-))^*$ is explained by the

spin orbit coupling ISC mechanism (SOC-ISC) and radical pair ISC mechanism (RP-ISC) respectively (Scheme 4.1)[162].

In principle the rate of charge recombination could be retarded if the ground and intermediate excited states of the system has different spin multiplicity. Recently, there has been greater interest in optically dark charge-transfer (CT) states that affect excited-state processes, in particular, spin-state interconversion. Investigation of this phenomenon in carbazole-tetrachlorophthalimide, D-A system, had shown that the singlet charge separated state ($^1(D^+-A^-)^*$) is short lived (ca. 20 ns) and triplet charge separated state ($^3(D^+-A^-)^*$) has a lifetime in the micro-millisecond

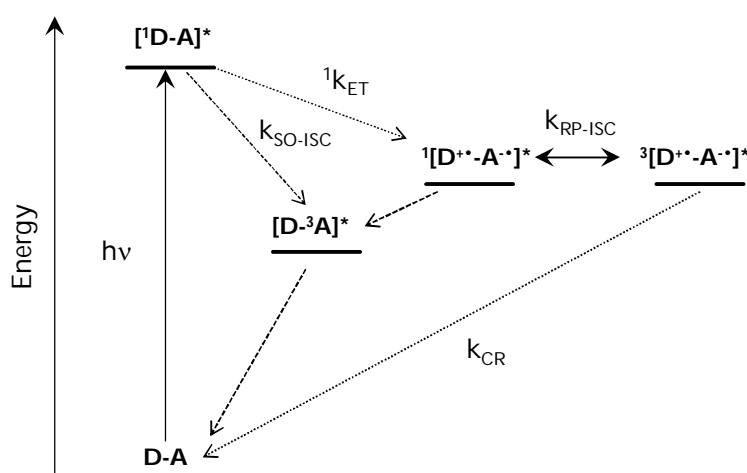


Figure 4.1. An energy level diagram for the donor-acceptor (D-A) dyads illustrates the different photoinduced processes that occur in these molecules. The triplet state that is reached through RP-ISC can be localized on either the donor or the acceptor.

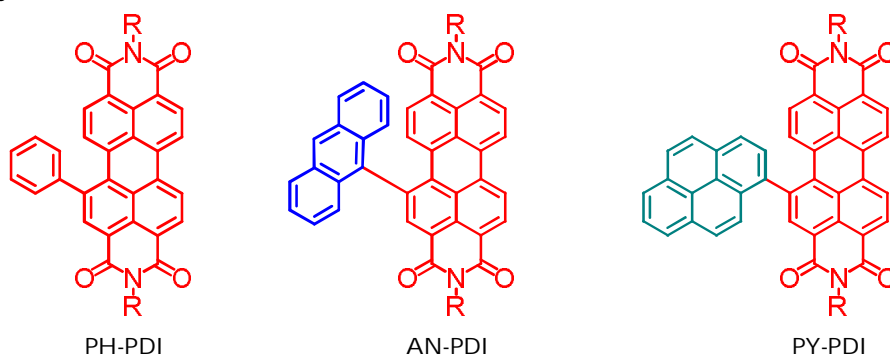
range[163-164]. In the absence of a strong external magnetic field, the most reasonable mechanisms for intersystem crossing in general involve either spin-orbit coupling or hyperfine interactions[25]. Spin-orbit coupling is unlikely to induce the

alternate intersystem crossing process k_{isc}^{CT} . Lim has shown that in the one-electron approximation, spin-orbit coupling between the $^1(A^{\bullet-}-D^{\bullet+})$ and $^3(A^{\bullet-}-D^{\bullet+})$ states is zero, since the orbital occupation is the same in each system[165]. Thus, the hyperfine interaction is the most reasonable mechanism for the intersystem crossing from $^1(A^{\bullet-}-D^{\bullet+})$ to $^3(A^{\bullet-}-D^{\bullet+})$. Indeed, direct evidence for this mechanism has been obtained in some covalently linked donor/acceptor systems[166]. In some favorable cases, the triplet radical pair state has been directly observed, confirming the mechanism[167].

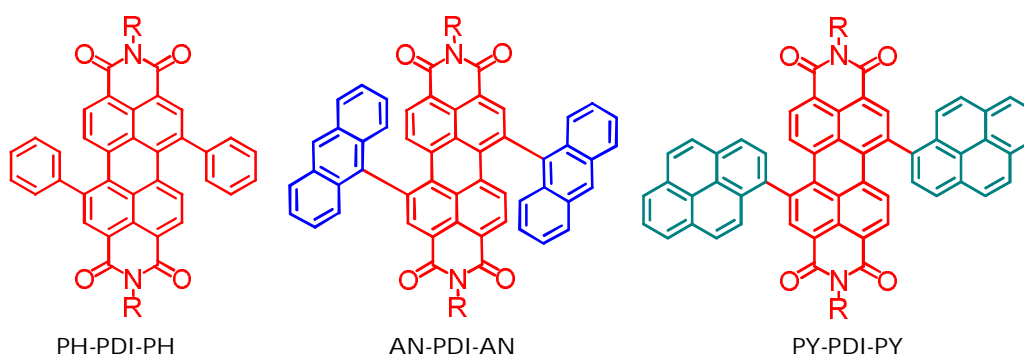
However, the weak hyperfine interactions can only induce intersystem crossing when the energy difference between the singlet and triplet CT states is small, i.e., when electronic coupling is weak[168]. In both bimolecular and covalently linked donor/acceptor CT systems, electronic coupling tends to decrease with increasing separation distance between the radical sites. In most of the covalently linked charge-transfer systems that have been studied, the distance between the donor and the acceptor is usually large, to reduce electronic coupling[168]. Orthogonal donor-acceptor systems tend to show negligible orbital overlap due to the improper orientation between the constituent donor and acceptor units[169]. In the present work, we have designed some orthogonal D-A dyads and D-A-D triads for reduced electronic coupling and studied their ISC properties in the excited state.

The present work describes the synthesis, steady state and ultrafast (femto and nanosecond) photophysical properties of orthogonal dyads (AN-PDI and PY-PDI) and triads (AN-PDI-AN and PY-PDI-PY) (Scheme 4.1) along with the model

Dyads



Triads



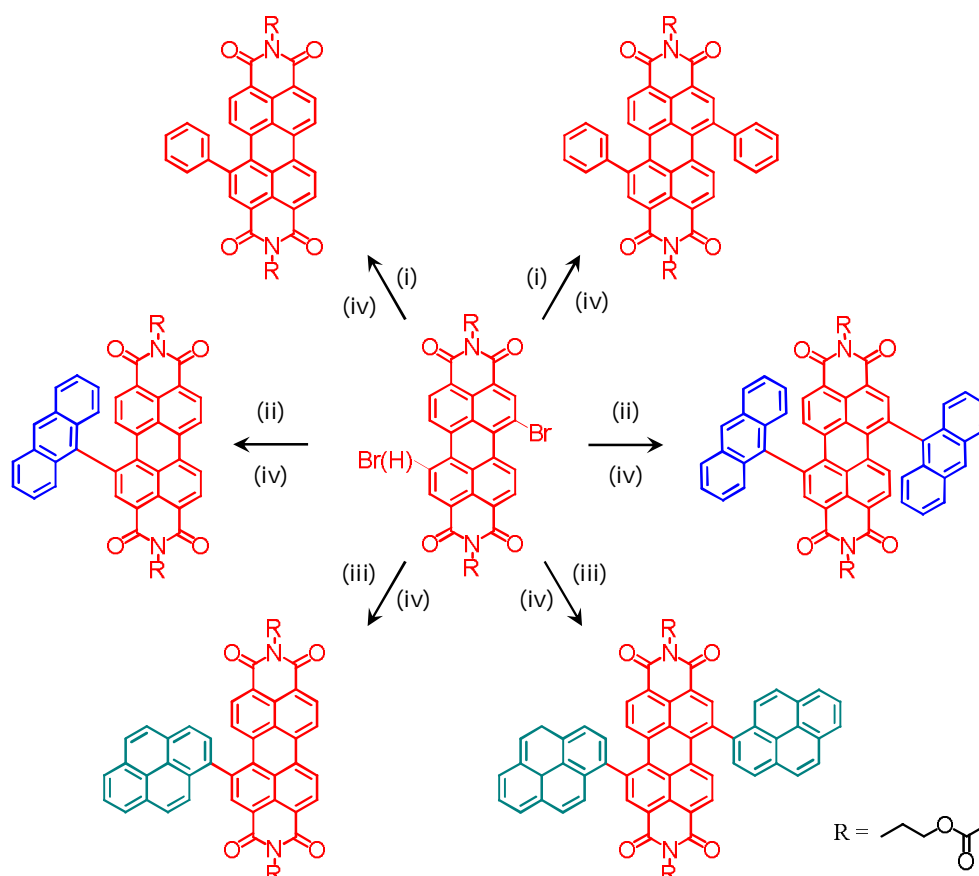
Scheme 4.1. Molecular structures of the PDI based D-A dyad and D-A-D triad.

derivative PH-PDI and PH-PDI-PH which show extended delocalization between the units. Solvent dependent nTA spectra of the dyads and triads show that non-polar solvent facilitate the formation of ^3PDI while long lived triplet charge separated states are formed in polar solvents. Fully conjugated PH-PDI and PH-PDI-PH exhibit neither CT nor ^3PDI , but only nearly quantitative fluorescence is observed. The present chapter offers the correlation between solvent polarity vs. excited state photophysical properties in near-orthogonal donor-acceptor systems.

4.2. Synthesis and characterisation

All the derivatives were synthesised by performing Suzuki coupling of bromo derivative of PDI with arylboronic acids in the presence of Pd^0 catalyst as reported

earlier. Suzuki reaction of 1-bromo PDI (PDI-Br; synthesis is reported in chapter 2) with one equivalent of 1-phenyl, 9-anthracene and 1-pyrene boronic acids in the presence of tetrakis(triphenylphosphine)palladium(0) catalyst offered the dyads PH-PDI, AN-PDI and PY-PDI respectively (Scheme 4.2). In the same way, reaction of 1,7-dibromo PDI (PDI-Br₂; synthesis reported in chapter 2) with 2 equivalents of 1-phenyl, 9-anthracene and 1-pyrene boronic acids offered the triads PH-PDI-PH, AN-PDI-AN and PY-PDI-PY respectively (Scheme 4.2). All the derivatives have been purified by column chromatographic techniques and characterised by spectroscopic and analytical techniques.



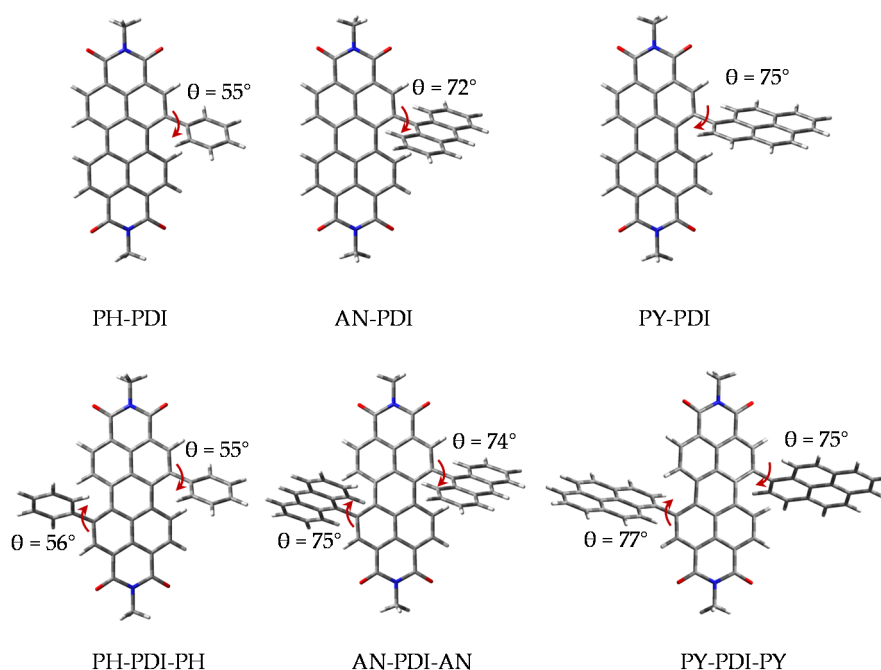
i) Phenylboronic acid; ii) anthracene-9-boronic acid; iii) pyrene-1-boronic acid and iv) Pd(PPh₃)₄, K₂CO₃, THF/H₂O, 65°C

Scheme 4.2. Syntheses scheme for the PDI based dyads and triads.

4.3. Results and discussions

4.3.1. Structure optimization

As the X-ray analyses of the compounds were unsuccessful; the molecular structures of the dyad and triad derivatives were geometry optimised calculated using DFT analysis (Scheme 4.3). All the derivatives were optimised at B3LYP/6-311G (d,p) theory level. In PH-PDI and PH-PDI-PH, freely rotating phenyl groups at the bay region are at a dihedral angle of 50-55° to the PDI plane (Scheme 4.3). But in the case of AN and PY based derivatives (AN/PY-PDI; AN/PY-PDI-AN/PY), AN/PY units are near orthogonal with respect to the PDI plane with the dihedral angle of 75-80°. Frontier molecular orbital (FMO) analysis shows that the phenyl substitution in the bay region extends the π surface of PDI while anthracene and pyrene based



Scheme 4.3. Optimised geometries of the dyads and triads obtained using B3LYP/6-311G (d,p) level of theory; θ show the dihedral angle between the donor and acceptor units; inside alkyl chain is omitted for the clarity.

derivatives show negligible orbital overlap between AN/PY and PDI units (Figure 4.2B). Highest occupied and lowest unoccupied molecular orbitals (HOMO and LUMO) exhibit delocalised PDI π surface in phenyl derivatives. Conversely, in AN and PY based derivatives, HOMO is localised on AN/PY unit while LUMO is concentrated in PDI unit, establishing a donor-acceptor relation between AN/PY and PDI.

4.3.2. Electrochemical analysis

Cyclic voltammogram of the dyads and triads along with model derivatives anthracene (AN), pyrene (PY) and perylenediimide (PDI) in dichloromethane are indicated in the table 4.1. Model donor molecules AN and PY show the oxidation

Table 4.1. *Electrochemical properties of the derivatives along with the model derivatives in dichloromethane; HOMO and LUMO energy levels obtained from DFT calculations.*

Molecule	E_{red}^1 , eV	E_{red}^2 , eV	E_{ox} , eV	HOMO, eV	LUMO, eV
Anthracene	-	-	1.50		
Pyrene	-2.51	-	1.28		
PDI	-0.52	-0.69	1.80		
PH-PDI	-0.57	-0.74	-	-5.99	-3.66
AN-PDI	-0.53	-0.70	1.51	-5.85	-3.70
PY-PDI	-0.54	-0.71	1.30	-5.89	-3.71
PH-PDI-PH	-0.59	-0.76	1.82	-6.20	-3.79
AN-PDI-AN	-0.54	-0.70	1.52, 1.79	-5.85	-3.72
PY-PDI-PY	-0.54	-0.71	1.30, 1.79	-5.87	-3.75

peak at 1.5 and 1.28 V respectively while unsubstituted PDI exhibits an oxidation potential at 1.80 V and two reversible reduction peaks at -0.52 and -0.69 V (Figure 4.2A). Upon substituting one/two phenyl units at the bay region, first and second reduction potential of PDI is shifted to -0.57/-0.59 and -0.74/-0.76 respectively (Table 4.1). This decrease in the electron accepting ability of the phenyl derivatives is readily explained by the extended π -conjugation from the phenyl unit to PDI. AN/PY substituted PDI exhibit very feeble change in the reduction potential of PDI unit and oxidation potential of donor units in both dyads and triads (Table 4.1). Cyclic voltammogram of the near orthogonal dyads (PH-PDI, AN-PDI and PY-PDI) and triads (PH-PDI-PH, AN-PDI-AN and PY-PDI-PY) (Figure 4.2A) in dichloromethane show that the donor and acceptor units retain their individual electronic properties even though they are connected to each other.

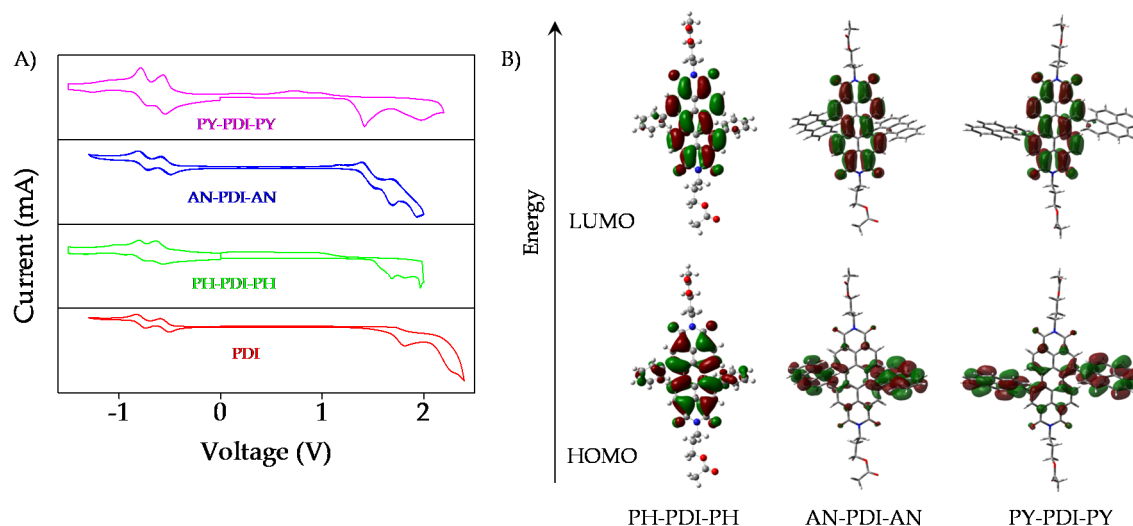


Figure 4.2. A) Electrochemical analysis of the triads (1 mM) in dichloromethane along with PDI in the presence of tetrabutylhexafluoroammoniumphosphate (100 mM) with respect to Ag/Ag⁺ electrode; B) frontier molecular orbital diagram of the triads calculated from DFT calculations.

4.3.2.1. Rehm-Weller analysis

In order to prove the possibility of CT in the derivatives, change in free energy of charge separation was calculated according to Rehm–Weller relation,

$$\Delta G_{ET} = E_{D/D^+} - E_{A/A^-} - E_{00} - \frac{e^2}{\epsilon r} \quad \text{---(4.1)}$$

where ΔG_{ET} is the change in free energy of electron transfer, 'e' is the electronic charge, 'r' is the centroid to centroid distance between the donor and the acceptor. 'r' for AN and PY based derivatives are estimated to be 5 Å and 6 Å respectively from the energy optimized structure. 'ε' is the static dielectric constant of the solvent in which the redox potentials are being measured (dichloromethane in this case, ε=8.93). Rehm-Weller analysis of AN/PY based derivatives shows the free energy change, $\Delta G_{ET} = -1.1$ eV for electron transfer from singlet excited state of $^1\text{AN}^*$ to PDI and $\Delta G_{ET} = -1.4$ eV for ET from $^1\text{PY}^*$ to PDI in dichloromethane.

4.3.3. Photophysical properties of dyads and triads

Absorption spectra: The UV-vis absorption spectra of the dyads PH-PDI, AN-PDI and PY-PDI along with the model derivative PDI in toluene is shown in the Figure 4.3A. All the three derivatives show the PDI characteristic $S_0 \rightarrow S_1$ transition at around 450-550 nm. PH-PDI exhibits a red shifted absorption spectrum when compared to the model derivative PDI, which is due to the extended conjugation from phenyl unit to PDI. The absorption spectra of AN-PDI and PY-PDI corresponds to the sum of AN/PY and PDI absorption along with the broad absorption at higher wavelength (550-650 nm). A blue shift of 10-30 nm is observed in the absorption of PDI unit in

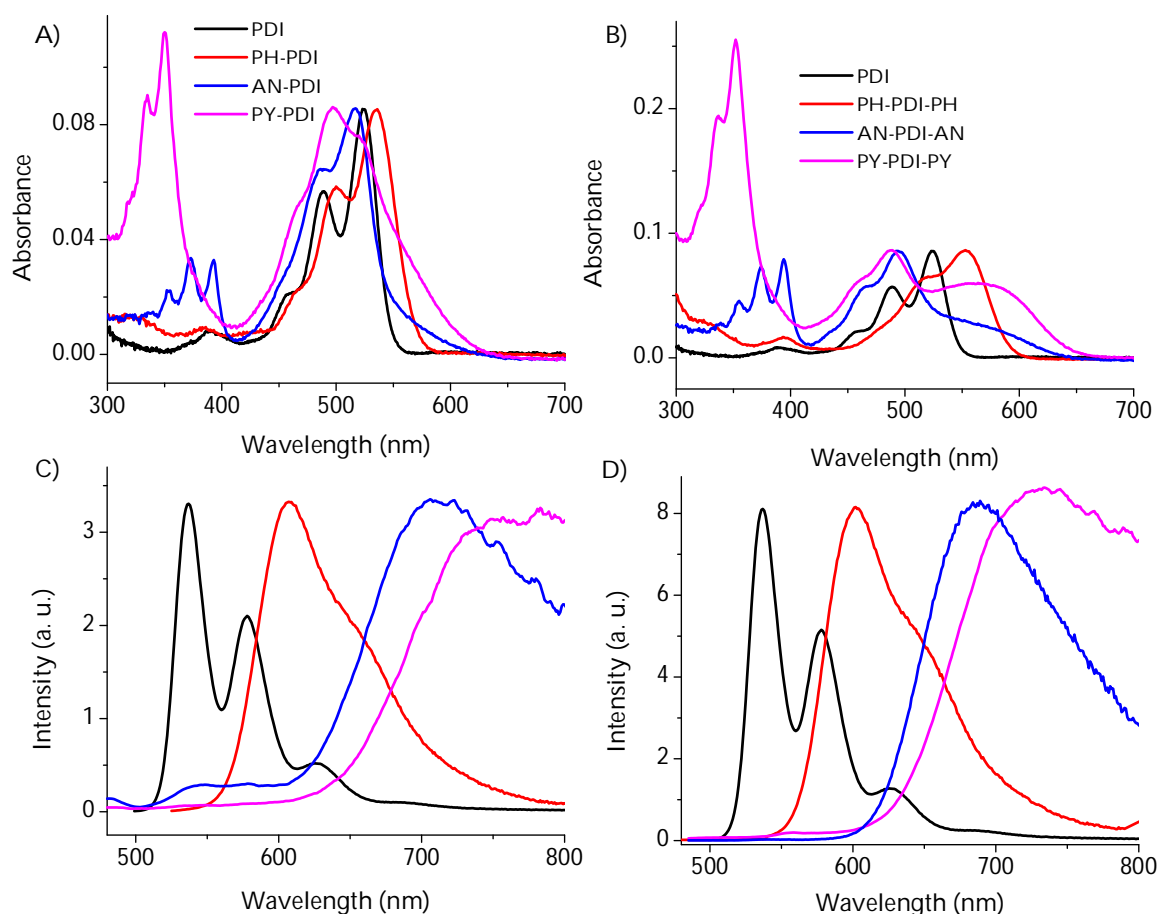


Figure 4.3. Steady-state absorption spectra of A) dyads and B) triads along with PDI in toluene; normalised steady state fluorescence spectra of C) dyads and D) triads along with PDI ($\lambda_{ex} = 350$ nm) in toluene.

the dyads of AN/PY-PDI when compared to the unsubstituted PDI (Table 4.2). The red shifted absorption observed at 550-650 nm is not witnessed in equimolar mixture of AN/PY and PDI. So the additional red shifted absorption and blue shift in the PDI unit absorption in the dyads could be attributed to the ground state charge transfer (GSCT) between the units. The same phenomenon was observed in the UV-vis absorption spectra of the triads PH-PDI-PH, AN-PDI-AN and PY-PDI-PY (Figure 4.3B). PH-PDI-PH exhibits a red shifted absorption spectrum compared to that of PDI due to higher π delocalisation, while AN and PY based triads show sum of

Table 4.2. Photophysical properties of the dyads and triads along with PDI in toluene.

Molecule	λ_{abs} , nm	λ_{em} , ns	τ_{F} , ns	Φ_{F}	Φ_{CS}	Φ_{T}	τ_{T} , μs
PDI	488, 525	536, 577	4	0.98	-	<0.01	-
PH-PDI	500, 535	560, 600	5.0	0.95	-	<0.01	-
AN-PDI	486, 515, 580	665 (bs)	3.1	0.04	0.55	0.30	0.50
PY-PDI	333, 351, 468, 496, 580	680 (bs)	5.3	0.18	0.43	0.25	0.46
PH-PDI-PH	518, 555	600, 650	5.2	0.92	-	<0.01	-
AN-PDI-AN	463, 494, 580	675 (bs)	3.8	0.02	0.59	0.40	0.55
PY-PDI-PY	335, 351, 455, 485, 585	690 (bs)	5.0	0.16	0.48	0.35	0.50

absorption bands of individual units along with the additional GSCT band at higher wavelength region. Similar observations were made in the UV-Vis spectrum of 1,7-(Ph₂NC₆H₄)₂PDI that is attributed to the charge transfer interactions between Ph₂NC₆H₄ and PDI units[170].

Emission spectra: Fluorescence spectra of the dyad and triad derivatives were collected by exciting at the donor unit (AN/PY; 350 nm), acceptor unit (PDI; 480 nm) and GSCT region (570 nm). Upon excitation at 350 nm, PH-PDI in toluene exhibit red shifted vibration less emission when compared to the unsubstituted PDI which is attributed to the π conjugation from the freely rotating phenyl units (Figure 4.3C). Fluorescence quantum yield (Φ_{F}) of PH-PDI is found to be nearly quantitative (0.95) which is in agreement with the reported literatures (Table 4.2). Upon exciting donor or acceptor units in the AN/PY-PDI in toluene, highly quenched, broad emission spectrum was observed at higher wavelength region (650-800 nm). Φ_{F} was found to

be 0.04 for AN-PDI and 0.18 for PY-PDI in toluene solution (Table 4.2). Similar spectral features were obtained by exciting at the acceptor ($\lambda_{\text{ex}} = 480 \text{ nm}$) and GSCT ($\lambda_{\text{ex}} = 480 \text{ nm}$) region of the derivatives in toluene solvent. The quenched fluorescence in AN-PDI and PY-PDI is attributed to the photo induced electron transfer when compared to extended conjugation in PH-PDI which is in agreement with the earlier reports. Triads PH-PDI-PH, AN-PDI-AN and PY-PDI-PY also show similar behaviour (Figure 4.3D) in the emission spectra which is in agreement with the UV-vis absorption studies. Zhu and co-workers showed that instead of GSCT interactions, conjugation effect was observed in 2-anthracene substituted 1,7-perylenediimide dyads and triads[171]. While, aryloxy substituents at the bay position of PDI exhibited photoinduced electron transfer from the electron-rich substituent to the PDI core. Similarly, AN-(CH₂)_n-PDI-(CH₂)_n-AN triad connected through flexible alkyl linkers also exhibited photoinduced electron transfer based quenching in the PDI fluorescence[172]. In other context, 1,7-(Ph₂NC₆H₄)₂PDI exhibited EDA interactions in the ground state, showed a negligible fluorescence emission[170].

4.3.4. Characterization of singlet excited CT states

The red shifted absorption band in PH-PDI and PH-PDI-PH appears as extended vibronic progression of the PDI state, whereas those of dyads (AN/PY-PDI) and triads (AN/PY-PDI-AN/PY) appear as significant broadening on the red edge of their spectra. The quenched fluorescence observed for dyads and triads is the

characteristics of excited state CT as observed for PDI based donor-acceptor dyads. The magnitude of the excited-state dipole, which is indicative of the intramolecular charge distribution, was established using the Lippert–Mataga method (Figure 4.4)[12, 173]. The theory predicts a linear relationship between the Stokes shift $\nu_A - \nu_E$, and the polarisability function Δf according to the following equation,

$$\nu_A - \nu_E = \frac{2(\Delta\mu)^2}{hca_0^3} \left[\frac{(\epsilon-1)}{2\epsilon+1} - \frac{(\eta^2-1)}{2(2\eta^2+1)} \right] \quad \text{---(4.2)}$$

$$\Delta f = \left[\frac{(\epsilon-1)}{2\epsilon+1} - \frac{(\eta^2-1)}{2(2\eta^2+1)} \right] \quad \text{---(4.3)}$$

$$\nu_A - \nu_E = \frac{2(\Delta\mu)^2}{hca_0^3} \Delta f + \text{constant} \quad \text{---(4.4)}$$

where h is Planck's constant, c is the speed of light, ν_A is the absorption maximum and ν_E is the energy of the CT emission band measured in several solvents with dielectric constant ϵ and index of refraction η . The radius of the Onsager spherical cavity, a_0 , was determined to be (6.94 Å for AN-PDI; 7.24 Å for PY-PDI; 7.14 Å for AN-PDI-AN and 7.64 Å for PY-PDI-PY) using the DFT optimized structures, which

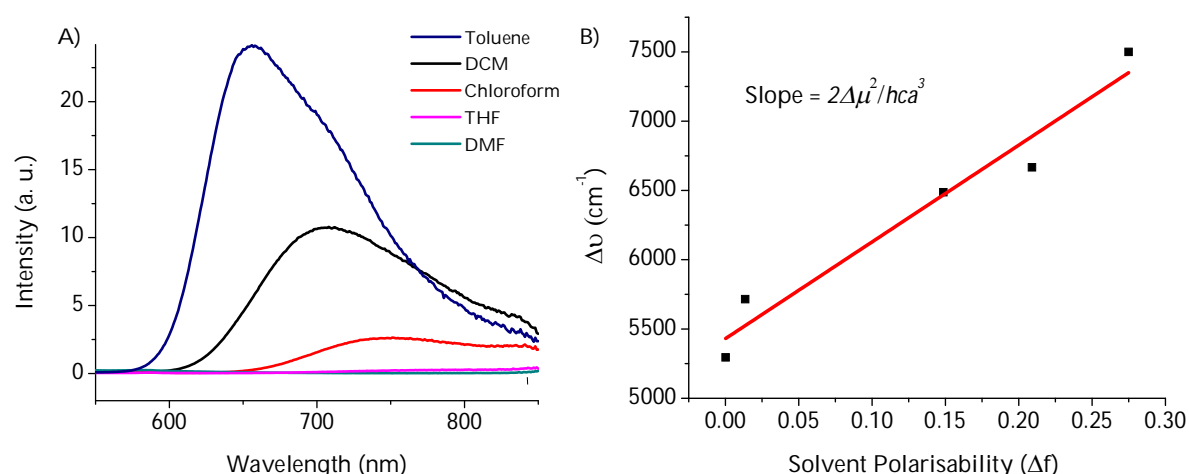


Figure 4.4. A) Solvent dependent fluorescence spectra of the triad AN-PDI-AN upon excitation with 350 nm; B) corresponding Lippert-Mataga plot.

is in agreement with that previously estimated for PDI based dyads[174]. $\Delta\mu$ is the change in electric dipole moment of the molecule between the excited state and the ground state, can be estimated from the slope of the plot of $\nu_A - \nu_E$ vs. Δf . The dipole moment change ($\Delta\mu$) is calculated to be 14.5 D for AN-PDI; 15.8 D for PY-PDI; 15.2 D for AN-PDI-AN and 17.1 D for PY-PDI-PY. We estimated the degree of charge separation in the ^1CT states by using the formula, $\Delta\mu/4.8 \text{ D esu}^{-1} \text{ \AA}^{-1}$ (3.16 esu \AA for AN-PDI; 3.29 esu \AA for PY-PDI; 3.17 esu \AA for AN-PDI-AN and 3.57 esu \AA for PY-PDI-PY). Using the centers of the spin density distributions in $\text{AN}^{+\bullet}/\text{PY}^{+\bullet}$ and $\text{PDI}^{\bullet-}$ the distance that a full charge is transferred to yield $\text{AN}^{+\bullet}/\text{PY}^{+\bullet}\text{-PDI}^{\bullet-}$ is 5.6 \AA . Thus, the estimated percentage of charge separation in ^1CT is 55% in AN-PDI; 43% in PY-PDI; 59% in AN-PDI-AN and 48% in PY-PDI-PY (Table 4.2).

Figure 4.5 shows the time-resolved fluorescence decay profile of AN/PY based PDI dyads and triads in solvents of varying polarity when excited at 375 nm and monitored at the charge transfer band at 700 nm. All the four derivatives exhibit

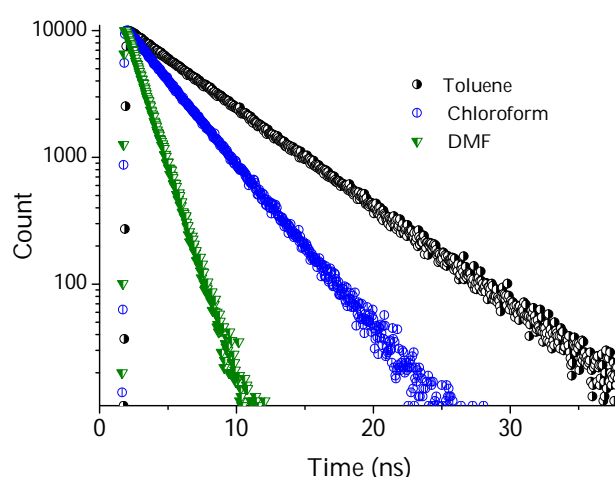
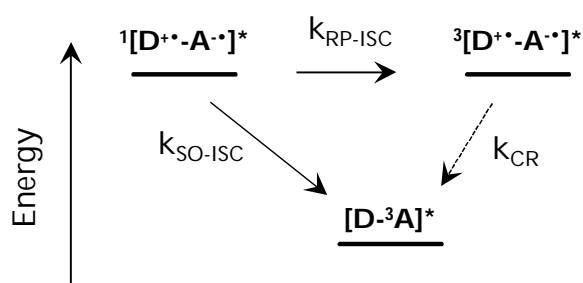


Figure 4.5. Time resolved fluorescence emission profile of the triad AN-PDI-AN in toluene, chloroform and DMF upon excitation with 375 nm.

solvent dependent change in fluorescence lifetime. For example, the triad AN–PDI–AN in toluene exhibited a mono-exponential decay having a lifetime of 5 ns. A systematic decrease in the lifetime with increase in solvent polarity was observed leading to a shorter lifetime of 2 ns in chloroform. In DMF, the triad AN–PDI–AN exhibited a bi-exponential decay having the lifetimes of 0.58 ns (96%) and 4.21 ns (4%). The minor long lived component corresponds to the LE state emission of PDI unit. We observed a systematic decrease in the lifetime of the CT state with increase in solvent polarity (upto THF) resulting in the complete disappearance of the CT state in DMF.

4.3.5. Charge recombination

For singlet excited charge-transfer states, two basic mechanisms for intersystem crossing can be considered, as illustrated in Scheme 4.4[162]. In the first case, the CT state undergoes ISC to the triplet CT state, k_{RP-ISC} , which is followed by return electron transfer in the triplet manifold to give the locally excited triplet, k_{CR} . In the second, ISC occurs as a result of a simultaneous spin-flip and electron-transfer process, k_{SO-ISC} , and the singlet CT state is converted directly into the locally excited



Scheme 4.4. Basic ISC mechanism from singlet excited CT state (Adopted with permission from ref. 168. Copyright © 2016, American Chemical Society).

triplet state in a spin-forbidden electron-transfer reaction. Unless an intermediate state can be directly detected, or some specific spectroscopic information is obtained, it is difficult for one to distinguish between these mechanisms. For several covalently linked donor/acceptor excited CT states, direct experimental evidence has been obtained using time-resolved ESR spectroscopy that demonstrates that either mechanism may operate, depending upon the system. In order to understand the presence of triplet excited state in our derivatives upon excitation, steady state CW-EPR was performed in chloroform solution.

General features of transient EPR spectra: Solutions of triad AN-PDI-AN and PY-PDI-PY in chloroform (~0.005 M) were deaerated by several freeze-thaw cycles and sealed under vacuum. These were placed in the cavity of an X-band EPR spectrometer, cooled to 20 K where the solvent is a glass, and irradiated with continuous wave of light. Continuous wave (CW) steady-state EPR spectra of the ground state were obtained using the same set-up but without light excitation (Figure 4.6). In the ground state (Figure 4.6 A and C) both the triads show negligible EPR signal due to the diamagnetic nature, while in the excited state both the triads exhibit broad signals which could correspond to paramagnetic transient species generated upon excitation (Figure 4.6B and D). The paramagnetic intermediate generated could be attributed to photoinduced generation of a radical ion-pair species in the excited state. Time resolved EPR measurements are very important to further characterise the dynamics of the radical ion-pair system which can lead to the triplet excited state via ISC (not studied in this present thesis).

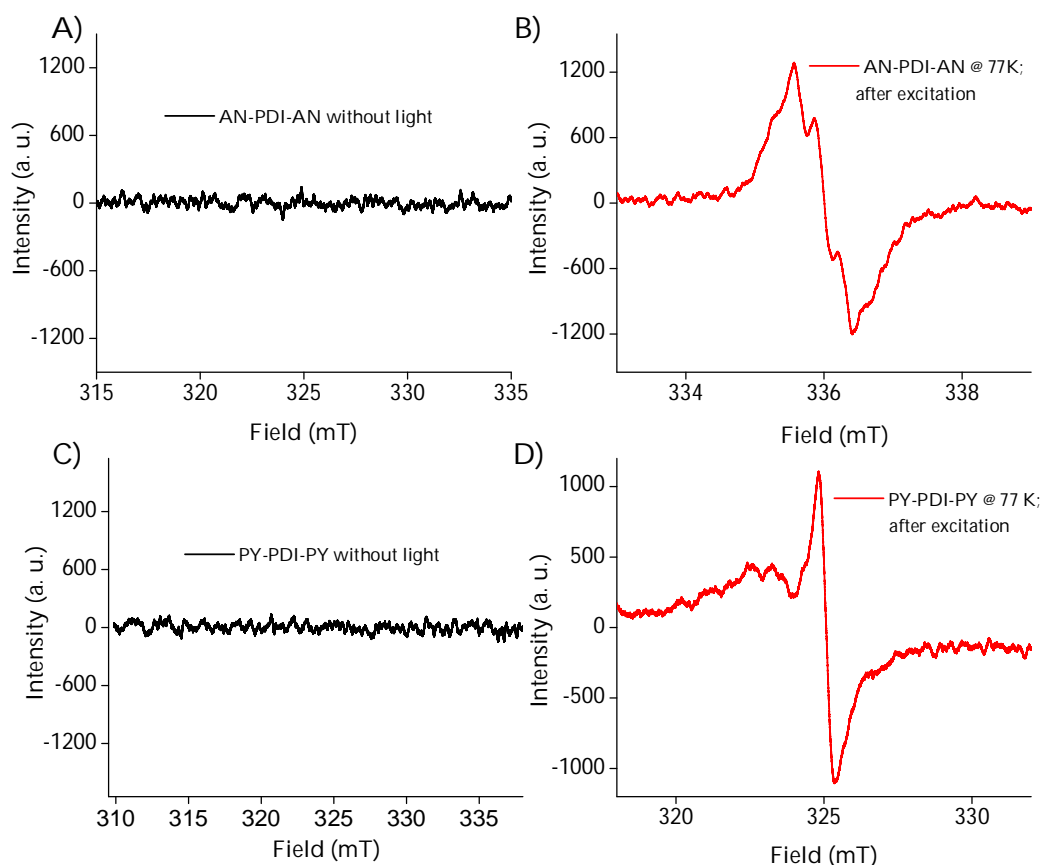


Figure 4.6. Steady state CW-EPR spectra of A) and B) AN-PDI-AN in the absence and presence of light of excitation at 77 K; C) and D) PY-PDI-PY in the absence and presence of light of excitation at 77 K.

4.3.6. Transient absorption spectroscopy

4.3.6.1. Nanosecond transient absorption measurements

In order to understand the fate of excited CT states, we have performed solvent dependent nTA measurement by exciting the solution at 355 and 532 nm, 10 ns laser pulse (Figure 4.7). PH-PDI and PH-PDI-PH derivatives exhibit negligible transient absorption due to the nearly quantitative fluorescence. The transient absorption spectra of PY-PDI and PY-PDI-PY in toluene (Figure 4.7A) upon excitation with 355 nm, reveals clearly the PDI triplet state with absorption maxima at 450, 540 and 660 nm which decay on a microsecond time scale ($\tau_T = 0.46 \mu\text{s}$ for PY-PDI; $0.50 \mu\text{s}$ for PY-

PDI-PY). As the unsubstituted PDI exhibits negligible ISC, PDI triplet can be observed only from the charge recombination process in PY based dyad and triad. The efficiency of triplet formation (Φ_T) in toluene is calculated to be $25\pm 2\%$ and $35\pm 2\%$ in PY-PDI and PY-PDI-PY respectively. In a moderately polar solvent like chloroform (Figure 4.7B), PY-PDI and PY-PDI-PY exhibit broad transient absorption having maxima at 400, 450, 550, 580 and 650 nm which decay with different rates. In order to deconvolute the complex spectrum obtained in chloroform, we have performed SVD followed by global analysis (which is explained in the chapter 1). The right singular vector at 450, 540 and 650 nm decaying with the lifetime of ≈ 0.45 μs is attributed to the localised triplet state of PDI while the long lived transient absorption observed at 400, 550 and 650 nm corresponding to $\text{PY}^{+\bullet}$ and $\text{PDI}^{\bullet-}$ ($\tau_T = 5$ μs). In the polar medium like N, N-dimethylformamide (DMF), nTA spectra of PY

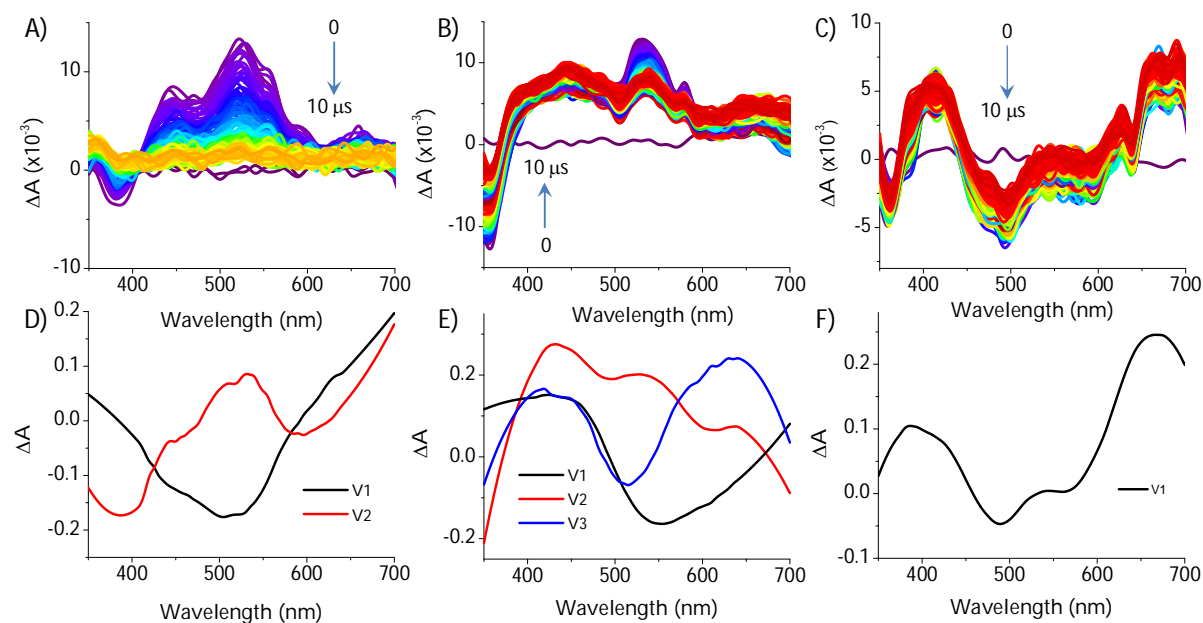


Figure 4.7. nTA spectra of the derivative PY-PDI-PY in A) toluene; B) chloroform and C) DMF upon excitation with 355 nm, 10 ns pulse. D), E) and F) corresponding SVD analysis.

derivatives exhibit transient absorption at 400, 550, 640, 660 and 680 nm along with the broad ground state bleach at 500 and 600 nm (Figure 4.7C). The peaks are corresponding to the connected $\text{PY}^{+\bullet}$ and PDI^{\bullet} which decay with the same time constant *ca.* 5 μs . No signal corresponding to localised triplet state on PDI (^3PDI) is observed in PY based derivatives in polar solvent such as DMF.

Solvent dependent transient absorption spectra could be explained from the energy level diagram which is obtained from the combination of experimental and computational analysis (Figure 4.8). In non-polar solvents such as toluene upon excitation, instantaneous electron transfer occurs from the electron donor acceptor complex to generate singlet excited charge transfer (^1CT) state. The decay pathways of ^1CT consist of i) ISC to generate ^3PDI and ii) radiative decay to ground state (Figure 4.8A). Upon excitation at 440 nm, picosecond lifetime measurements show

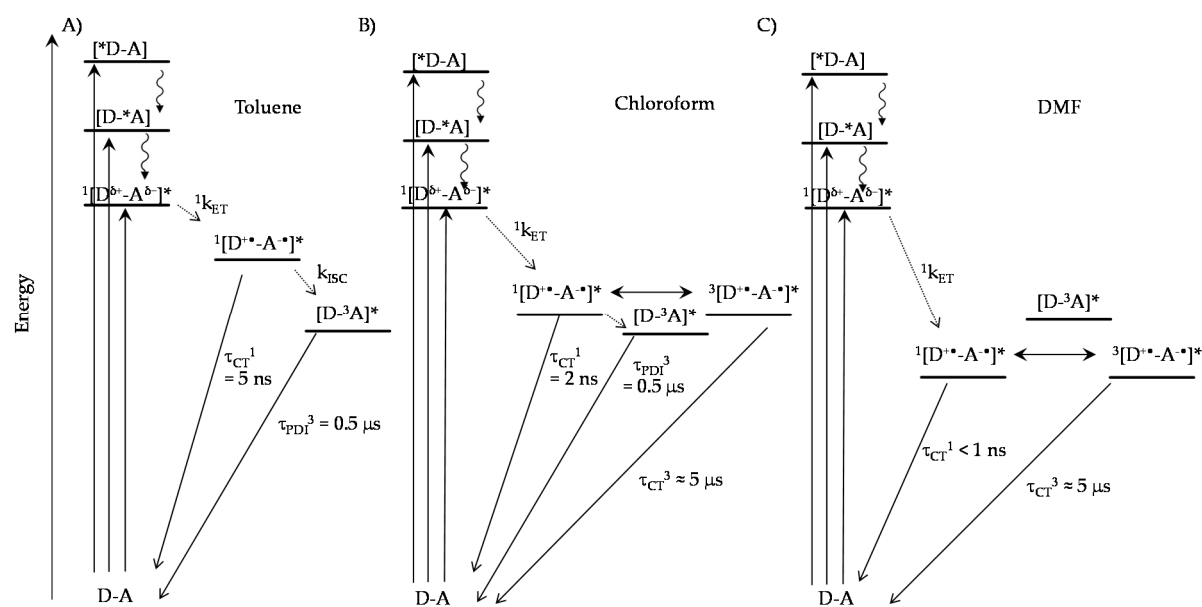


Figure 4.8. Model energy level diagrams for the excited states of dyads and triads in toluene, chloroform and DMF.

that radiative decay life time of 5 ns for PY derivatives in toluene solution and nTA spectra clearly establishes the presence of ^3PDI which has lifetime of 0.5 μs in toluene. On increasing the solvent polarity to chloroform, ^1CT is more stabilised when compared to that in toluene (Figure 4.8B). Upon excitation with 440 nm, ^1CT exhibits quenched radiative lifetime of 2 ns in chloroform. Interestingly, nTA spectra exhibit transient absorption corresponding to ^3PDI and $\text{PY}^{\bullet+}\text{-PDI}^{\bullet-}$ having lifetime of 0.5 μs and $\approx 5 \mu\text{s}$ respectively in chloroform solution (Figure 4.8B). The radical ion absorption bands indicate only the presence of $\text{PY}^{\bullet+}\text{-PDI}^{\bullet-}$, but do not give any information about the spin state. The very long lifetime, however, can only be explained assuming that the $\text{PY}^{\bullet+}\text{-PDI}^{\bullet-}$ is in triplet state. In addition, reduced lifetime of the transient species upon purging with oxygen further confirms the triplet nature of the excited CT state. In extremely polar solvent such as DMF, only the signal corresponding to $\text{PY}^{\bullet+}\text{-PDI}^{\bullet-}$ is observed (Figure 4.8C). In DMF, ^1CT is stabilised well below the ^3PDI thereby, only the long lived triplet excited state of radical ions are observed in the nTA spectra as reported earlier[175]. AN based derivatives AN-PDI and AN-PDI-AN also exhibit similar behaviour in solvent dependent nTA measurements.

4.3.6.2. Femtosecond transient absorption measurements

In order to characterize the formation of transient intermediates involved in the excited state of the derivatives we have carried out the femtosecond transient absorption measurements of the triads AN-PDI-AN and PY-PDI-PY in chloroform

with excitation at 400 nm. Figure 4.9A shows fTA spectra of the derivative AN-PDI-AN in chloroform upon excitation with 400 nm. Negative band centered around 500 nm that corresponds to the ground state bleach which is in accordance with UV-vis absorption spectrum of AN-PDI-AN in chloroform. Positive absorption is attributed to excited state transient species such as excited singlet, triplet and radical ions.

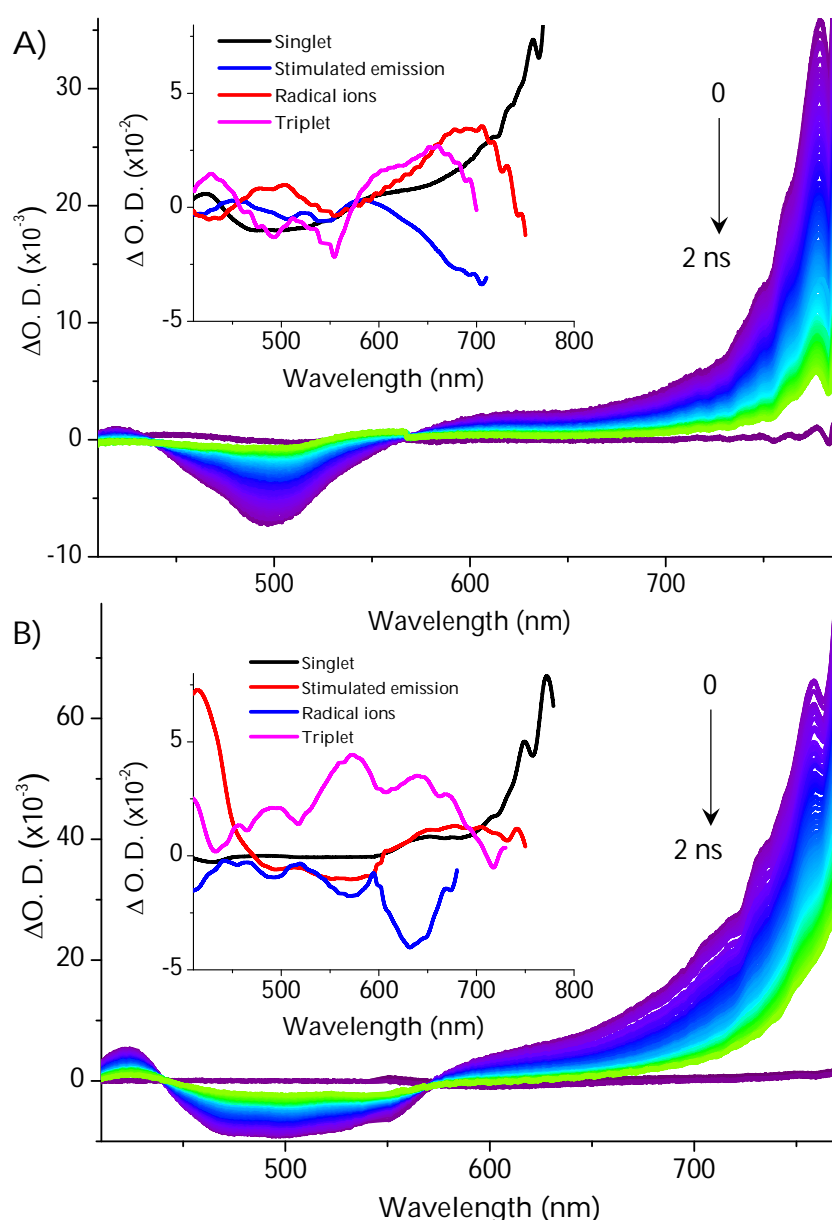


Figure 4.9. fTA spectra of the triads A) AN-PDI-AN and B) PY-PDI-PY in chloroform upon excitation with 400 nm laser; insets show the spectra obtained from the corresponding SVD analysis.

Singular value decomposition (SVD) of ΔA versus time and the wavelength based three-dimensional map followed by global analysis yielded four principle components (inset of Figure 4.8A). i) absorption from lower singlet excited state (600-770 nm) to higher singlet excited state (black trace; $S_1 \rightarrow S_n$); ii) stimulated emission at 600-750 nm (blue trace; $S_1 \rightarrow S_0$); iii) transient absorption of radical intermediates $AN^{\bullet+}$ - $PDI^{\bullet-}$ (red trace; 490 and 700 nm); iv) triplet absorption at 430, 550 and 630 nm (pink trace; $T_1 \rightarrow T_n$). Due to the ultrafast nature of ISC, no growth is observed for the triplet formation in the fTA spectra. So we could not extract any kinetic parameters from the fTA spectra analysis. A similar behaviour is observed in PY-PDI-PY in chloroform upon excitation with 400 nm (Figure 4.9B).

4.4. Conclusions

We have demonstrated the successful synthesis of PDI acceptor based near-orthogonal D-A dyads and D-A-D triads. Structure optimisation and electrochemical analysis of the derivatives confirm the near-orthogonality between the units. Phenyl substituted PDIs exhibit extended conjugation while anthracene and pyrene substituted PDIs show donor-acceptor character due to the negligible orbital overlap between AN/PY and PDI. Existence of ground state electron donor acceptor interactions in AN/PY derivatives facilitates the instantaneous charge separation between the units to generate $AN^{\bullet+}$ - $PDI^{\bullet-}$ and $PY^{\bullet+}$ - $PDI^{\bullet-}$. Phenyl substituted PDIs exhibit nearly quantitative fluorescence quantum yield ($\Phi_F \approx 0.95$) while the AN and PY substituted show highly quenched fluorescence ($\Phi_F \approx 0.05$) due to the

photoinduced electron transfer. Feasibility of electron transfer in the derivatives was estimated by calculating the free energy change for electron transfer from Rehm-Weller analysis. Charge transfer states were further characterised from solvent dependent time resolved fluorescence and Lippert-Mataga analysis. Excited state intersystem crossing properties of the derivatives were studied by femtosecond and nanosecond transient absorption spectroscopy by varying the solvent polarity. Solvent dependent nTA spectra of the dyads and triads show that non-polar solvent facilitate the formation of ^3PDI while long lived triplet charge separated states $^3(\text{D}^{+\bullet}-\text{A}^{-\bullet})$ are formed in polar solvents. Fully conjugated PH-PDI and PH-PDI-PH show neither CT nor ISC in the excited state, but only nearly quantitative fluorescence.

4.5. Experimental section:

Materials and methods: As described in the Chapter 2.

Computational details: Geometry optimisation of all the derivatives was performed by DFT calculations using nonlocal hybrid three-parameter Lee-Yang-Parr (B3LYP) level of theory (B3LYP/6-311G++(2d,2p)) as implemented in the Gaussian 09W program suite.

Electron paramagnetic resonance (EPR) spectroscopy: Continuous wave EPR (CW-EPR) measurements with X band (8.75-9.65 GHz) were carried using JEOL JES-FA200 ESR spectrometer at room temperature and liquid nitrogen (77 K) temperatures. Samples were prepared by loading the THF solutions of PA in 5 mm o.d. (4 mm i.d.) quartz tubes, subjecting them to nitrogen purging cycles and was sealed later using a rubber septum. Samples were photoexcited inside the EPR cavity with a USHIO Optical Modulex-XENON lamp-ES-UXL 500 with an input current of 20 amperes.

Synthesis and characterisation

General Procedure: 200 mg of PDI-Br₂ (synthesis of PDI-Br₂ is explained in chapter 2) was taken with 20 mL of distilled THF in nitrogen atmosphere. 10 mL of 2 M K₂CO₃ solution was added and the mixture was stirred under nitrogen flushing to remove the dissolved oxygen. (0.1 eq) of Pd(PPh₃)₄ was added and flushed with nitrogen for 10 more minutes. One and two equivalents of aryl boronic acid (phenylboronic acid, 9-anthracenylboronic acid and 1-pyrene-boronic acid) were added to synthesise desired dyads and triads respectively. The reaction mixture was refluxed at 65 °C for 12 hours. After the completion of the reaction, reaction mixture was poured into 50 mL of 1N HCl and the product was extracted with dichloromethane. Organic layer was washed with water, brine solution and it was dehydrated using anhydrous sodium sulphate. Dichloromethane was distilled out under reduced pressure to get crude product. The product was purified using column chromatography using dichloromethane as eluent.

PH-PDI: Yield: 60%; m. p. >300 °C. ¹H NMR (500 MHz, CDCl₃, δ): 8.62 (m, 2H), 8.59 (m, 3H), 8.06 (m, 1H), 7.78 (m, 1H), 7.46 (m, 3H), 7.39 (m, 2H), 4.27(t, 2H), 4.22 (t, 2H), 4.13 (m, 4H), 1.97 (m, 4H), 1.95 (m, 6H) ; ¹³C NMR (125 MHz, CDCl₃, δ): 171.20, 163.35, 163.25, 141.80, 137.96, 137.39, 136.45, 136.18, 134.99, 133.08, 132.57, 129.45, 128.87, 128.42, 128.31, 128.21, 127.44, 125.78, 124.68, 122.36, 122.09, 62.25, 37.54, 27.22, 20.87; IR (KBr): 3060, 2948, 1730, 1694, 1645, 1592 and 1405 cm⁻¹; Anal. Calcd for C₄₀H₃₀N₂O₈: C, 72.06; H, 4.54; N, 4.20. Found: C, 72.00; H, 4.48; N, 4.18.

AN-PDI: Yield: 40%; m. p. >300 °C. ¹H NMR (500 MHz, CDCl₃, δ): 8.75 (m, 2H), 8.64 (m, 3H), 8.45 (s, 1H), 8.09 (d, J = 8.6 Hz, 2H), 7.60 (d, J = 8.6 Hz, 1H), 7.47 (d, J = 8.8 Hz, 2H), 7.42 (m, 2H), 7.34 (d, J=7.85, 1H), 7.21 (m, 2H), 4.27 (t, J = 7.1 Hz, 2H), 4.11 (t, J = 6.3, 2H), 4.09 (m, 4H), 2.06 (m, 2H), 1.96 (s, 3H), 1.92 (m, 2H), 1.88 (s, 3H); ¹³C NMR (125 MHz, CDCl₃, δ): 171.07, 171.00, 163.60, 163.48, 163.19, 163.08, 138.14, 138.09, 135.82, 135.43, 134.90, 134.76, 134.69, 132.12, 131.34, 131.09, 131.06, 129.22,

129.03, 128.93, 128.54, 128.41, 128.10, 128.02, 127.16, 125.93, 124.81, 123.70, 123.25, 123.20, 123.01, 122.66, 122.28, 62.32, 60.39, 37.74, 37.54, 27.38, 27.22, 21.04, 20.93, 20.85 and 14.20; IR (KBr): 3041, 2964, 1738, 1701, 1650, 1587 and 1410 cm^{-1} ; Anal. Calcd for $\text{C}_{48}\text{H}_{34}\text{N}_2\text{O}_8$: C, 75.19; H, 4.47; N, 3.65. Found: C, 75.22; H, 4.45; N, 3.58.

PY-PDI: Yield: 45%; m. p. >300 °C. ^1H NMR (500 MHz, CDCl_3 , δ): 8.70 (m, 1H), 8.65 (m, 2H), 8.59 (m, 2H), 8.24 (m, 2H), 8.12 (m, 3H) 7.98 (m, 1H), 7.90 (m, 1H), 7.85 (m, 1H), 7.79 (m, 1H), 7.59 (m, 1H), 7.41 (m, 1H), 4.15 (m, 2H), 4.11 (m, 4H), 4.02 (m, 2H), 2.07 (m, 2H), 1.96 (s, 3H), 1.92 (m, 2H), 1.91 (s, 3H); ^{13}C NMR (125 MHz, CDCl_3 , δ): 171.03, 170.94, 163.57, 163.46, 163.31, 163.03, 140.33, 137.56, 137.01, 135.24, 134.95, 134.66, 134.06, 131.75, 131.47, 131.16, 131.10, 131.07, 130.55, 129.20, 129.18, 128.91, 128.71, 128.52, 128.08, 127.69, 127.38, 127.34, 126.58, 126.44, 126.40, 126.06, 125.74, 125.65, 124.84, 123.67, 123.53, 123.15, 122.88, 122.19, 122.09, 62.30, 62.25, 60.35, 37.73, 37.53, 31.56, 27.42, 27.26, 22.62, 20.90, 20.80, 14.18, 14.06; IR (KBr): 3061, 2966, 1730, 1690, 1654, 1600, 1440 cm^{-1} ; Anal. Calcd for $\text{C}_{50}\text{H}_{34}\text{N}_2\text{O}_8$: C, 75.94; H, 4.33; N, 3.54. Found: C, 75.90; H, 4.35; N, 3.58.

PH-PDI-PH: Yield: 55%; m. p. >300 °C. ^1H NMR (500 MHz, CDCl_3 , δ): 8.54 (s, 2H), 8.07 (d, $J=8.15$, 2H), 7.73 (d, $J = 8.15$ Hz, 2H), 7.46 (m, 10H), 4.24(t, $J = 7.05$ Hz, 4H), 4.09 (t, $J = 6.25$ Hz, 4H), 1.99 (m, 4H), 1.94 (s, 6H) ; ^{13}C NMR (125 MHz, CDCl_3 , δ): 171, 163.48, 142.19, 141.21, 135.40, 134.43, 130.23, 129.66, 129.01, 128.45, 128.21, 127.86, 127.27, 125.91, 124.65, 122.36, 62.28, 37.67, 27.37, 20.92; IR (KBr): 3043, 2930, 1745, 1690, 1650 and 1587 cm^{-1} ; Anal. Calcd for $\text{C}_{46}\text{H}_{34}\text{N}_2\text{O}_8$: C, 74.38; H, 4.61; N, 3.77. Found: C, 74.50; H, 4.55; N, 3.78.

AN-PDI-AN: Yield: 60%; m. p. >300 °C. ^1H NMR (500 MHz, CDCl_3 , δ): 8.73 (s, 2H), 8.54 (s, 2H), 8.20 (d, $J = 8.6$ Hz, 4H), 7.78 (d, 8.4 Hz, 2H), 7.64 (m, 6H), 7.53 (t, $J = 3.5$ Hz, 4H), 7.35 (t, $J = 3.7$ Hz, 4H), 4.18(t, $J = 7.1$ Hz, 4H), 4.09 (t, $J = 6.3$ Hz, 4H), 1.99 (m, 4H), 1.94 (s, 6H) ; ^{13}C NMR (125 MHz, CDCl_3 , δ): 171.00, 163.25, 163.2, 137.56, 137.34, 136.0, 135.18, 134.99, 132.08, 130.57, 129.31, 128.88, 128.45, 128.31, 128.26, 127.24,

125.88, 124.88, 122.56, 122.19, 62.25, 37.54, 27.22, 20.87; IR (KBr): 3051, 2956, 1737, 1697, 1658, 1597, 1400, 1330, 1244, 1178, , 813, 734 cm^{-1} ; Anal. Calcd for $\text{C}_{64}\text{H}_{42}\text{N}_2\text{O}_8$: C, 78.97; H, 4.49; N, 2.97. Found: C, 78.60; H, 4.35; N, 2.78.

PY-PDI-PY: Yield: 50%; m. p. >300 °C. ^1H NMR (500 MHz, CDCl_3 , δ): 8.72 (s, 2H), 8.31 (m, 1H), 8.25 (m, 2H), 8.18 (m, 5H), 8.14 (m, 5H), 8.10 (m, 1H), 8.05 (m, 1H), 7.91 (m, 3H), 7.70 (m, 2H), 7.55 (m, 2H), 4.10 (m, 4H), 4.05 (m, 4H), 1.97 (m, 4H), 1.94 (s, 6H) ; ^{13}C NMR (125 MHz, CDCl_3 , δ): 171.10, 163.25, 163.20, 139.74, 139.62, 137.06, 136.98, 135.19, 134.14, 134.09, 131.74, 131.68, 131.44, 131.11, 131.00, 129.99, 129.90, 129.85, 129.40, 129.19, 129.17, 128.87, 128.54, 128.50, 128.45, 127.92, 127.85, 127.74, 127.42, 127.33, 127.03, 126.64, 126.58, 126.37, 126.18, 126.06, 125.82, 125.68, 125.65, 125.59, 124.86, 124.80, 123.84, 123.62, 122.18, 121.91, 121.83, 121.76, 62.24, 37.54, 27.30, 27.27, 20.90, 20.87, 14.21; IR (KBr): 3060, 2970, 1724, 1690, 1668, 1607, 1390 cm^{-1} ; Anal. Calcd for $\text{C}_{66}\text{H}_{42}\text{N}_2\text{O}_8$: C, 79.99; H, 4.27; N, 2.83. Found: C, 79.90; H, 4.25; N, 2.80.

5. Bibliography

- [1] Muccini, M., A Bright Future for Organic Field-Effect Transistors, *Nat. Mater.* **2006**, *5*, 605-613.
- [2] O'Neill, M.; Kelly, S. M., Ordered Materials for Organic Electronics and Photonics, *Adv. Mater.* **2011**, *23*, 566-584.
- [3] Cao, W.; Xue, J., Recent Progress in Organic Photovoltaics: Device Architecture and Optical Design, *Energy Environ. Sci.* **2014**, *7*, 2123-2144.
- [4] Müller, T. J. J.; Bunz, U. H. F., *Functional Organic Materials : Syntheses, Strategies and Applications*. Wiley-VCH: Weinheim; Chichester, 2007.
- [5] Mukherjee, S.; Thilagar, P., Recent Advances in Purely Organic Phosphorescent Materials, *Chem. Commun.* **2015**, *51*, 10988-11003.
- [6] Wardle, B., *Principles and Applications of Photochemistry*. Wiley: Chichester, U.K., 2009.
- [7] Turro, N. J.; Ramamurthy, V.; Scaiano, J. C., *Principles of Molecular Photochemistry : An Introduction*. University Science Books: Sausalito, Calif., 2009.
- [8] Köhler, A.; Bässler, H., Triplet States in Organic Semiconductors, *Mater. Sci. Eng. R-Rep.* **2009**, *66*, 71-109.
- [9] Anslyn, E. V.; Dougherty, D. A., *Modern Physical Organic Chemistry*. University Science: Sausalito, CA, 2006.
- [10] Turro, N. J., The Triplet State, *J. Chem. Educ.* **1969**, *46*, 2.
- [11] Lower, S. K.; El-Sayed, M. A., The Triplet State and Molecular Electronic Processes in Organic Molecules, *Chem. Rev.* **1966**, *66*, 199-241.
- [12] Lakowicz, J. R., *Principles of Fluorescence Spectroscopy*. Springer: New York, 2006.
- [13] Köhler, A.; Wilson, J. S.; Friend, R. H., Fluorescence and Phosphorescence in Organic Materials, *Adv. Mater.* **2002**, *14*, 701-707.
- [14] Yang, C.-M.; Wu, C.-H.; Liao, H.-H.; Lai, K.-Y.; Cheng, H.-P.; Horng, S.-F.; Meng, H.-F.; Shy, J.-T., Enhanced Photovoltaic Response of Organic Solar Cell by Singlet-to-Triplet Exciton Conversion, *Appl. Phys. Lett.* **2007**, *90*, 133509.
- [15] Heremans, P.; Cheyns, D.; Rand, B. P., Strategies for Increasing the Efficiency of Heterojunction Organic Solar Cells: Material Selection and Device Architecture, *Acc. Chem. Res.* **2009**, *42*, 1740-1747.
- [16] Liu, S.; Qiao, W.; Cao, G.; Chen, Y.; Ma, Y.; Huang, Y.; Liu, X.; Xu, W.; Zhao, Q.; Huang, W., Smart Poly(N-isopropylacrylamide) Containing Iridium(III) Complexes as Water-Soluble Phosphorescent Probe for Sensing and Bioimaging of Homocysteine and Cysteine, *Macromol. Rapid Commun.* **2013**, *34*, 81-86.

- [17] Ma, Y.; Liu, S.; Yang, H.; Wu, Y.; Yang, C.; Liu, X.; Zhao, Q.; Wu, H.; Liang, J.; Li, F.; Huang, W., Water-Soluble Phosphorescent Iridium(III) Complexes as Multicolor Probes for Imaging of Homocysteine and Cysteine in Living Cells, *J. Mater. Chem.* **2011**, *21*, 18974-18982.
- [18] Plaetzer, K.; Krammer, B.; Berlanda, J.; Berr, F.; Kiesslich, T., Photophysics and Photochemistry of Photodynamic Therapy: Fundamental Aspects, *Lasers Med. Sci.* **2009**, *24*, 259-268.
- [19] Lee, J.; Chen, H.-F.; Batagoda, T.; Coburn, C.; Djurovich, P. I.; Thompson, M. E.; Forrest, S. R., Deep Blue Phosphorescent Organic Light-Emitting Diodes with Very High Brightness and Efficiency, *Nat. Mater.* **2016**, *15*, 92-98.
- [20] Hudson, Z. M.; Helander, M. G.; Lu, Z.-H.; Wang, S., Highly Efficient Orange Electrophosphorescence from a Trifunctional Organoboron-Pt(II) Complex, *Chem. Commun.* **2011**, *47*, 755-757.
- [21] Lund, A.; Shiotani, M.; Shimada, S., *Principles and Applications of ESR Spectroscopy*. Springer: Dordrecht; London, 2010.
- [22] Ogilby, P. R., Singlet Oxygen: There Is Indeed Something New under the Sun, *Chem. Soc. Rev.* **2010**, *39*, 3181-3209.
- [23] Berera, R.; van Grondelle, R.; Kennis, J. T. M., Ultrafast Transient Absorption Spectroscopy: Principles and Application to Photosynthetic Systems, *Photosynth. Res.* **2009**, *101*, 105-118.
- [24] Marian, C. M., Spin-Orbit Coupling and Intersystem Crossing in Molecules, *WIREs Comput. Mol. Sci.* **2012**, *2*, 187-203.
- [25] Dance, Z. E. X.; Mickley, S. M.; Wilson, T. M.; Ricks, A. B.; Scott, A. M.; Ratner, M. A.; Wasielewski, M. R., Intersystem Crossing Mediated by Photoinduced Intramolecular Charge Transfer: Julolidine-Anthracene Molecules with Perpendicular π Systems, *J. Phys. Chem. A* **2008**, *112*, 4194-4201.
- [26] Smith, M. B.; Michl, J., Recent Advances in Singlet Fission, *Annu. Rev. Phys. Chem.* **2013**, *64*, 361-386.
- [27] Smith, M. B.; Michl, J., Singlet Fission, *Chem. Rev.* **2010**, *110*, 6891-6936.
- [28] Singh, S.; Jones, W. J.; Siebrand, W.; Stoicheff, B. P.; Schneider, W. G., Laser Generation of Excitons and Fluorescence in Anthracene Crystals, *J. Chem. Phys.* **1965**, *42*, 330-342.
- [29] Swenberg, C. E.; Stacy, W. T., Bimolecular Radiationless Transitions in Crystalline Tetracene, *Chem. Phys. Lett.* **1968**, *2*, 327-328.
- [30] Wilson, M. W. B.; Rao, A.; Ehrler, B.; Friend, R. H., Singlet Exciton Fission in Polycrystalline Pentacene: From Photophysics toward Devices, *Acc. Chem. Res.* **2013**, *46*, 1330-1338.

- [31] Johnson, J. C.; Nozik, A. J.; Michl, J., High Triplet Yield from Singlet Fission in a Thin Film of 1,3-Diphenylisobenzofuran, *J. Am. Chem. Soc.* **2010**, *132*, 16302-16303.
- [32] Najafov, H.; Lee, B.; Zhou, Q.; Feldman, L. C.; Podzorov, V., Observation of Long-Range Exciton Diffusion in Highly Ordered Organic Semiconductors, *Nat. Mater.* **2010**, *9*, 938-943.
- [33] Wilson, M. W. B.; Rao, A.; Clark, J.; Kumar, R. S. S.; Brida, D.; Cerullo, G.; Friend, R. H., Ultrafast Dynamics of Exciton Fission in Polycrystalline Pentacene, *J. Am. Chem. Soc.* **2011**, *133*, 11830-11833.
- [34] Musser, A. J.; Maiuri, M.; Brida, D.; Cerullo, G.; Friend, R. H.; Clark, J., The Nature of Singlet Exciton Fission in Carotenoid Aggregates, *J. Am. Chem. Soc.* **2015**, *137*, 5130-5139.
- [35] Busby, E.; Berkelbach, T. C.; Kumar, B.; Chernikov, A.; Zhong, Y.; Hlaing, H.; Zhu, X. Y.; Heinz, T. F.; Hybertsen, M. S.; Sfeir, M. Y.; Reichman, D. R.; Nuckolls, C.; Yaffe, O., Multiphonon Relaxation Slows Singlet Fission in Crystalline Hexacene, *J. Am. Chem. Soc.* **2014**, *136*, 10654-10660.
- [36] Pensack, R. D.; Tilley, A. J.; Parkin, S. R.; Lee, T. S.; Payne, M. M.; Gao, D.; Jahnke, A. A.; Oblinsky, D. G.; Li, P.-F.; Anthony, J. E.; Seferos, D. S.; Scholes, G. D., Exciton Delocalization Drives Rapid Singlet Fission in Nanoparticles of Acene Derivatives, *J. Am. Chem. Soc.* **2015**, *137*, 6790-6803.
- [37] Wu, Y.; Liu, K.; Liu, H.; Zhang, Y.; Zhang, H.; Yao, J.; Fu, H., Impact of Intermolecular Distance on Singlet Fission in a Series of Tips Pentacene Compounds, *J. Phys. Chem. Lett.* **2014**, *5*, 3451-3455.
- [38] Wang, C.; Tauber, M. J., High-Yield Singlet Fission in a Zeaxanthin Aggregate Observed by Picosecond Resonance Raman Spectroscopy, *J. Am. Chem. Soc.* **2010**, *132*, 13988-13991.
- [39] Eaton, S. W.; Miller, S. A.; Margulies, E. A.; Shoer, L. E.; Schaller, R. D.; Wasielewski, M. R., Singlet Exciton Fission in Thin Films of Tert-Butyl-Substituted Terrylenes, *J. Phys. Chem. A* **2015**, *119*, 4151-4161.
- [40] Kasai, Y.; Tamai, Y.; Ohkita, H.; Bente, H.; Ito, S., Ultrafast Singlet Fission in a Push-Pull Low-Bandgap Polymer Film, *J. Am. Chem. Soc.* **2015**, *137*, 15980-15983.
- [41] Eaton, S. W.; Shoer, L. E.; Karlen, S. D.; Dyar, S. M.; Margulies, E. A.; Veldkamp, B. S.; Ramanan, C.; Hartzler, D. A.; Savikhin, S.; Marks, T. J.; Wasielewski, M. R., Singlet Exciton Fission in Polycrystalline Thin Films of a Slip-Stacked Perylenediimide, *J. Am. Chem. Soc.* **2013**, *135*, 14701-14712.
- [42] Lefler, K. M.; Brown, K. E.; Salamant, W. A.; Dyar, S. M.; Knowles, K. E.; Wasielewski, M. R., Triplet State Formation in Photoexcited Slip-Stacked Perylene-3,4:9,10-

- Bis(Dicarboximide) Dimers on a Xanthene Scaffold, *J. Phys. Chem. A* **2013**, *117*, 10333-10345.
- [43] Veldman, D.; Chopin, S. M. A.; Meskers, S. C. J.; Groeneveld, M. M.; Williams, R. M.; Janssen, R. A. J., Triplet Formation Involving a Polar Transition State in a Well-Defined Intramolecular Perylenediimide Dimeric Aggregate, *J. Phys. Chem. A* **2008**, *112*, 5846-5857.
- [44] Li, C.; Wonneberger, H., Perylene Imides for Organic Photovoltaics: Yesterday, Today, and Tomorrow, *Adv. Mater.* **2012**, *24*, 613-636.
- [45] Huang, C.; Barlow, S.; Marder, S. R., Perylene-3,4,9,10-Tetracarboxylic Acid Diimides: Synthesis, Physical Properties, and Use in Organic Electronics, *J. Org. Chem.* **2011**, *76*, 2386-2407.
- [46] Würthner, F.; Saha-Möller, C. R.; Fimmel, B.; Ogi, S.; Leowanawat, P.; Schmidt, D., Perylene Bisimide Dye Assemblies as Archetype Functional Supramolecular Materials, *Chem. Rev.* **2016**, *116*, 962-1052.
- [47] Guo, Y.; Li, Y.; Awartani, O.; Zhao, J.; Han, H.; Ade, H.; Zhao, D.; Yan, H., A Vinylene-Bridged Perylenediimide-Based Polymeric Acceptor Enabling Efficient All-Polymer Solar Cells Processed under Ambient Conditions, *Adv. Mater.* **2016**, *28*, 8483-8489.
- [48] Chen, Z.; Fimmel, B.; Würthner, F., Solvent and Substituent Effects on Aggregation Constants of Perylene Bisimide π -Stacks - A Linear Free Energy Relationship Analysis, *Org. Biomol. Chem.* **2012**, *10*, 5845-5855.
- [49] Rybtchinski, B.; Sinks, L. E.; Wasielewski, M. R., Combining Light-Harvesting and Charge Separation in a Self-Assembled Artificial Photosynthetic System Based on Perylenediimide Chromophores, *J. Am. Chem. Soc.* **2004**, *126*, 12268-12269.
- [50] Chen, Z.; Lohr, A.; Saha-Möller, C. R.; Würthner, F., Self-Assembled π -Stacks of Functional Dyes in Solution: Structural and Thermodynamic Features, *Chem. Soc. Rev.* **2009**, *38*, 564-584.
- [51] Ford, W. E.; Kamat, P. V., Photochemistry of 3,4,9,10-Perylenetetracarboxylic Dianhydride Dyes. 3. Singlet and Triplet Excited-State Properties of the bis(2,5-di-tert-butylphenyl)imide Derivative, *J. Phys. Chem.* **1987**, *91*, 6373-6380.
- [52] Tilley, A. J.; Pensack, R. D.; Lee, T. S.; Djukic, B.; Scholes, G. D.; Seferos, D. S., Ultrafast Triplet Formation in Thionated Perylene Diimides, *J. Phys. Chem. C* **2014**, *118*, 9996-10004.
- [53] Vagnini, M. T.; Smeigh, A. L.; Blakemore, J. D.; Eaton, S. W.; Schley, N. D.; D'Souza, F.; Crabtree, R. H.; Brudvig, G. W.; Co, D. T.; Wasielewski, M. R., Ultrafast Photodriven Intramolecular Electron Transfer from an Iridium-Based Water-Oxidation Catalyst to Perylene Diimide Derivatives, *Proc. Natl. Acad. Sci. U.S.A.* **2012**, *109*, 15651-15656.

- [54] Rachford, A. A.; Goeb, S.; Castellano, F. N., Accessing the Triplet Excited State in Perylenediimides, *J. Am. Chem. Soc.* **2008**, *130*, 2766-2767.
- [55] Schulze, M.; Steffen, A.; Würthner, F., Near-Ir Phosphorescent Ruthenium(II) and Iridium(III) Perylene Bisimide Metal Complexes, *Angew. Chem. Int. Ed.* **2015**, *54*, 1570-1573.
- [56] Jiménez, Á. J.; Spänig, F.; Rodríguez-Morgade, M. S.; Ohkubo, K.; Fukuzumi, S.; Guldi, D. M.; Torres, T., A Tightly Coupled Bis(Zinc(II) Phthalocyanine)–Perylenediimide Ensemble to Yield Long-Lived Radical Ion Pair States, *Org. Lett.* **2007**, *9*, 2481-2484.
- [57] Ventura, B.; Langhals, H.; Bock, B.; Flamigni, L., Phosphorescent Perylene Imides, *Chem. Commun.* **2012**, *48*, 4226-4228.
- [58] Zhan, X.; Facchetti, A.; Barlow, S.; Marks, T. J.; Ratner, M. A.; Wasielewski, M. R.; Marder, S. R., Rylene and Related Diimides for Organic Electronics, *Adv. Mater.* **2011**, *23*, 268-284.
- [59] Gao, X.; Hu, Y., Development of N-Type Organic Semiconductors for Thin Film Transistors: A Viewpoint of Molecular Design, *J. Mater. Chem. C* **2014**, *2*, 3099-3117.
- [60] Zhan, X.; Facchetti, A.; Barlow, S.; Marks, T. J.; Ratner, M. A.; Wasielewski, M. R.; Marder, S. R., Rylene and Related Diimides for Organic Electronics, *Advanced Materials (Weinheim, Germany)* **2011**, *23*, 268-284.
- [61] Ryan, S. T.; Young, R. M.; Henkelis, J. J.; Hafezi, N.; Vermeulen, N. A.; Hennig, A.; Dale, E. J.; Wu, Y.; Krzyaniak, M. D.; Fox, A.; Nau, W. M.; Wasielewski, M. R.; Stoddart, J. F.; Scherman, O. A., Energy and Electron Transfer Dynamics within a Series of Perylene Diimide/Cyclophane Systems, *J. Am. Chem. Soc.* **2015**, *137*, 15299-307.
- [62] Wu, Y.; Young, R. M.; Frasconi, M.; Schneebeli, S. T.; Spenst, P.; Gardner, D. M.; Brown, K. E.; Würthner, F.; Stoddart, J. F.; Wasielewski, M. R., Ultrafast Photoinduced Symmetry-Breaking Charge Separation and Electron Sharing in Perylenediimide Molecular Triangles, *J. Am. Chem. Soc.* **2015**, *137*, 13236-13239.
- [63] Kumar, M.; George, S. J., Homotropic and Heterotropic Allosteric Regulation of Supramolecular Chirality, *Chem. Sci.* **2014**, *5*, 3025-3030.
- [64] Neelakandan, P. P.; Zeidan, T. A.; McCullagh, M.; Schatz, G. C.; Vura-Weis, J.; Kim, C. H.; Wasielewski, M. R.; Lewis, F. D., Ground and Excited State Electronic Spectra of Perylenediimide Dimers with Flexible and Rigid Geometries in DNA Conjugates, *Chem. Sci.* **2014**, *5*, 973-981.
- [65] Hariharan, M.; Zheng, Y.; Long, H.; Zeidan, T. A.; Schatz, G. C.; Vura-Weis, J.; Wasielewski, M. R.; Zuo, X.; Tiede, D. M.; Lewis, F. D., Hydrophobic Dimerization and Thermal Dissociation of Perylenediimide-Linked DNA Hairpins, *J. Am. Chem. Soc.* **2009**, *131*, 5920-5929.

- [66] Ajayaghosh, A.; Praveen, V. K.; Vijayakumar, C., Organogels as Scaffolds for Excitation Energy Transfer and Light Harvesting, *Chem. Soc. Rev.* **2008**, *37*, 109-122.
- [67] De Schryver, F. C.; Vosch, T.; Cotlet, M.; Van der Auweraer, M.; Müllen, K.; Hofkens, J., Energy Dissipation in Multichromophoric Single Dendrimers, *Acc. Chem. Res.* **2005**, *38*, 514-522.
- [68] Shahar, C.; Baram, J.; Tidhar, Y.; Weissman, H.; Cohen, S. R.; Pinkas, I.; Rybtchinski, B., Self-Assembly of Light-Harvesting Crystalline Nanosheets in Aqueous Media, *ACS Nano* **2013**, *7*, 3547-3556.
- [69] Nelson, C. A.; Monahan, N. R.; Zhu, X. Y., Exceeding the Shockley-Queisser Limit in Solar Energy Conversion, *Energy Environ. Sci.* **2013**, *6*, 3508-3519.
- [70] Arias, D. H.; Ryerson, J. L.; Cook, J. D.; Damrauer, N. H.; Johnson, J. C., Polymorphism Influences Singlet Fission Rates in Tetracene Thin Films, *Chem. Sci.* **2016**, *7*, 1185-1191.
- [71] Paci, I.; Johnson, J. C.; Chen, X.; Rana, G.; Popović, D.; David, D. E.; Nozik, A. J.; Ratner, M. A.; Michl, J., Singlet Fission for Dye-Sensitized Solar Cells: Can a Suitable Sensitizer Be Found?, *J. Am. Chem. Soc.* **2006**, *128*, 16546-16553.
- [72] Walker, B. J.; Musser, A. J.; Beljonne, D.; Friend, R. H., Singlet Exciton Fission in Solution, *Nat. Chem.* **2013**, *5*, 1019-1024.
- [73] Sanders, S. N.; Kumarasamy, E.; Pun, A. B.; Trinh, M. T.; Choi, B.; Xia, J.; Taffet, E. J.; Low, J. Z.; Miller, J. R.; Roy, X.; Zhu, X. Y.; Steigerwald, M. L.; Sfeir, M. Y.; Campos, L. M., Quantitative Intramolecular Singlet Fission in Bipentacenes, *J. Am. Chem. Soc.* **2015**, *137*, 8965-8972.
- [74] Schrauben, J. N.; Ryerson, J. L.; Michl, J.; Johnson, J. C., Mechanism of Singlet Fission in Thin Films of 1,3-Diphenylisobenzofuran, *J. Am. Chem. Soc.* **2014**, *136*, 7363-7373.
- [75] Yost, S. R.; Lee, J.; Wilson, M. W. B.; Wu, T.; McMahon, D. P.; Parkhurst, R. R.; Thompson, N. J.; Congreve, D. N.; Rao, A.; Johnson, K.; Sfeir, M. Y.; Bawendi, M. G.; Swager, T. M.; Friend, R. H.; Baldo, M. A.; Van Voorhis, T., A Transferable Model for Singlet-Fission Kinetics, *Nat. Chem.* **2014**, *6*, 492-497.
- [76] Renaud, N.; Grozema, F. C., Intermolecular Vibrational Modes Speed up Singlet Fission in Perylenediimide Crystals, *J. Phys. Chem. Lett.* **2015**, *6*, 360-365.
- [77] Wu, Y.; Zhen, Y.; Ma, Y.; Zheng, R.; Wang, Z.; Fu, H., Exceptional Intersystem Crossing in Di(perylene bisimide)s: A Structural Platform toward Photosensitizers for Singlet Oxygen Generation, *J. Phys. Chem. Lett.* **2010**, *1*, 2499-2502.
- [78] Cheriya, R. T.; Mallia, A. R.; Hariharan, M., Light Harvesting Vesicular Donor-Acceptor Scaffold Limits the Rate of Charge Recombination in the Presence of an Electron Donor, *Energy Environ. Sci.* **2014**, *7*, 1661-1669.

- [79] Nagarajan, K.; Rajagopal, S. K.; Hariharan, M., C-H•••H-C and C-H••• π Contacts Aid Transformation of Dimeric to Monomeric Anthracene in the Solid State, *CrystEngComm* **2014**, *16*, 8946-8949.
- [80] Joy, J.; Cheriya, R. T.; Nagarajan, K.; Shaji, A.; Hariharan, M., Breakdown of Exciton Splitting through Electron Donor–Acceptor Interaction: A Caveat for the Application of Exciton Chirality Method in Macromolecules, *J. Phys. Chem. C* **2013**, *117*, 17927-17939.
- [81] Mallia, A. R.; Salini, P. S.; Hariharan, M., Nonparallel Stacks of Donor and Acceptor Chromophores Evade Geminate Charge Recombination, *J. Am. Chem. Soc.* **2015**, *137*, 15604-15607.
- [82] Nagarajan, K.; Mallia, A. R.; Reddy, V. S.; Hariharan, M., Access to Triplet Excited State in Core-Twisted Perylenediimide, *J. Phys. Chem. C* **2016**, *120*, 8443-8450.
- [83] Qiu, W.; Chen, S.; Sun, X.; Liu, Y.; Zhu, D., Suzuki Coupling Reaction of 1,6,7,12-Tetrabromoperylene Bisimide, *Org. Lett.* **2006**, *8*, 867-870.
- [84] Rajasingh, P.; Cohen, R.; Shirman, E.; Shimon, L. J. W.; Rybtchinski, B., Selective Bromination of Perylene Diimides under Mild Conditions, *J. Org. Chem.* **2007**, *72*, 5973-5979.
- [85] Osswald, P.; Würthner, F., Effects of Bay Substituents on the Racemization Barriers of Perylene Bisimides: Resolution of Atropo-Enantiomers, *J. Am. Chem. Soc.* **2007**, *129*, 14319-14326.
- [86] Handa, N. V.; Mendoza, K. D.; Shirtcliff, L. D., Syntheses and Properties of 1,6 and 1,7 Perylene Diimides and Tetracarboxylic Dianhydrides, *Org. Lett.* **2011**, *13*, 4724-4727.
- [87] Dubey, R. K.; Niemi, M.; Kaunisto, K.; Efimov, A.; Tkachenko, N. V.; Lemmetyinen, H., Direct Evidence of Significantly Different Chemical Behavior and Excited-State Dynamics of 1,7- and 1,6-Regioisomers of Pyrrolidinyl-Substituted Perylene Diimide, *Chem. Eur. J.* **2013**, *19*, 6791-6806.
- [88] Schmidt, R.; Oh, J. H.; Sun, Y.-S.; Deppisch, M.; Krause, A.-M.; Radacki, K.; Braunschweig, H.; Könemann, M.; Erk, P.; Bao, Z.; Würthner, F., High-Performance Air-Stable N-Channel Organic Thin Film Transistors Based on Halogenated Perylene Bisimide Semiconductors, *J. Am. Chem. Soc.* **2009**, *131*, 6215-6228.
- [89] Gautrot, J. E.; Hodge, P.; Cupertino, D.; Helliwell, M., Experimental Evidence for Carbonyl– π Electron Cloud Interactions, *New Journal of Chemistry* **2006**, *30*, 1801-1807.
- [90] Kim, C.-Y.; Chandra, P. P.; Jain, A.; Christianson, D. W., Fluoroaromatic–Fluoroaromatic Interactions between Inhibitors Bound in the Crystal Lattice of Human Carbonic Anhydrase II, *J. Am. Chem. Soc.* **2001**, *123*, 9620-9627.

- [91] Rajagopal, S. K.; Philip, A. M.; Nagarajan, K.; Hariharan, M., Progressive Acylation of Pyrene Engineers Solid State Packing and Colour Via C-H•••H-C, C-H•••O and π - π Interactions, *Chem. Commun.* **2014**, *50*, 8644-8647.
- [92] Matter, H.; Nazaré, M.; Güssregen, S.; Will, D. W.; Schreuder, H.; Bauer, A.; Urmann, M.; Ritter, K.; Wagner, M.; Wehner, V., Evidence for C-Cl/C-Br••• π Interactions as an Important Contribution to Protein-Ligand Binding Affinity, *Angew. Chem. Int. Ed.* **2009**, *48*, 2911-2916.
- [93] Mallia, A. R.; Sethy, R.; Bhat, V.; Hariharan, M., Crystallization Induced Enhanced Emission in Conformational Polymorphs of a Rotationally Flexible Molecule, *J. Mater. Chem. C* **2016**, *4*, 2931-2935.
- [94] Seifert, S.; Schmidt, D.; Würthner, F., An Ambient Stable Core-Substituted Perylene Bisimide Dianion: Isolation and Single Crystal Structure Analysis, *Chem. Sci.* **2015**, *6*, 1663-1667.
- [95] Chen, Z.; Baumeister, U.; Tschierske, C.; Würthner, F., Effect of Core Twisting on Self-Assembly and Optical Properties of Perylene Bisimide Dyes in Solution and Columnar Liquid Crystalline Phases, *Chem. Eur. J.* **2007**, *13*, 450-465.
- [96] Sadrai, M.; Hadel, L.; Sauers, R. R.; Husain, S.; Krogh-Jespersen, K.; Westbrook, J. D.; Bird, G. R., Lasing Action in a Family of Perylene Derivatives: Singlet Absorption and Emission Spectra, Triplet Absorption and Oxygen Quenching Constants, and Molecular Mechanics and Semiempirical Molecular Orbital Calculations, *J. Phys. Chem.* **1992**, *96*, 7988-7996.
- [97] Fron, E.; Schweitzer, G.; Osswald, P.; Würthner, F.; Marsal, P.; Beljonne, D.; Mullen, K.; De Schryver, F. C.; Van der Auweraer, M., Photophysical Study of Bay Substituted Perylenediimides, *Photochem. Photobiol. Sci.* **2008**, *7*, 1509-1521.
- [98] Dreeskamp, H.; Koch, E.; Zander, M., Fluorescence of Bromoperylene and the Requirements of Heavy-Atom Quenching, *Chem. Phys. Lett.* **1975**, *31*, 251-253.
- [99] Caldwell, R. A.; Jacobs, L. D.; Furlani, T. R.; Nalley, E. A.; Laboy, J., Conformationally Dependent Heavy Atom Effect of Chlorine on Alkene Triplet Lifetimes. Experimental and Ab Initio Calculations, *J. Am. Chem. Soc.* **1992**, *114*, 1623-1625.
- [100] Becke, A. D., *J. Chem. Phys.* **1993**, *98*, 5648-5652.
- [101] Lee, C.; Yang, W.; Parr, R. G., *Phys. Rev. B* **1988**, *37*, 785-789.
- [102] Brown, K. E.; Veldkamp, B. S.; Co, D. T.; Wasielewski, M. R., Vibrational Dynamics of a Perylene-Perylenediimide Donor-Acceptor Dyad Probed with Femtosecond Stimulated Raman Spectroscopy, *J. Phys. Chem. Lett.* **2012**, *3*, 2362-2366.
- [103] Kaiser, T. E.; Stepanenko, V.; Würthner, F., Fluorescent J-Aggregates of Core-Substituted Perylene Bisimides: Studies on Structure-Property Relationship,

- Nucleation–Elongation Mechanism, and Sergeants-and-Soldiers Principle, *J. Am. Chem. Soc.* **2009**, *131*, 6719-6732.
- [104] Reineke, S.; Baldo, M. A., Room Temperature Triplet State Spectroscopy of Organic Semiconductors, *Sci. Rep.* **2014**, *4*, 3797.
- [105] Hinoue, T.; Shigenoi, Y.; Sugino, M.; Mizobe, Y.; Hisaki, I.; Miyata, M.; Tohnai, N., Regulation of π -Stacked Anthracene Arrangement for Fluorescence Modulation of Organic Solid from Monomer to Excited Oligomer Emission, *Chem. Eur. J.* **2012**, *18*, 4634-4643.
- [106] Eaton, D. F., Reference Materials for Fluorescence Measurement, *Pure Appl. Chem.* **1988**, *60*, 1107-1114.
- [107] Cölle, M.; Gmeiner, J.; Milius, W.; Hillebrecht, H.; Brütting, W., Preparation and Characterization of Blue-Luminescent Tris(8-Hydroxyquinoline)-Aluminum (Alq3), *Adv. Funct. Mater.* **2003**, *13*, 108-112.
- [108] Snellenburg, J. J.; Laptinok, S. P.; Seger, R.; Mullen, K. M.; van Stokkum, I. H. M., Glotaran: A Java-Based Graphical User Interface for the R Package Timp., *J. Stat. Soft.* **2012**, *49*, 1–22.
- [109] Sandros, K., *Acta Chem. Scand.* **1964**, *18*, 2355-2374.
- [110] Frisch, M. J.; Trucks, G. W.; Schlegel, H. B.; Scuseria, G. E.; Rob, M. A.; Cheeseman, J. R.; Montgomery Jr., J. A.; Vreven, T. K., K. N.; Burant, J. C.; Millam, J. M.; Iyengar, S. S.; Tomasi, J.; Barone, V.; Mennucci, B.; Cossi, M.; Scalmani, G.; Rega, N.; Petersson, G. A.; Nakatsuji, H.; Hada, M.; Ehara, M.; Toyota, K.; Fukuda, R.; Hasegawa, J.; Ishida, M.; Nakajima, Y.; Honda, O.; Kitao, H.; Nakai, M.; Klene, X.; Li, J. E.; Knox, H. P.; Hratchian, J. B.; Cross, T.; Bakken, V.; Adamo, C.; Jaramillo, J.; Gomperts, R.; Stratmann, R. E.; Yazyev, O.; Austin, A. J.; Cammi, R.; Pomelli, C.; Ochterski, J. W.; Ayala, P. Y.; Morokuma, K.; Voth, G. A.; Salvador, P.; Dannenberg, J. J.; Zakrzewski, V. G.; Dapprich, S.; Daniels, A. D.; Strain, M. C.; Farkas, O.; Malick, D. K.; Rabuck, A. D.; Raghavachari, K.; Foresman, J. B.; Ortiz, J. V.; Cui, Q.; Baboul, A. G.; Clifford, S.; Cioslowski, J.; Stefanov, B. B.; Liu, G.; Liashenko, A.; Piskorz, P.; Komaromi, I.; Martin, R. L.; Fox, D. J.; Keith, T.; Al-Laham, M. A.; Peng, C. Y.; Nanayakkara, A.; Challacombe, M.; Gill, P. M. W.; Johnson, B.; Chen, W.; Wong, M. W.; Gonzalez, C.; Pople, J. A. *Gaussian 03* (Gaussian, Inc., Wallingford, CT, 2003).
- [111] Ball, M.; Zhong, Y.; Wu, Y.; Schenck, C.; Ng, F.; Steigerwald, M.; Xiao, S.; Nuckolls, C., Contorted Polycyclic Aromatics, *Acc. Chem. Res.* **2015**, *48*, 267-276.
- [112] Sanchez-Valencia, J. R.; Dienel, T.; Groning, O.; Shorubalko, I.; Mueller, A.; Jansen, M.; Amsharov, K.; Ruffieux, P.; Fasel, R., Controlled Synthesis of Single-Chirality Carbon Nanotubes, *Nature* **2014**, *512*, 61-64.

- [113] Liu, Z.; Fan, A. C.; Rakhra, K.; Sherlock, S.; Goodwin, A.; Chen, X.; Yang, Q.; Felsher, D. W.; Dai, H., Supramolecular Stacking of Doxorubicin on Carbon Nanotubes for in Vivo Cancer Therapy, *Angew. Chem. Int. Ed.* **2009**, *48*, 7668-7672.
- [114] Suzuki, N.; Wang, Y.; Elvati, P.; Ou, Z.-B.; Kim, K.; Jiang, S.; Baumeister, E.; Lee, J.; Yeom, B.; Bahng, J. H.; Lee, J.; Violi, A.; Kotov, N. A., Chiral Graphene Quantum Dots, *ACS Nano* **2016**, *10*, 1744-1755.
- [115] Modi, A.; Koratkar, N.; Lass, E.; Wei, B.; Ajayan, P. M., Miniaturized Gas Ionization Sensors Using Carbon Nanotubes, *Nature* **2003**, *424*, 171-174.
- [116] Geim, A. K.; Novoselov, K. S., The Rise of Graphene, *Nat. Mater.* **2007**, *6*, 183-191.
- [117] Mueller, M. L.; Yan, X.; McGuire, J. A.; Li, L.-S., Triplet States and Electronic Relaxation in Photoexcited Graphene Quantum Dots, *Nano Lett.* **2010**, *10*, 2679-2682.
- [118] Balakrishnan, J.; Kok Wai Koon, G.; Jaiswal, M.; Castro Neto, A. H.; Ozyilmaz, B., Colossal Enhancement of Spin-Orbit Coupling in Weakly Hydrogenated Graphene, *Nat. Phys.* **2013**, *9*, 284-287.
- [119] Irmer, S.; Frank, T.; Putz, S.; Gmitra, M.; Kochan, D.; Fabian, J., Spin-Orbit Coupling in Fluorinated Graphene, *Phys. Rev. B*, **2015**, *91*, 115141.
- [120] Avsar, A.; Tan, J. Y.; Taychatanapat, T.; Balakrishnan, J.; Koon, G. K.; Yeo, Y.; Lahiri, J.; Carvalho, A.; Rodin, A. S.; O'Farrell, E. C.; Eda, G.; Castro Neto, A. H.; Ozyilmaz, B., Spin-Orbit Proximity Effect in Graphene, *Nat. Commun.* **2014**, *5*, 1-6.
- [121] Marchenko, D.; Varykhalov, A.; Scholz, M. R.; Bihlmayer, G.; Rashba, E. I.; Rybkin, A.; Shikin, A. M.; Rader, O., Giant Rashba Splitting in Graphene Due to Hybridization with Gold, *Nat. Commun.* **2012**, *3*, 1232.
- [122] Kralj, M., Graphene Spintronics: Intercalated Boosters, *Nat. Phys.* **2015**, *11*, 11-12.
- [123] Weeks, C.; Hu, J.; Alicea, J.; Franz, M.; Wu, R., Engineering a Robust Quantum Spin Hall State in Graphene Via Adatom Deposition, *Phys. Rev. X* **2011**, *1*, 021001-021015.
- [124] Arbogast, J. W.; Foote, C. S., Photophysical Properties of C70, *J. Am. Chem. Soc.* **1991**, *113*, 8886-8889.
- [125] Lewis, F. D.; Zuo, X., Activated Decay Pathways for Planar vs Twisted Singlet Phenylalkenes, *J. Am. Chem. Soc.* **2003**, *125*, 8806-8813.
- [126] Huertas-Hernando, D.; Guinea, F.; Brataas, A., Spin-Orbit Coupling in Curved Graphene, Fullerenes, Nanotubes, and Nanotube Caps, *Phys. Rev. B*, **2006**, *74*, 155426.
- [127] Bolton, O.; Lee, K.; Kim, H.-J.; Lin, K. Y.; Kim, J., Activating Efficient Phosphorescence from Purely Organic Materials by Crystal Design, *Nat. Chem.* **2011**, *3*, 205-210.
- [128] Li, Y.; Jia, Z.; Xiao, S.; Liu, H.; Li, Y., A Method for Controlling the Synthesis of Stable Twisted Two-Dimensional Conjugated Molecules, *Nat. Commun.* **2016**, *7*.

- [129] Ravat, P.; Šolomek, T.; Rickhaus, M.; Häussinger, D.; Neuburger, M.; Baumgarten, M.; Juríček, M., Cethrene: A Helically Chiral Biradicaloid Isomer of Heptazethrene, *Angew. Chem. Int. Ed.* **2016**, *55*, 1183-1186.
- [130] Dutta, A. K.; Linden, A.; Zoppi, L.; Baldrige, K. K.; Siegel, J. S., Extended Corannulenes: Aromatic Bowl/Sheet Hybridization, *Angew. Chem. Int. Ed.* **2015**, *54*, 10792-6.
- [131] Fujikawa, T.; Segawa, Y.; Itami, K., Synthesis, Structures, and Properties of π -Extended Double Helicene: A Combination of Planar and Nonplanar π -Systems, *J. Am. Chem. Soc.* **2015**.
- [132] Qiao, X.; Ho, D. M.; Pascal, R. A., An Extraordinarily Twisted Polycyclic Aromatic Hydrocarbon, *Angew. Chem. Int. Ed.* **1997**, *36*, 1531-1532.
- [133] Tan, Y.-Z.; Yang, B.; Parvez, K.; Narita, A.; Osella, S.; Beljonne, D.; Feng, X.; Müllen, K., Atomically Precise Edge Chlorination of Nanographenes and Its Application in Graphene Nanoribbons, *Nat. Commun.* **2013**, *4*.
- [134] Kawasumi, K.; Zhang, Q.; Segawa, Y.; Scott, L. T.; Itami, K., A Grossly Warped Nanographene and the Consequences of Multiple Odd-Membered-Ring Defects, *Nat. Chem.* **2013**, *5*, 739-744.
- [135] Xiao, S.; Myers, M.; Miao, Q.; Saur, S.; Pang, K.; Steigerwald, M. L.; Nuckolls, C., Molecular Wires from Contorted Aromatic Compounds, *Angew. Chem. Int. Ed.* **2005**, *44*, 7390-7394.
- [136] Baumgärtner, K.; Meza Chinchá, A. L.; Dreuw, A.; Rominger, F.; Mastalerz, M., A Conformationally Stable Contorted Hexabenzoovalene, *Angew. Chem. Int. Ed.* **2016**, *55*, 15594-15598.
- [137] Chiu, C.-Y.; Kim, B.; Gorodetsky, A. A.; Sattler, W.; Wei, S.; Sattler, A.; Steigerwald, M.; Nuckolls, C., Shape-Shifting in Contorted Dibenzotetrathienocoronenes, *Chem. Sci.* **2011**, *2*, 1480-1486.
- [138] Xiao, S.; Kang, S. J.; Wu, Y.; Ahn, S.; Kim, J. B.; Loo, Y.-L.; Siegrist, T.; Steigerwald, M. L.; Li, H.; Nuckolls, C., Supersized Contorted Aromatics, *Chem. Sci.* **2013**, *4*, 2018-2023.
- [139] Zhong, Y.; Kumar, B.; Oh, S.; Trinh, M. T.; Wu, Y.; Elbert, K.; Li, P.; Zhu, X.; Xiao, S.; Ng, F.; Steigerwald, M. L.; Nuckolls, C., Helical Ribbons for Molecular Electronics, *J. Am. Chem. Soc.* **2014**, *136*, 8122-8130.
- [140] Sanyal, S.; Manna, A. K.; Pati, S. K., Effect of Imide Functionalization on the Electronic, Optical, and Charge Transport Properties of Coronene: A Theoretical Study, *J. Phys. Chem. C* **2013**, *117*, 825-836.
- [141] Dai, L., Functionalization of Graphene for Efficient Energy Conversion and Storage, *Acc. Chem. Res.* **2013**, *46*, 31-42.

- [142] Yoonessi, M.; Shi, Y.; Scheiman, D. A.; Lebron-Colon, M.; Tigelaar, D. M.; Weiss, R. A.; Meador, M. A., Graphene Polyimide Nanocomposites; Thermal, Mechanical, and High-Temperature Shape Memory Effects, *ACS Nano* **2012**, *6*, 7644-7655.
- [143] Nagarajan, K.; Mallia, A. R.; Muraleedharan, K.; Hariharan, M., Enhanced Intersystem Crossing in Core-Twisted Aromatics, *Chem. Sci.* **2017**, DOI: 10.1039/C6SC05126J.
- [144] Lütke Eversloh, C.; Li, C.; Müllen, K., Core-Extended Perylene Tetracarboxdiimides: The Homologous Series of Coronene Tetracarboxdiimides, *Org. Lett.* **2011**, *13*, 4148-4150.
- [145] Flamigni, L.; Zanelli, A.; Langhals, H.; Böck, B., Photophysical and Redox Properties of Perylene Bis- and Tris-Dicarboximide Fluorophores with Triplet State Formation: Transient Absorption and Singlet Oxygen Sensitization, *J. Phys. Chem. A* **2012**, *116*, 1503-1509.
- [146] Henry, B. R.; Siebrand, W., Spin-Orbit Coupling in Aromatic Hydrocarbons. Analysis of Nonradiative Transitions between Singlet and Triplet States in Benzene and Naphthalene, *J. Chem. Phys.* **1971**, *54*, 1072-1085.
- [147] Wasielewski, M. R., Photoinduced Electron Transfer in Supramolecular Systems for Artificial Photosynthesis, *Chem. Rev.* **1992**, *92*, 435-461.
- [148] Scholes, G. D.; Fleming, G. R.; Olaya-Castro, A.; van Grondelle, R., Lessons from Nature About Solar Light Harvesting, *Nat. Chem.* **2011**, *3*, 763-774.
- [149] Gust, D.; Moore, T. A.; Moore, A. L., Molecular Mimicry of Photosynthetic Energy and Electron Transfer, *Acc. Chem. Res.* **1993**, *26*, 198-205.
- [150] Flors, C.; Oesterling, I.; Schnitzler, T.; Fron, E.; Schweitzer, G.; Sliwa, M.; Herrmann, A.; van der Auweraer, M.; de Schryver, F. C.; Müllen, K.; Hofkens, J., Energy and Electron Transfer in Ethynylene Bridged Perylene Diimide Multichromophores, *J. Phys. Chem. C* **2007**, *111*, 4861-4870.
- [151] Antoniuk-Pablant, A.; Kodis, G.; Moore, A. L.; Moore, T. A.; Gust, D., Photoinduced Electron and Energy Transfer in a Molecular Triad Featuring a Fullerene Redox Mediator, *J. Phys. Chem. B* **2016**, *120*, 6687-6697.
- [152] Megiatto, J. D.; Antoniuk-Pablant, A.; Sherman, B. D.; Kodis, G.; Gervaldo, M.; Moore, T. A.; Moore, A. L.; Gust, D., Mimicking the Electron Transfer Chain in Photosystem II with a Molecular Triad Thermodynamically Capable of Water Oxidation, *Proc. Natl. Acad. Sci. U.S.A.* **2012**, *109*, 15578-15583.
- [153] Sautter, A.; Kaletaş, B. K.; Schmid, D. G.; Dobrawa, R.; Zimine, M.; Jung, G.; van Stokkum, I. H. M.; De Cola, L.; Williams, R. M.; Würthner, F., Ultrafast Energy-Electron Transfer Cascade in a Multichromophoric Light-Harvesting Molecular Square, *J. Am. Chem. Soc.* **2005**, *127*, 6719-6729.

- [154] Oraziotti, M.; Kuss-Petermann, M.; Hamm, P.; Wenger, O. S., Light-Driven Electron Accumulation in a Molecular Pentad, *Angew. Chem. Int. Ed.* **2016**, *55*, 9407-9410.
- [155] Kc, C. B.; Lim, G. N.; Zandler, M. E.; D'Souza, F., Synthesis and Photoinduced Electron Transfer Studies of a Tri(Phenothiazine)–Subphthalocyanine–Fullerene Pentad, *Org. Lett.* **2013**, *15*, 4612-4615.
- [156] Gust, D.; Moore, T. A.; Moore, A. L.; Lee, S.-J.; Bittersmann, E.; Luttrull, D. K.; Rehms, A. A.; DeGraziano, J. M.; Ma, X. C.; Gao, F.; Belford, R. E.; Trier, T. T., Efficient Multistep Photoinitiated Electron Transfer in a Molecular Pentad, *Science* **1990**, *248*, 199-201.
- [157] Peterman, E. J. G.; van Amerongen, H.; van Grondelle, R.; Dekker, J. P., The Nature of the Excited State of the Reaction Center of Photosystem II of Green Plants: A High-Resolution Fluorescence Spectroscopy Study, *Proc. Natl. Acad. Sci. U.S.A.* **1998**, *95*, 6128-6133.
- [158] Kobori, Y.; Yamauchi, S.; Akiyama, K.; Tero-Kubota, S.; Imahori, H.; Fukuzumi, S.; Norris, J. R., Primary Charge-Recombination in an Artificial Photosynthetic Reaction Center, *Proc. Natl. Acad. Sci. U.S.A.* **2005**, *102*, 10017-10022.
- [159] Fukuzumi, S.; Ohkubo, K.; Suenobu, T., Long-Lived Charge Separation and Applications in Artificial Photosynthesis, *Acc. Chem. Res.* **2014**, *47*, 1455-1464.
- [160] Imahori, H.; Guldi, D. M.; Tamaki, K.; Yoshida, Y.; Luo, C.; Sakata, Y.; Fukuzumi, S., Charge Separation in a Novel Artificial Photosynthetic Reaction Center Lives 380 ms, *J. Am. Chem. Soc.* **2001**, *123*, 6617-6628.
- [161] Van Dijk, S. I.; Groen, C. P.; Hartl, F.; Brouwer, A. M.; Verhoeven, J. W., Long-Lived Triplet State Charge Separation in Novel Piperidine-Bridged Donor–Acceptor Systems, *J. Am. Chem. Soc.* **1996**, *118*, 8425-8432.
- [162] Gould, I. R.; Boiani, J. A.; Gaillard, E. B.; Goodman, J. L.; Farid, S., Intersystem Crossing in Charge-Transfer Excited States, *J. Phys. Chem. A* **2003**, *107*, 3515-3524.
- [163] Borkent, J. H.; De Jong, A. W. J.; Verhoeven, J. W.; De Boer, T. J., Photophysics of Intramolecular Electron Donor–Acceptor Systems; N-carbazolyl—(CH₂)_n—tetrachlorophthalimide, *Chem. Phys. Lett.* **1978**, *57*, 530-534.
- [164] Smit, K. J.; Warman, J. M., The Formation of Singlet and Triplet Charge Transfer States on Photo-Excitation of Carbazole-(CH₂)N-Tetrachlorophthalimide Compounds Studied by Time-Resolved Microwave Conductivity, *J. Lumin.* **1988**, *42*, 149-154.
- [165] Lim, B. T.; Okajima, S.; Chandra, A. K.; Lim, E. C., Radiationless Transitions in Electron Donor-Acceptor Complexes: Selection Rules for S₁ → T Intersystem Crossing and Efficiency of S₁ → S₀ Internal Conversion, *Chem. Phys. Lett.* **1981**, *79*, 22-27.

- [166] Wiederrecht, G. P.; Svec, W. A.; Wasielewski, M. R.; Galili, T.; Levanon, H., Novel Mechanism for Triplet State Formation in Short Distance Covalently Linked Radical Ion Pairs, *J. Am. Chem. Soc.* **2000**, *122*, 9715-9722.
- [167] Carbonera, D.; Di Valentin, M.; Corvaja, C.; Agostini, G.; Giacometti, G.; Liddell, P. A.; Kuciauskas, D.; Moore, A. L.; Moore, T. A.; Gust, D., Epr Investigation of Photoinduced Radical Pair Formation and Decay to a Triplet State in a Carotene–Porphyrin–Fullerene Triad, *J. Am. Chem. Soc.* **1998**, *120*, 4398-4405.
- [168] Gould, I. R.; Farid, S., Dynamics of Bimolecular Photoinduced Electron-Transfer Reactions, *Acc. Chem. Res.* **1996**, *29*, 522-528.
- [169] Cheriya, R. T.; Joy, J.; Alex, A. P.; Shaji, A.; Hariharan, M., Energy Transfer in near-Orthogonally Arranged Chromophores Separated through a Single Bond, *J. Phys. Chem. C* **2012**, *116*, 12489-12498.
- [170] Chao, C.-C.; Leung, M.-k.; Su, Y. O.; Chiu, K.-Y.; Lin, T.-H.; Shieh, S.-J.; Lin, S.-C., Photophysical and Electrochemical Properties of 1,7-Diaryl-Substituted Perylene Diimides, *J. Org. Chem.* **2005**, *70*, 4323-4331.
- [171] Li, Y.; Xu, L.; Liu, T.; Yu, Y.; Liu, H.; Li, Y.; Zhu, D., Anthraceno-Perylene Bisimides: The Precursor of a New Acene, *Org. Lett.* **2011**, *13*, 5692-5695.
- [172] Supur, M.; Sung, Y. M.; Kim, D.; Fukuzumi, S., Enhancement of Photodriven Charge Separation by Conformational and Intermolecular Adaptations of an Anthracene–Perylenediimide–Anthracene Triad to an Aqueous Environment, *J. Phys. Chem. C* **2013**, *117*, 12438-12445.
- [173] Noboru, M.; Yozo, K.; Masao, K., Solvent Effects Upon Fluorescence Spectra and the Dipolemoments of Excited Molecules, *Bull. Chem. Soc. Jpn.* **1956**, *29*, 465-470.
- [174] Ahrens, M. J.; Tauber, M. J.; Wasielewski, M. R., Bis(n-octylamino)perylene-3,4:9,10-bis(dicarboximide)s and Their Radical Cations: Synthesis, Electrochemistry, and Endor Spectroscopy, *J. Org. Chem.* **2006**, *71*, 2107-2114.
- [175] Verhoeven, J. W.; van Ramesdonk, H. J.; Groeneveld, M. M.; Benniston, A. C.; Harriman, A., Long-Lived Charge-Transfer States in Compact Donor–Acceptor Dyads, *ChemPhysChem* **2005**, *6*, 2251-2260.

6. List of publications

- 1) Enhanced Intersystem Crossing in Core-Twisted Aromatics
Nagarajan, K.; Mallia, A. R.; Muraleedharan, K.; Hariharan, M.*
Chem. Sci. **2017**, DOI: 10.1039/C6SC05126J.
- 2) Access to Triplet Excited State in Core-Twisted Perylenediimide
Nagarajan, K.; Mallia, A. R.; Reddy, V. S.; Hariharan, M.*
J. Phys. Chem. C **2016**, *120*, 8443-8450.
- 3) A Polyimide based all-organic sodium ion battery
Banda, H.; Damien, D.; **Nagarajan, K.**; Hariharan, M.; Shaijumon, M. M.*
J. Mater. Chem. A **2015**, *3*, 10453-10458.
- 4) Progressive Acylation of Pyrene Engineers Solid State Packing and Colour via C–H...H–C, C–H...O and π - π Interactions
Rajagopal, S. K.; Philip, A. M.; **Nagarajan, K.**; Hariharan, M.*
Chem. Commun. **2014**, *50*, 8644-8647.
- 5) C–H...H–C and C–H... π Contacts Aid Transformation of Dimeric to Monomeric Anthracene in the Solid State
Nagarajan, K.; Rajagopal, S. K.; Hariharan, M.*
CrystEngComm **2014**, *16*, 8946-8949.
- 6) Breakdown of Exciton Splitting through Electron Donor–Acceptor Interaction: A Caveat for the Application of Exciton Chirality Method in Macromolecules
Joy, J.; Cheriya, R. T.; **Nagarajan, K.**; Shaji, A.; Hariharan, M.*
J. Phys. Chem. C **2013**, *117*, 17927-17939.
- 7) Single Component Organic Light-Harvesting Red Luminescent Crystal
Cheriya, R. T.; **Nagarajan, K.**; Hariharan, M.*
J. Phys. Chem. C **2013**, *117*, 3240-3248.
- 8) Perylene Polyimide based Organic Electrode Materials for Rechargeable Lithium Batteries
Sharma, P.; Damien, D.; **Nagarajan, K.**; Shaijumon, M. M.; Hariharan, M.*
J. Phys. Chem. Lett. **2013**, *4*, 3192-3197.
- 9) DNA-Enforced Conformational Restriction of an Atropisomer
Cheriya, R. T.; Joy, J.; Rajagopal, S. K.; **Nagarajan, K.**; Hariharan, M.*
J. Phys. Chem. C **2012**, *116*, 22631-22636.

7. Presentations at conferences

- 1) Presented a poster in the **Gordon Research Conference and Seminar (GRC-2016) on "Electronic Processes in Organic Materials"** (June 4-10, 2016), held at Lucca (Barga), Italy (**Best Poster Award**).
- 2) **Presented a poster in Inter-IISER Chemistry Meet-2015** (December 11-13, 2016) held at Thiruvananthapuram, India.
- 3) Presented a poster and oral presentation in the Conference on "**Modern Trends in Electron Transfer Chemistry: From Molecular Electronics to Devices**" (January 28-29, 2016), ICTS, Bangalore, India.
- 4) Presented a poster and oral presentation in the "**11th JNC Research Conference on Chemistry of Materials**" (October 02-04, 2015), Alleppey, Kerala, India.
- 5) Presented a poster in the 8th "**Asian Photochemistry Conference (APC-2014)**", (November 10-13, 2014), Thiruvananthapuram, Kerala, India.
- 6) Presented a poster and oral presentation in the "**DAE-BRNS conference on Organic Device: A Future Ahead (ODeFA-2014)**" (March 03-06, 2014), BARC, Mumbai, India. (**Best Poster and Innovative Research Award**).
- 7) Attended one day conference "**ACS on Campus**" an initiative from American Chemical Society held at NIIST-Thiruvananthapuram, India, November 23, 2013.
- 8) Presented a poster and oral presentation in the "**8th JNC Research Conference on Chemistry of Materials**" (September 30- October 02, 2012), Thiruvananthapuram, Kerala, India.
- 9) Attended **Inter-IISER Chemistry Meet-2011** held at IISER-Thiruvananthapuram, India, December, 2011.

8. Copyrights and Permission

10/27/2016

Rightslink® by Copyright Clearance Center

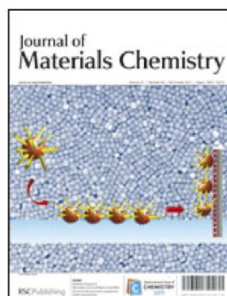


RightsLink®

Home

Account Info

Help



Title: Water-soluble phosphorescent iridium(iii) complexes as multicolor probes for imaging of homocysteine and cysteine in living cells

Author: Yun Ma, Shujuan Liu, Huiran Yang, Yongquan Wu, Chengjiang Yang, Xiangmei Liu, Qiang Zhao, Huazhou Wu, Jiakai Liang, Fuyou Li, Wei Huang

Publication: Journal of Materials Chemistry

Publisher: Royal Society of Chemistry

Date: Nov 2, 2011

Copyright © 2011, Royal Society of Chemistry

Logged in as:

Kalaivanan Nagarajan

[LOGOUT](#)

Review Order

Please review the order details and the associated [terms and conditions](#).

No royalties will be charged for this reuse request although you are required to obtain a license and comply with the license terms and conditions. To obtain the license, click the Accept button below.

Licensed Content Publisher	Royal Society of Chemistry
Licensed Content Publication	Journal of Materials Chemistry
Licensed Content Title	Water-soluble phosphorescent iridium(iii) complexes as multicolor probes for imaging of homocysteine and cysteine in living cells
Licensed Content Author	Yun Ma, Shujuan Liu, Huiran Yang, Yongquan Wu, Chengjiang Yang, Xiangmei Liu, Qiang Zhao, Huazhou Wu, Jiakai Liang, Fuyou Li, Wei Huang
Licensed Content Date	Nov 2, 2011
Licensed Content Volume	21
Licensed Content Issue	47
Type of Use	Thesis/Dissertation
Requestor type	non-commercial (non-profit)
Portion	figures/tables/images
Number of figures/tables/images	1
Distribution quantity	1
Format	print and electronic
Will you be translating?	no
Order reference number	
Title of the thesis/dissertation	Strategies to access triplet excited state in perylenediimide based chromophores
Expected completion date	Oct 2016
Estimated size	150
Requestor Location	Kalaivanan Nagarajan School of Chemistry CET Campus Thiruvananthapuram, 695016 India Attn: Kalaivanan Nagarajan
Total	0.00 USD

10/27/2016

Rightslink® by Copyright Clearance Center



RightsLink®

Home

Account
Info

Help

ACS Publications
Most Trusted. Most Cited. Most Read.

Title: Intersystem Crossing Mediated
by Photoinduced Intramolecular
Charge Transfer: Julolidine
–Anthracene Molecules with
Perpendicular n Systems

Author: Zachary E. X. Dance, Sarah M.
Mickley, Thea M. Wilson, et al

Publication: The Journal of Physical Chemistry
A

Publisher: American Chemical Society

Date: May 1, 2008

Copyright © 2008, American Chemical Society

Logged in as:

Kalaivanan Nagarajan

Account #:

3001077792

LOGOUT

PERMISSION/LICENSE IS GRANTED FOR YOUR ORDER AT NO CHARGE

This type of permission/license, instead of the standard Terms & Conditions, is sent to you because no fee is being charged for your order. Please note the following:

- Permission is granted for your request in both print and electronic formats, and translations.
- If figures and/or tables were requested, they may be adapted or used in part.
- Please print this page for your records and send a copy of it to your publisher/graduate school.
- Appropriate credit for the requested material should be given as follows: "Reprinted (adapted) with permission from (COMPLETE REFERENCE CITATION). Copyright (YEAR) American Chemical Society." Insert appropriate information in place of the capitalized words.
- One-time permission is granted only for the use specified in your request. No additional uses are granted (such as derivative works or other editions). For any other uses, please submit a new request.

If credit is given to another source for the material you requested, permission must be obtained from that source.

BACK

CLOSE WINDOW

Copyright © 2016 Copyright Clearance Center, Inc. All Rights Reserved. [Privacy statement](#). [Terms and Conditions](#).
Comments? We would like to hear from you. E-mail us at customercare@copyright.com

10/27/2016

Rightslink® by Copyright Clearance Center

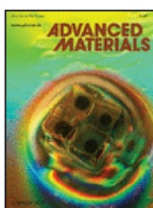


RightsLink®

Home

Account
Info

Help



Title: Perylene Imides for Organic Photovoltaics: Yesterday, Today, and Tomorrow

Author: Chen Li, Henrike Wonneberger

Publication: Advanced Materials

Publisher: John Wiley and Sons

Date: Jan 9, 2012

Copyright © 2012 WILEY-VCH Verlag GmbH & Co. KGaA, Weinheim

Logged in as:
Kalaivanan Nagarajan
Account #:
3001077792

LOGOUT

Review Order

Please review the order details and the associated [terms and conditions](#).

No royalties will be charged for this reuse request although you are required to obtain a license and comply with the license terms and conditions. To obtain the license, click the Accept button below.

Licensed Content Publisher	John Wiley and Sons
Licensed Content Publication	Advanced Materials
Licensed Content Title	Perylene Imides for Organic Photovoltaics: Yesterday, Today, and Tomorrow
Licensed Content Author	Chen Li, Henrike Wonneberger
Licensed Content Date	Jan 9, 2012
Licensed Content Pages	24
Type of use	Dissertation/Thesis
Requestor type	University/Academic
Format	Print and electronic
Portion	Figure/table
Number of figures/tables	1
Original Wiley figure/table number(s)	Figure 2
Will you be translating?	No
Title of your thesis / dissertation	Strategies to access triplet excited state in perylenediimide base chromophores
Expected completion date	Oct 2016
Expected size (number of pages)	150
Requestor Location	Kalaivanan Nagarajan School of Chemistry CET Campus Thiruvananthapuram, 695016 India Attn: Kalaivanan Nagarajan
Publisher Tax ID	EU826007151
Total	0.00 USD

10/27/2016

Rightslink® by Copyright Clearance Center



RightsLink®

Home

Account
Info

Help

ACS Publications
Most Trusted. Most Cited. Most Read.**Title:** Perylene Bisimide Dye Assemblies
as Archetype Functional
Supramolecular Materials**Author:** Frank Würthner, Chantu R.
Saha-Möller, Benjamin Fimmel,
et al**Publication:** Chemical Reviews**Publisher:** American Chemical Society**Date:** Feb 1, 2016

Copyright © 2016, American Chemical Society

Logged in as:
Kalaivanan Nagarajan
Account #:
3001077792

LOGOUT

PERMISSION/LICENSE IS GRANTED FOR YOUR ORDER AT NO CHARGE

This type of permission/license, instead of the standard Terms & Conditions, is sent to you because no fee is being charged for your order. Please note the following:

- Permission is granted for your request in both print and electronic formats, and translations.
- If figures and/or tables were requested, they may be adapted or used in part.
- Please print this page for your records and send a copy of it to your publisher/graduate school.
- Appropriate credit for the requested material should be given as follows: "Reprinted (adapted) with permission from (COMPLETE REFERENCE CITATION). Copyright (YEAR) American Chemical Society." Insert appropriate information in place of the capitalized words.
- One-time permission is granted only for the use specified in your request. No additional uses are granted (such as derivative works or other editions). For any other uses, please submit a new request.

If credit is given to another source for the material you requested, permission must be obtained from that source.

BACK

CLOSE WINDOW

Copyright © 2016 [Copyright Clearance Center, Inc.](#) All Rights Reserved. [Privacy statement](#). [Terms and Conditions](#).
Comments? We would like to hear from you. E-mail us at customer@copyright.com

10/27/2016

Rightslink® by Copyright Clearance Center

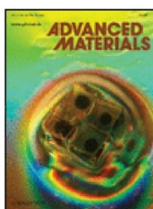


RightsLink®

Home

Account
Info

Help



Title: A Vinylene-Bridged Perylenediimide-Based Polymeric Acceptor Enabling Efficient All-Polymer Solar Cells Processed under Ambient Conditions

Author: Yikun Guo, Yunke Li, Omar Awartani, Jingbo Zhao, Han Han, Harald Ade, Dahui Zhao, He Yan

Publication: Advanced Materials

Publisher: John Wiley and Sons

Date: Aug 8, 2016

© 2016 WILEY-VCH Verlag GmbH & Co. KGaA, Weinheim

Logged in as:

Kalaivanan Nagarajan

Account #:
3001077792
[LOGOUT](#)

Review Order

Please review the order details and the associated [terms and conditions](#).

No royalties will be charged for this reuse request although you are required to obtain a license and comply with the license terms and conditions. To obtain the license, click the Accept button below.

Licensed Content Publisher	John Wiley and Sons
Licensed Content Publication	Advanced Materials
Licensed Content Title	A Vinylene-Bridged Perylenediimide-Based Polymeric Acceptor Enabling Efficient All-Polymer Solar Cells Processed under Ambient Conditions
Licensed Content Author	Yikun Guo, Yunke Li, Omar Awartani, Jingbo Zhao, Han Han, Harald Ade, Dahui Zhao, He Yan
Licensed Content Date	Aug 8, 2016
Licensed Content Pages	7
Type of use	Dissertation/Thesis
Requestor type	University/Academic
Format	Print and electronic
Portion	Figure/table
Number of figures/tables	1
Original Wiley figure/table number(s)	Figure 1
Will you be translating?	No
Title of your thesis / dissertation	Strategies to access triplet excited state in perylenediimide based chromophores
Expected completion date	Oct 2016
Expected size (number of pages)	150
Requestor Location	Kalaivanan Nagarajan School of Chemistry CET Campus Thiruvananthapuram, 695016 India Attn: Kalaivanan Nagarajan
Publisher Tax ID	EU826007151
Total	0.00 USD

10/27/2016

Rightslink® by Copyright Clearance Center

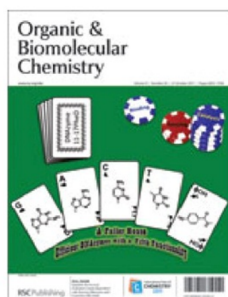


RightsLink®

Home

Account
Info

Help



Title: Solvent and substituent effects on aggregation constants of perylene bisimide n-stacks – a linear free energy relationship analysis

Logged in as:
Kalaivanan Nagarajan
Account #:
3001077792

Author: Zhijian Chen, Benjamin Fimmel, Frank Würthner

Publication: Organic & Biomolecular Chemistry

Publisher: Royal Society of Chemistry

Date: Mar 5, 2012

Copyright © 2012, Royal Society of Chemistry

LOGOUT

Review Order

Please review the order details and the associated [terms and conditions](#).

No royalties will be charged for this reuse request although you are required to obtain a license and comply with the license terms and conditions. To obtain the license, click the Accept button below.

Licensed Content Publisher	Royal Society of Chemistry
Licensed Content Publication	Organic & Biomolecular Chemistry
Licensed Content Title	Solvent and substituent effects on aggregation constants of perylene bisimide n-stacks – a linear free energy relationship analysis
Licensed Content Author	Zhijian Chen, Benjamin Fimmel, Frank Würthner
Licensed Content Date	Mar 5, 2012
Licensed Content Volume	10
Licensed Content Issue	30
Type of Use	Thesis/Dissertation
Requestor type	academic/educational
Portion	figures/tables/images
Number of figures/tables/images	1
Distribution quantity	1
Format	print and electronic
Will you be translating?	no
Order reference number	
Title of the thesis/dissertation	Strategies to access triplet excited state in perylenediimide based chromophores
Expected completion date	Oct 2016
Estimated size	150
Requestor Location	Kalaivanan Nagarajan School of Chemistry CET Campus Thiruvananthapuram, 695016 India Attn: Kalaivanan Nagarajan
Total	0.00 USD

10/27/2016

Rightslink® by Copyright Clearance Center



RightsLink®

Home

Account
Info

Help

ACS Publications
Most Trusted. Most Cited. Most Read.

Title:

Combining Light-Harvesting and
Charge Separation in a Self-
Assembled Artificial
Photosynthetic System Based on
Perylenediimide Chromophores

Logged in as:

Kalaivanan Nagarajan

Account #:

3001077792

LOGOUT

Author:

Boris Rybtchinski, Louise E.
Sinks, Michael R. WasielewskiPublication: Journal of the American Chemical
Society

Publisher: American Chemical Society

Date: Oct 1, 2004

Copyright © 2004, American Chemical Society

PERMISSION/LICENSE IS GRANTED FOR YOUR ORDER AT NO CHARGE

This type of permission/license, instead of the standard Terms & Conditions, is sent to you because no fee is being charged for your order. Please note the following:

- Permission is granted for your request in both print and electronic formats, and translations.
- If figures and/or tables were requested, they may be adapted or used in part.
- Please print this page for your records and send a copy of it to your publisher/graduate school.
- Appropriate credit for the requested material should be given as follows: "Reprinted (adapted) with permission from (COMPLETE REFERENCE CITATION). Copyright (YEAR) American Chemical Society." Insert appropriate information in place of the capitalized words.
- One-time permission is granted only for the use specified in your request. No additional uses are granted (such as derivative works or other editions). For any other uses, please submit a new request.

If credit is given to another source for the material you requested, permission must be obtained from that source.

BACK

CLOSE WINDOW

Copyright © 2016 [Copyright Clearance Center, Inc.](#) All Rights Reserved. [Privacy statement.](#) [Terms and Conditions.](#)
Comments? We would like to hear from you. E-mail us at customercare@copyright.com

10/27/2016

Rightslink® by Copyright Clearance Center



RightsLink®

Home

Account
Info

Help



Title: Access to Triplet Excited State in Core-Twisted Peryleneimide
Author: Kalaivanan Nagarajan, Ajith R. Mallia, V. Sivarajana Reddy, et al
Publication: The Journal of Physical Chemistry C
Publisher: American Chemical Society
Date: Apr 1, 2016
Copyright © 2016, American Chemical Society

Logged in as:
Kalaivanan Nagarajan
Account #:
3001077792

LOGOUT

PERMISSION/LICENSE IS GRANTED FOR YOUR ORDER AT NO CHARGE

This type of permission/license, instead of the standard Terms & Conditions, is sent to you because no fee is being charged for your order. Please note the following:

- Permission is granted for your request in both print and electronic formats, and translations.
- If figures and/or tables were requested, they may be adapted or used in part.
- Please print this page for your records and send a copy of it to your publisher/graduate school.
- Appropriate credit for the requested material should be given as follows: "Reprinted (adapted) with permission from (COMPLETE REFERENCE CITATION). Copyright (YEAR) American Chemical Society." Insert appropriate information in place of the capitalized words.
- One-time permission is granted only for the use specified in your request. No additional uses are granted (such as derivative works or other editions). For any other uses, please submit a new request.

BACK

CLOSE WINDOW

Copyright © 2016 [Copyright Clearance Center, Inc.](#) All Rights Reserved. [Privacy statement.](#) [Terms and Conditions.](#) Comments? We would like to hear from you. E-mail us at customercare@copyright.com

10/27/2016

Rightslink® by Copyright Clearance Center



RightsLink®

Home

Account Info

Help



ACS Publications
Most Trusted. Most Cited. Most Read.

Title: Singlet Fission
Author: Millicent B. Smith, Josef Michl
Publication: Chemical Reviews
Publisher: American Chemical Society
Date: Nov 1, 2010

Logged in as:
Kalaivanan Nagarajan
Account #:
3001077792

LOGOUT

Copyright © 2010, American Chemical Society

PERMISSION/LICENSE IS GRANTED FOR YOUR ORDER AT NO CHARGE

This type of permission/license, instead of the standard Terms & Conditions, is sent to you because no fee is being charged for your order. Please note the following:

- Permission is granted for your request in both print and electronic formats, and translations.
- If figures and/or tables were requested, they may be adapted or used in part.
- Please print this page for your records and send a copy of it to your publisher/graduate school.
- Appropriate credit for the requested material should be given as follows: "Reprinted (adapted) with permission from (COMPLETE REFERENCE CITATION). Copyright (YEAR) American Chemical Society." Insert appropriate information in place of the capitalized words.
- One-time permission is granted only for the use specified in your request. No additional uses are granted (such as derivative works or other editions). For any other uses, please submit a new request.

If credit is given to another source for the material you requested, permission must be obtained from that source.

BACK

CLOSE WINDOW

Copyright © 2016 [Copyright Clearance Center, Inc.](#) All Rights Reserved. [Privacy statement](#). [Terms and Conditions](#).
Comments? We would like to hear from you. E-mail us at customer@copyright.com

10/27/2016

Rightslink® by Copyright Clearance Center



RightsLink®

Home

Account
Info

Help

ACS Publications
Most Trusted. Most Cited. Most Read.**Title:**Singlet Exciton Fission in
Polycrystalline Thin Films of a
Slip-Stacked Perylenediimide**Author:**Samuel W. Eaton, Leah E. Shoer,
Steven D. Karlen, et al**Publication:**Journal of the American Chemical
Society**Publisher:**

American Chemical Society

Date:

Oct 1, 2013

Copyright © 2013, American Chemical Society

Logged in as:

Kalaivanan Nagarajan

Account #:

3001077792

LOGOUT

PERMISSION/LICENSE IS GRANTED FOR YOUR ORDER AT NO CHARGE

This type of permission/license, instead of the standard Terms & Conditions, is sent to you because no fee is being charged for your order. Please note the following:

- Permission is granted for your request in both print and electronic formats, and translations.
- If figures and/or tables were requested, they may be adapted or used in part.
- Please print this page for your records and send a copy of it to your publisher/graduate school.
- Appropriate credit for the requested material should be given as follows: "Reprinted (adapted) with permission from (COMPLETE REFERENCE CITATION). Copyright (YEAR) American Chemical Society." Insert appropriate information in place of the capitalized words.
- One-time permission is granted only for the use specified in your request. No additional uses are granted (such as derivative works or other editions). For any other uses, please submit a new request.

If credit is given to another source for the material you requested, permission must be obtained from that source.

BACK

CLOSE WINDOW

Copyright © 2016 [Copyright Clearance Center, Inc.](#) All Rights Reserved. [Privacy statement](#). [Terms and Conditions](#).
Comments? We would like to hear from you. E-mail us at customercare@copyright.com

10/27/2016

Rightslink® by Copyright Clearance Center



RightsLink®

Home

Account
Info

Help



Title: Intersystem Crossing in Charge-Transfer Excited States
Author: Ian R. Gould, James A. Boiani, Elizabeth B. Gaillard, et al
Publication: The Journal of Physical Chemistry A
Publisher: American Chemical Society
Date: May 1, 2003
Copyright © 2003, American Chemical Society

Logged in as:
Kalaivanan Nagarajan
Account #:
3001077792

LOGOUT

PERMISSION/LICENSE IS GRANTED FOR YOUR ORDER AT NO CHARGE

This type of permission/license, instead of the standard Terms & Conditions, is sent to you because no fee is being charged for your order. Please note the following:

- Permission is granted for your request in both print and electronic formats, and translations.
- If figures and/or tables were requested, they may be adapted or used in part.
- Please print this page for your records and send a copy of it to your publisher/graduate school.
- Appropriate credit for the requested material should be given as follows: "Reprinted (adapted) with permission from (COMPLETE REFERENCE CITATION). Copyright (YEAR) American Chemical Society." Insert appropriate information in place of the capitalized words.
- One-time permission is granted only for the use specified in your request. No additional uses are granted (such as derivative works or other editions). For any other uses, please submit a new request.

If credit is given to another source for the material you requested, permission must be obtained from that source.

BACK

CLOSE WINDOW

Copyright © 2016 [Copyright Clearance Center, Inc.](#) All Rights Reserved. [Privacy statement.](#) [Terms and Conditions.](#)
Comments? We would like to hear from you. E-mail us at customer@copyright.com